NASA CR-54636
PWA-3142


SUMMARY REPORT

# METHODS FOR PREDICTING THERMAL STRESS CRACKING IN TURBINE STATOR OR ROTOR BLADES

by
O. L. STEWART AND W. H. VOGEL

approved by
R. A. DOAK

prepared for
NATIONAL AERONAUTICS AND SPACE ADMINISTRATION

JULY 10, 1967

CONTRACT NAS3-7909

TECHNICAL MANAGEMENT
NASA LEWIS RESEARCH CENTER
CLEVELAND, OHIO
AIR BREATHING ENGINES DIVISION
E. L. WARREN

RESEARCH ADVISOR, MATERIALS AND STRUCTURES DIVISION
D. A. SPERA



Pratt & Whitney Aircraft
DIVISION OF UNITED AIRCRAFT CORPORATION

EAST HARTFORD, CONNECTICUT

Requests for copies of this report should be referred to

National Aeronautics and Space Administration
Office of Scientific and Technical Information
Attention: AFSS-A
Washington, D.C. 20546

NASA CR-54636
PWA-3142

# METHODS FOR PREDICTING THERMAL STRESS CRACKING IN TURBINE STATOR OR ROTOR BLADES

By

O. L. Stewart and W. H. Vogel

Approved By
R. A. Doak

Prepared For
NATIONAL AERONAUTICS AND SPACE ADMINISTRATION

CONTRACT NO. NAS 3-7909

# FOREWORD

The report was prepared in response to the requirements of Contract NAS3-7909 under the technical management of Mr. Edward L. Warren, NASA-Lewis Research Center, Cleveland, Ohio. It describes the design and construction of a single specimen cascade test rig, used to determine experimentally the lives of simulated turbine blade specimens subjected to various heating and cooling cycles, in accordance with Exhibit "A", Section III of the contract.

# TABLE OF CONTENTS

TABLE OF CONTENTS (Cont'd)

# LIST OF ILLUSTRATIONS

LIST OF ILLUSTRATIONS (Cont'd)

LIST OF ILLUSTRATIONS (Cont'd)

## LIST OF ILLUSTRATIONS (Cont'd)

LIST OF ILLUSTRATIONS (Cont'd)

LIST OF ILLUSTRATIONS (Cont'd)

# LIST OF TABLES

## SUMMARY

Pratt & Whitney Aircraft had developed a method of predicting thermal fatigue cracking in gas turbine blades and vanes prior to this contract. This prediction method was furnished to NASA as part of this program. The purposes of this program were:

- To develop the method of predicting initiation of thermal fatigue cracking in turbine blades and vanes, and
- To test simulated turbine blade specimens to verify the prediction method.

Isothermal strain cycling fatigue properties and other physical properties needed for prediction calculations were measured for B-1900 and IN-100 alloys.

A new test rig for subjecting simulated turbine blade specimens to controlled temperature cycles and mechanical loads which simulate the conditions experienced by a first-stage turbine blade in an aircraft gas turbine was designed and constructed.

Thermocouples were attached to specimens which were tested to measure mid-span metal surface temperature at several chordwise locations. The specimens simulated film cooled, convectively cooled, and uncooled turbine blades. Two temperature cycles (fast and slow accelerations) were studied in preparation for fatigue tests. Based on the measured surface metal temperatures, complete temperature distributions were predicted for the uncooled and convectively cooled specimens. Thermal fatigue life was predicted for the convectively cooled specimens using these temperature predictions for the fast acceleration cycle.

Fatigue testing of two convectively cooled specimens was started and bowing and premature fracturing of the specimens were encountered. Analytical and experimental investigations were performed to determine the reasons for these results. Seven additional specimens were fatigue tested to develop a satisfactory test method. Further testing was not funded when it was concluded by NASA that the uncertainty in the value of the bending moments induced in the specimens was too large to satisfy their requirements.

## INTRODUCTION

Thermal fatigue cracking in turbine rotor blades and stator vanes of high performance lightweight gas turbine engines is one of the important and demanding problems encountered by the turbine designer. To meet the performance and weight requirements of these advanced engine designs, it is necessary to operate the turbine at increasingly higher turbine inlet gas temperatures. During operation of the engine and, particularly, during start-up take-off and landing, the turbine blades and vanes are subjected to rapid heating and cooling. Various sections of the blades and vanes heat and cool at different rates due to factors such as airfoil geometry, mass distribution, local heat transfer coefficient distribution around the airfoils and, in the case of cooled turbines, coolant distribution in the airfoils. These non-uniform heating and cooling rates induce high local strain cycles in some sections of the airfoil which can cause thermal fatigue crack development. Other factors such as the relatively low ductility of most of the high strength, high temperature alloys used for blades and vanes contribute to initiation and propagation of these thermal fatigue cracks. Unless detected soon after initiation these cracks can propagate in a short time to the extent that they weaken the blade or vane sufficiently to result in fracture.

The thermal fatigue mechanism is a special case of low cycle fatigue in which cyclic stresses and strains are produced at least partially by temperature variations. In a typical high temperature gas turbine balde, the leading and trailing edge sections of the airfoil are heated and cooled more rapidly than the mid-chord section, as seen in Figure 1. Since the mid-chord section of the blade contains the greatest protion of the blade mass, it controls the average elongation of the blade and, during heat up and cool down, restrains the thermal growth of the loading and trailing edge sections. This induces large compressive strains in the leading and trailing edge sections during heat up and large tensile strains during cool down. Figure 2 shows the total strain in the leading edge section of a typical high temperature turbine blade during heat up and cool down. These strains are frequently great enough to produce local stresses substantially in excess of the elastic limit of the blade material. Repeated cycling will then cause fatigue cracks to initiate in the elements subjected to the greatest total strain range. Similar effects are found in high temperature turbine vanes and in both cooled and uncooled configurations. The thermally-induced strains are added to the mechanical strains caused by aerodynamic and, in the case of blades, centrifugal forces. Due to the airfoil geometry, heating and cooling rate differences in the various blade and vane sections cause spanwise bowing. For blades, centrifugal action induces bending stresses that oppose bowing and contribute to local stresses.

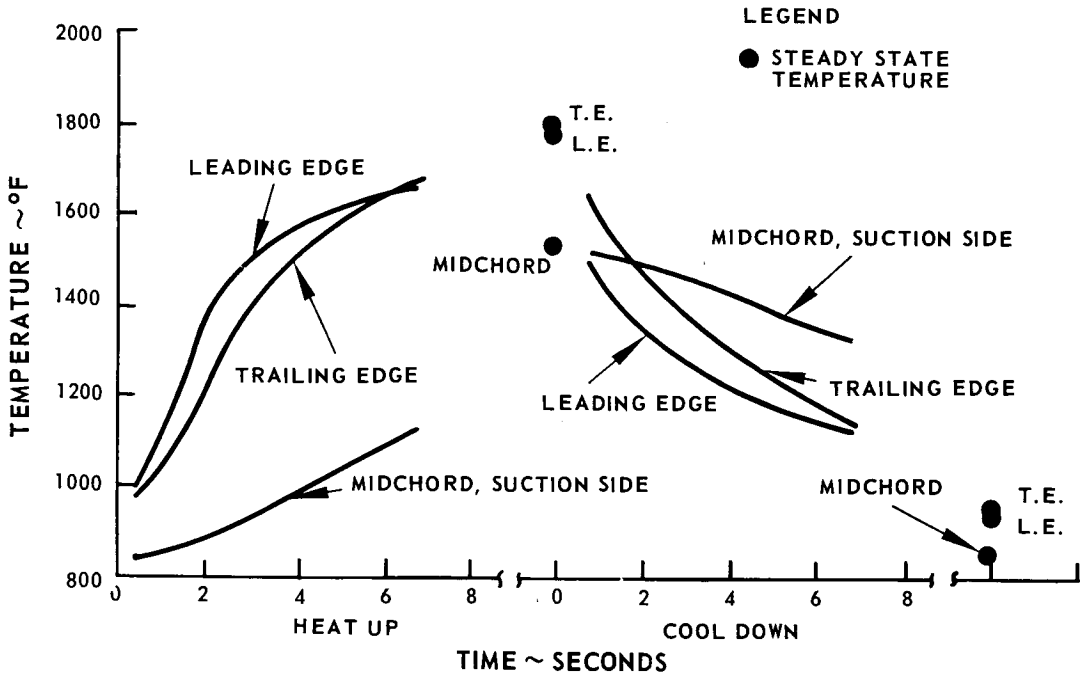


Figure 1 Cooled Turbine Blade Calculated Temperature vs. Time

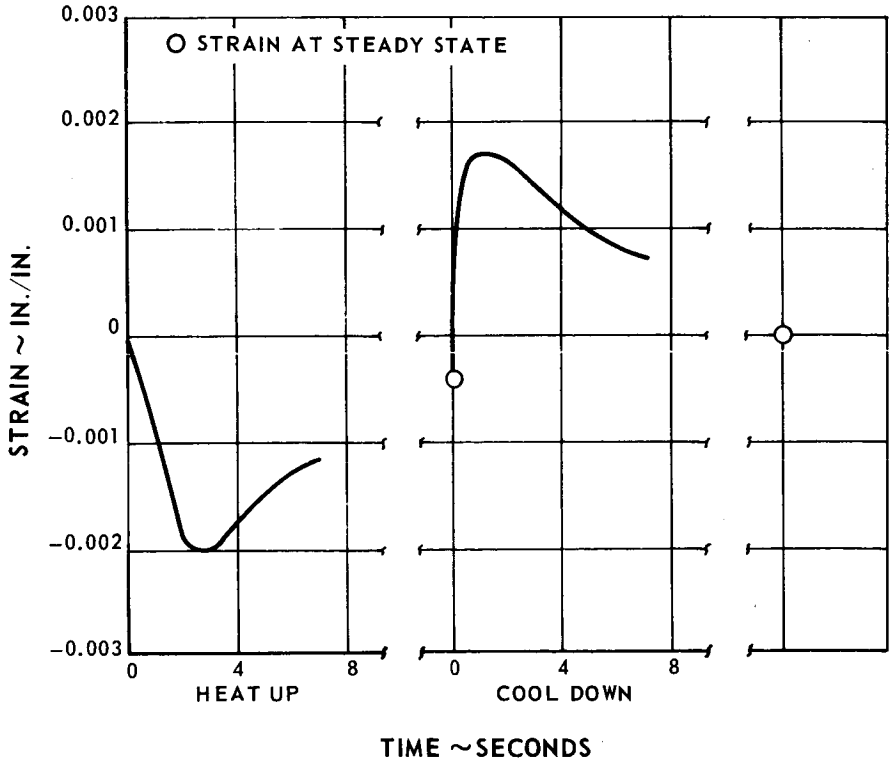


Figure 2 Cooled Turbine Blade Calculated Total Strain of the Leading Edge vs. Time

To design the necessary reliability and useful life into gas turbine engines being developed for advanced aircraft, the turbine designer must be able to predict and control thermal fatigue cracking in blades and vanes. Thermal fatigue cracking can be controlled by:

- Designing the airfoil and airfoil cooling configurations judiciously to minimize adverse temperature gradients during transient and steady state operation.
- Developing more fatigue resistant materials.
- Limiting the rates of temperature change during acceleration and deceleration of the engine.

The last two methods are obviously restricted; one by the slow rate of development and evaluation of new materials and the other by the practical limits that can be placed on the rates of power changes of an aircraft engine. Therefore, the turbine designer is usually restricted to the first method. A procedure for predicting the thermal fatigue life of a given design is necessary to evaluate the acceptability of the design to meet the engine requirements and the relative merits of one design against another.

Pratt and Whitney Aircraft initiated work on this problem in the late 1950's. During the period between 1961 and 1964, Pratt and Whitney Aircraft developed a method for predicting the initiation of thermal fatigue cracking in turbine blades and vanes. Limited verification of this method has been obtained from engine tests. The actual temperature conditions during these tests, however, were not known well enough to provide conclusive verification of this method and the rate of data acquisition was slow.

The work reported upon herein was accomplished by Pratt and Whitney Aircraft under contract NAS 3-7909 for the National Aeronautics and Space Administration-Lewis Research Laboratory. The purpose of this contract was to:

- Develop a method for predicting thermal stress cracking in turbine stator and rotor blades, and
- Verify experimentally this prediction method.

Under this contract Pratt and Whitney Aircraft:

- Furnished the prediction method it had previously developed to NASA
- Designed and constructed a test rig to subject simulated turbine blade specimens to controlled temperature and mechanical cycles and environmental conditions which closely simulated aircraft gas turbine conditions.

- Designed and fabricated simulated turbine blade specimens embodying two materials, cast B-1900 (PWA 663) and cast IN-100 (PWA 658), and three configurations; uncooled solid, convectively cooled and film cooled. A diffused aluminum-silicon coating was applied to all specimens in accordance with Specification PWA 47-14L.

- Provided basic material properties of the two specimen materials for the range of metal temperatures covered in this program including tensile and strain-cycling fatigue data.

- Tested instrumented specimens in each material and configuration and measured the transient and steady state metal temperatures at several chordwise locations at the mid-span section of the specimen for the gas temperature cycles and environmental conditions planned to be used for subsequent fatigue tests.

- Calculated the steady state and transient temperature distribution in the convectively cooled specimen to match the measured metal temperatures for the fast acceleration temperature cycle and predicted the number of cycles to initiate thermal fatigue cracking in this specimen for the thermal and mechanical load cycles shown in Figure 3. Substantially completed temperature syntheses for the uncooled solid specimens for the fast and slow acceleration temperature cycles and for the convectively cooled specimen for the slow acceleration temperature cycles.

- Devised a test program using two thermal-mechanical load cycles and commenced testing the convectively cooled specimens. These tests were discontinued after the first specimen bowed and the second specimen fractured in a very few cycles.

- Conducted analytical and experimental investigations to determine the cause of the bowing and premature fracture and to develop a test procedure which would produce meaningful data in 10 to 1000 test cycles per specimen.

- Devised a revised test program which would obtain meaningful test data.

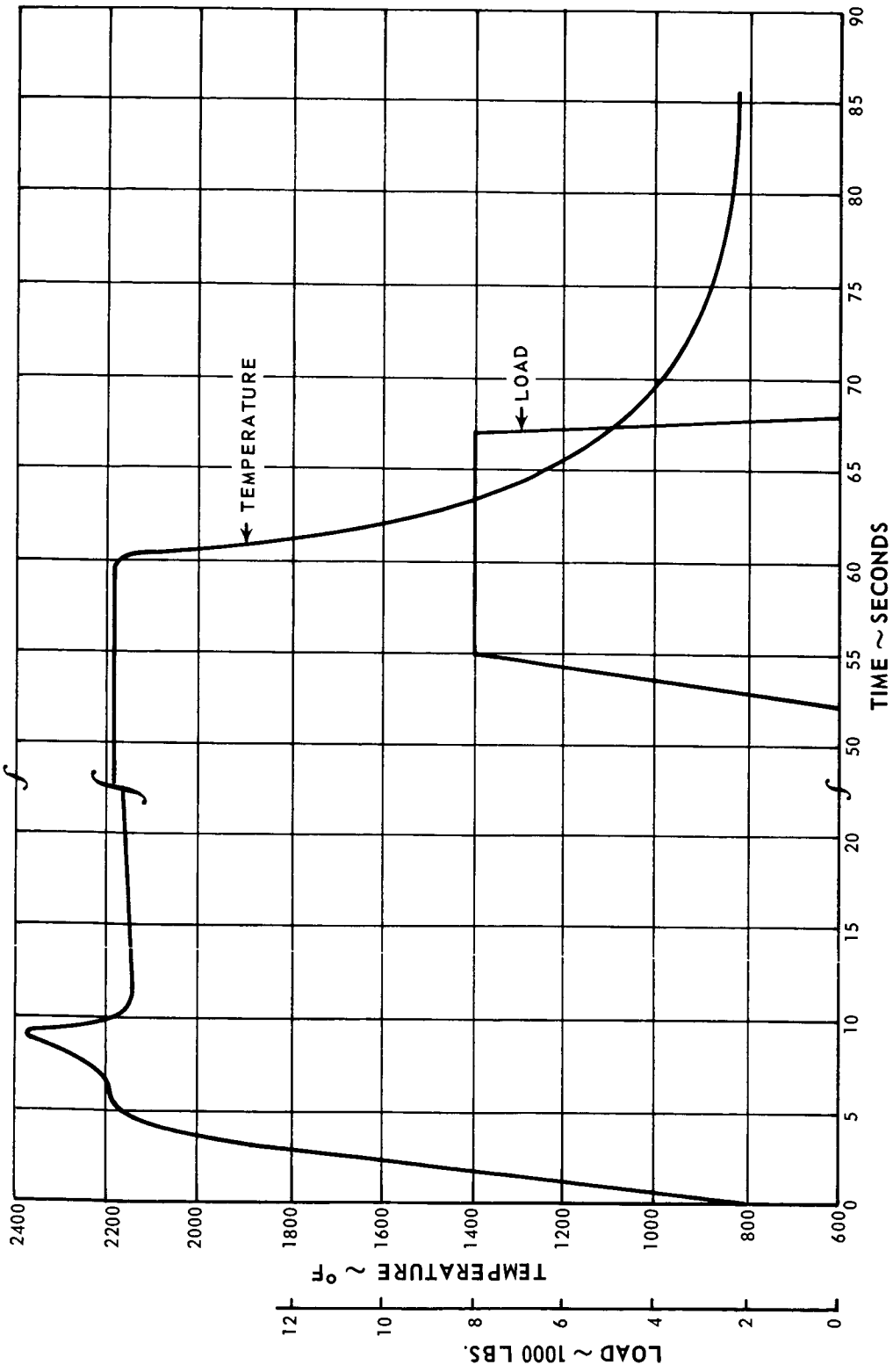


Figure 3 Primary Gas Temperature And Load Cycles for Cooled Specimens, Fast Acceleration Cycle

## TURBINE BLADE SPECIMENS

The design of the simulated turbine blade specimens is shown in Figure 4. The external shape of all specimens were identical. The airfoil design was based upon the 65 percent span section of the JT4 engine first-stage turbine blade. The airflow channel width was reduced approximately 18 percent to correspond to the test facility air flow capacity at design conditions. This necessitated minor modifications to the airfoil contour to assure a converging channel in the cascade. The design operating conditions for the cascade are shown in Figure 5.

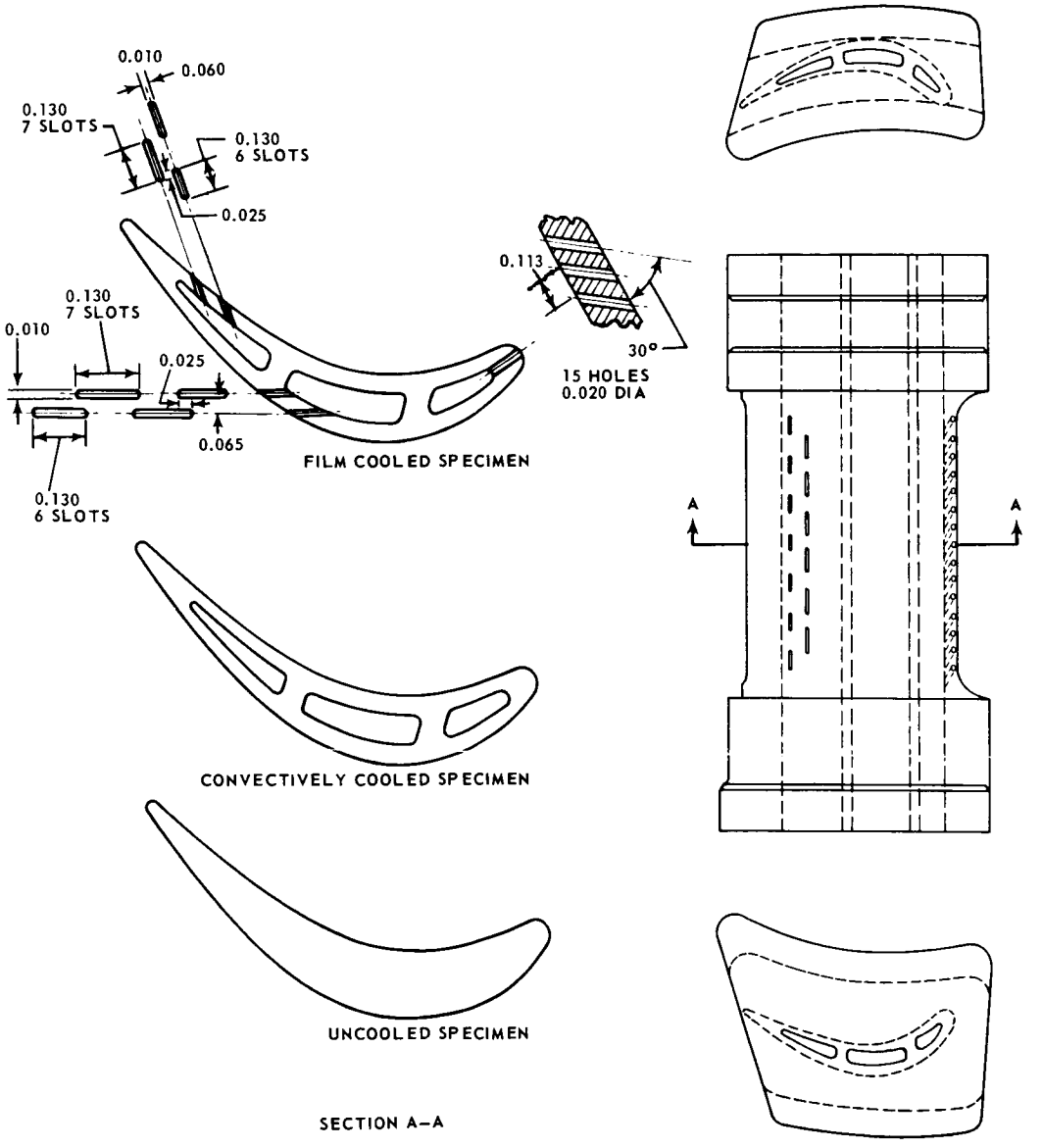


Figure 4 Simulated Turbine Blade Specimens

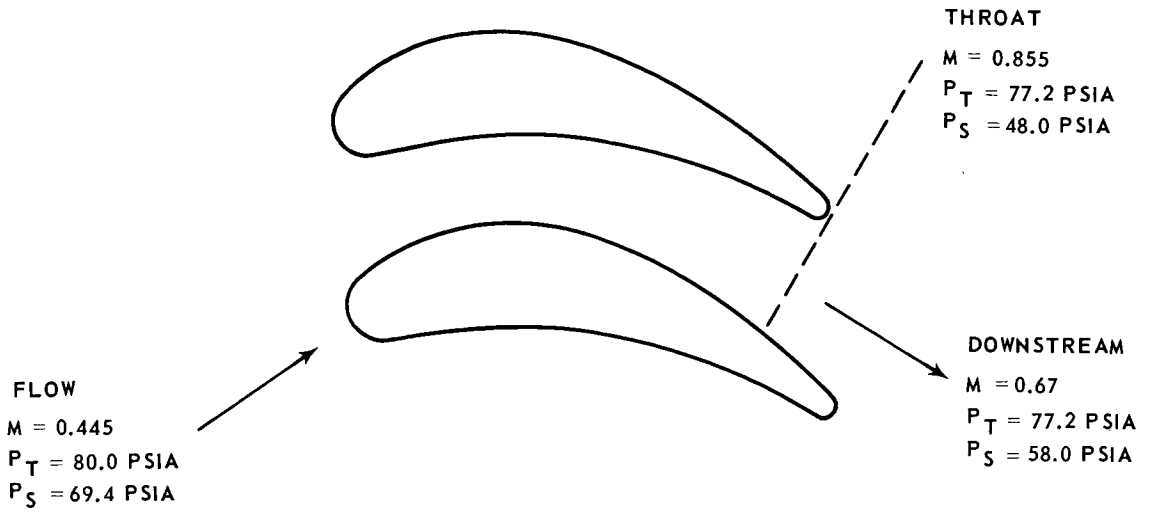


Figure 5 Cascade Design Operating Conditions

Lugs were provided on each end of the airfoil to permit tensile loading of the airfoil during test to simulate centrifugal forces in a turbine blade. These lugs were shaped to permit the upper lug to pass through the cascade duct of the test rig flow path liner. They fitted in openings in the top and bottom plates of the duct and were machined to very close tolerances to minimize gas leakage around them. A groove was machined in each side of the upper lug and a lip was provided on each side of the lower lug to engage the loading yokes. The lugs were machined relative to the airfoil section such that the line of action of the load passed through the airfoil section centroid. The lugs were designed for a stress rupture life at least four times as great as the stress rupture life of the airfoil.

The turbine blade specimens were precision cast in B-1900 (PWA 663) and IN-100 (PWA 658) materials, both of which are nickel base super alloys used for high temperature turbine blades. Internal passages for cooling air were cast through the airfoil and end lugs of the convectively cooled and film cooled specimens. These passages were identical for the two configurations. External surfaces of the airfoil and the end surfaces of the lugs adjacent to the airfoil were coated with a diffused aluminum-silica based slurry in accordance with Pratt and Whitney Aircraft Specification PWA 47-14L. Internal surfaces of the airfoil and the remaining external surfaces of the end lugs were uncoated. The leading edge holes and trailing edge staggered slots through the suction and pressure surfaces of the film cooled configuration were cut in the airfoils by electrical discharge machining (EDM) after coating. A sketch of the airfoils is presented in Figure 4.

Metering orifice plates were brazed to the end surfaces of the convectively cooled and film cooled specimens end lugs to control the division of cooling air between passages and between film and through flow. The design cooling air flow distributions are given in Table I.

TABLE I

COOLING AIR FLOW DISTRIBUTION

Primary air flow = 1.25 lbs/sec.
Cooling air inlet temperature = 700°F

| Description | Leading Edge Passage (lbs/sec) | Mid-Chord Passage (lbs/sec) | Trailing Edge Passage (lbs/sec) | Total (lbs/sec) |
|---|---|---|---|---|
| Film Cooled Specimen | | | | |
| Film Flow | 0.002 | 0.009 | 0.004 | 0.015 |
| Through Flow | 0.002 | 0.004 | 0.004 | 0.010 |
| Total Flow | 0.004 | 0.013 | 0.008 | 0.025 |
| Convectively Cooled Specimen | | | | |
| Total Flow | 0.004 | 0.007 | .005 | 0.016 |

Two specimens of each material and configuration were instrumented with chromel-alumel thermocouples at the airfoil mid-span to measure the transient and steady state metal temperatures. Uncooled and convectively cooled specimens were instrumented at six chordwise locations and film cooled specimens were instrumented at ten locations, as shown in Figure 6. The thermocouples were installed in spanwise grooves machined in the surface of the airfoil with the junction at the mid-span section. The lead wires were passed through holes in the lower lug, as shown in Figure 7. Two methods of attaching the thermocouples to the specimen were used. One method consisted of coating the surfaces of the grooves with Allen P-1 cement, laying bare 0.003 inch diameter chromel and alumel wires on the cement, spot welding the junctions to the airfoil surface at the ends of the grooves, and then filling the remainder of the

groove with Allen P-1 cement. The second method consisted of brazing 0.020 inch diameter Inconel-sheathed thermocouple wire in the grooves. In this case, the junction was formed by welding the end of the sheath and the ends of the chromel and alumel wires together. The junctions were located at the ends of the grooves flush with the airfoil surface and the entire thermocouple was brazed in place with Coast Metals 53 brazing alloy (82% nickel, 7% chromium, 2-3% boron, 3% iron, 3-5% silicon). Several gold-nickel-paladium alloys were tried but these attacked the sheath material. The mortality rate of the thermocouples during testing was high with both methods due to the development of open circuits and secondary junctions. The second method, however, proved somewhat superior for this application after a procedure was developed for installing the specimen in the loading yokes without bending the lead wires sharply and supporting the lead wires in areas where they were exposed to high velocity airflow to reduce vibrations. Figure 8 shows an instrumented specimen installed in the pull rod before installing the yoke end cover plates.

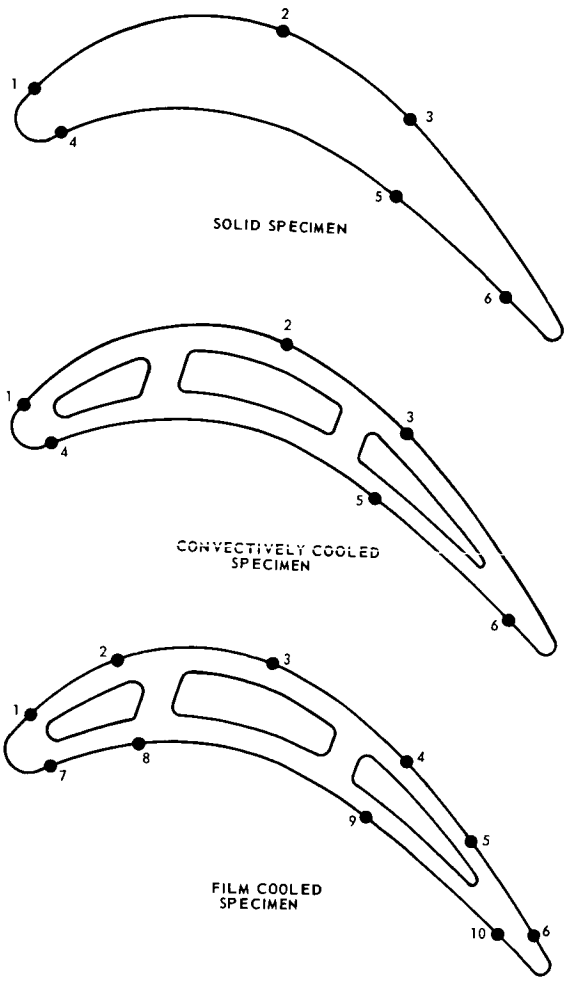


Figure 6 Blade Specimen Thermocouple Turbine Locations

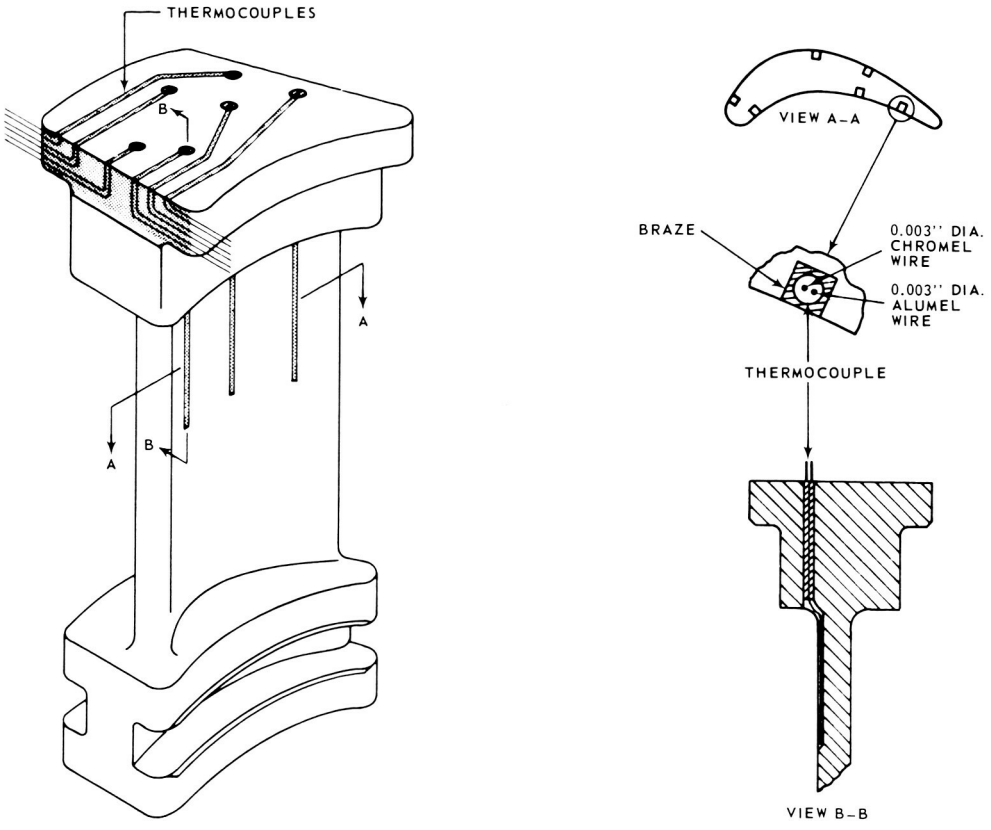


Figure 7 Thermocouple Installation On Specimen

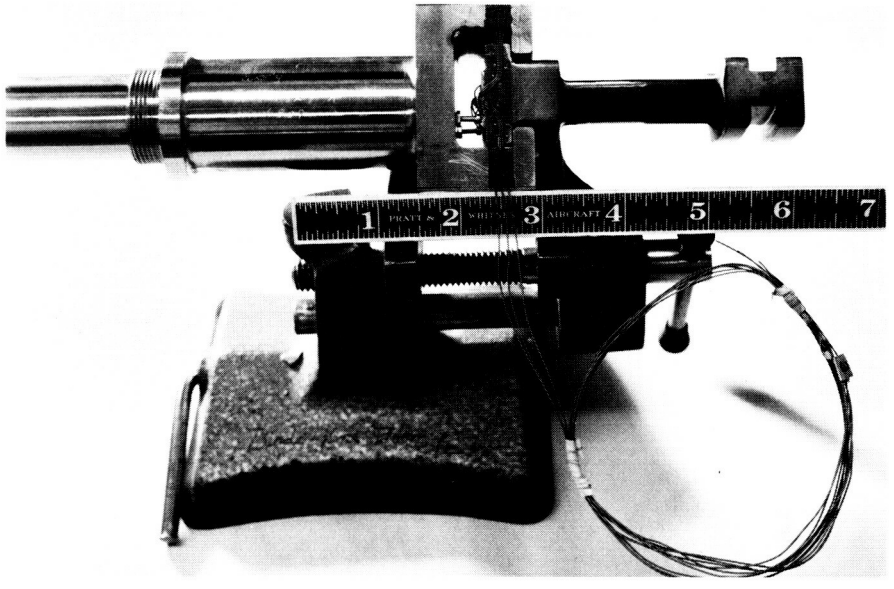

Figure 8 Instrumented Specimen Installed In Pull Rod (XP-69031)

## TEST FACILITY

The thermal-mechanical fatigue cascade rig, shown in Figure 9, was a new test facility designed and constructed for this program. It was a single specimen cascade rig designed to subject simulated turbine blade specimens to arbitrary thermal and mechanical cycles under environmental conditions simulating those experienced by a first-stage turbine blade in a high temperature aircraft gas turbine. Design conditions for this rig are shown in Table II. The rig consisted of a burner, a test chamber and a loading mechanism.

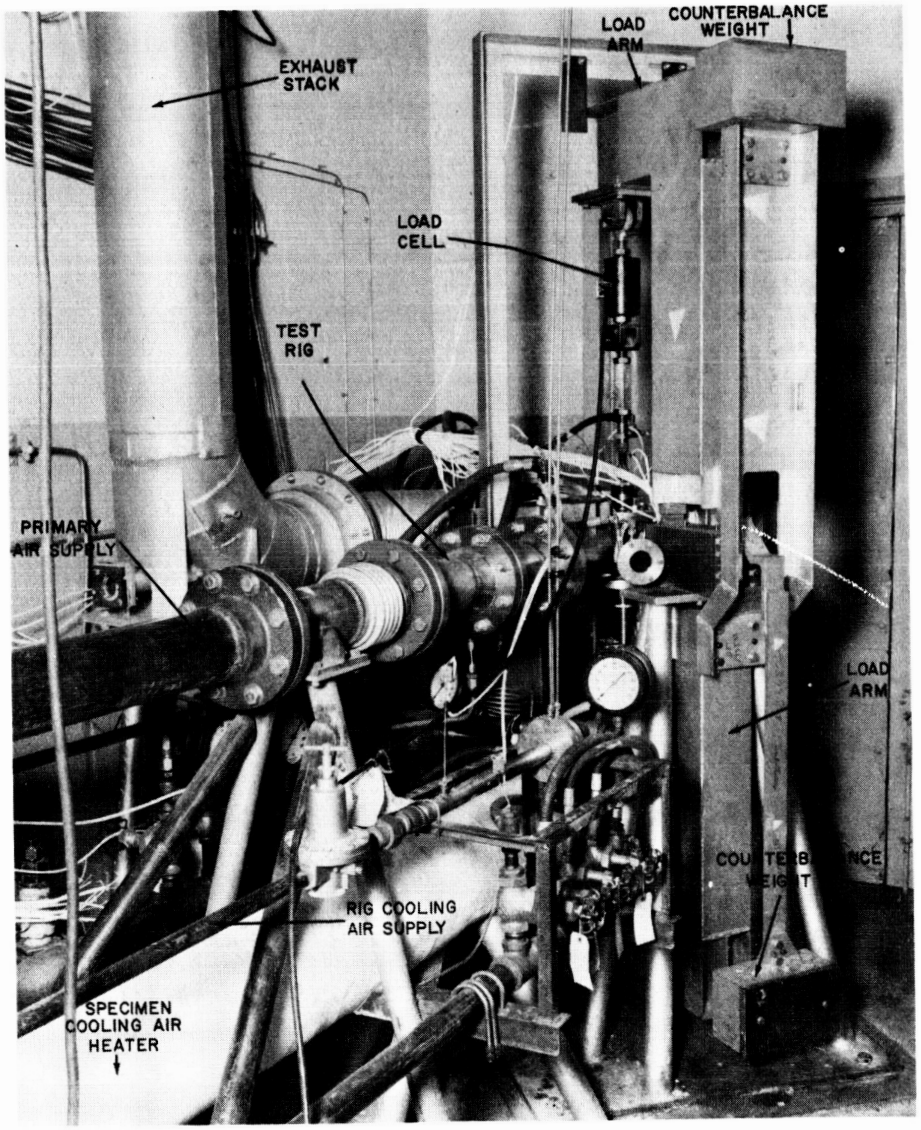


Figure 9 Thermal Mechanical Fatigue Cascade Rig (X-21890)

TABLE II

THERMAL-MECHANICAL FATIGUE CASCADE RIG
RATED DESIGN CONDITIONS

| | |
|---|---|
| **Primary Air** | |
| Flow Rate (lb/sec) | 1.25 |
| Temperature (°F, max.) | 2500 |
| Pressure (psig, max.) | 100 |
| **Specimen Cooling Air** | |
| Flow Rate (lb/sec) | 0.04 |
| Temperature (°F, max.) | 1200 |
| Pressure (psig, max.) | 120 |
| **Rig Cooling Air** | |
| Flow Rate (lb/sec) | 0.07 |
| Temperature (°F) | 200 |
| Pressure (psig, max.) | 120 |
| **Rig Cooling Water** | |
| Flow Rate (gal/min) | 12 |
| Temperature (°F, max.) | 100 |
| Pressure (psig) | 40 |
| **Specimen Loading Mechanism** | |
| Load (lb, max.) | 10,000 |
| **Fuel Supply** | |
| Type | JP-4 or JP-5 |
| Flow Rate (lb/hr, max) | 185 |

## Burner

The burner, shown in Figure 10, consists of an outer pressure case, a fuel nozzle assembly, and a burner can. The outer case was split and flanged immediately downstream of the fuel nozzle assembly to permit ease of maintenance. The fuel nozzle assembly consisted of a nozzle body supported by three

struts welded into the upstream section of the outer case. The fuel inlet passage was drilled through the center of one of the struts. A standard Delavan fuel nozzle with an integral strainer and a modified JT12 engine fuel nozzle swirler nut assembly were threaded to the nozzle body. The burner can was cantilevered from the swirler nut assembly at the upstream end and slipped into the transition duct in the test chamber at the downstream end. A split clamping ring, held together by a snap ring, attached the burner can to the swirler nut assembly. A spark plug igniter was threaded through the outer case and extended through a boss in the side of the burner can a short distance downstream of the fuel nozzle so that the end of the igniter was flush with the inside of the burner can.

Test Chamber

The test chamber, also shown in Figure 10, incorporated an outer pressure case, a flowpath liner, two specimen pull rods, and two liner side wall cooling air nozzles. The outer pressure case was cooled by water jackets on the inlet and exit sections and by copper coils brazed on the viewports and cascade housing. The case was split vertically and flanged in the cascade housing at a 45 degree angle to the inlet section to permit replacement of the flowpath liner.

The flowpath liner directed the primary gas flow from the burner past the test specimen and formed the cascade about the test specimen. The flowpath liner was made in two sections, a transition duct and a cascade duct. The transition duct was made of resistance-welded thoria-dispersed nickel (TD nickel) sheet metal assembly which made the transition from the circular flowpath cross section at the burner exit into the rectangular cross section at the cascade inlet. The duct was radiantly cooled by the water-jacketed inlet section of the outer case and shielded the specimen from excessive radiant heat loss to the cold walls of the outer case. The inlet end of the transition duct was riveted to a ring that snapped into a groove in the flange which mated to the burner section. Besides supporting and centering the inlet end of the transition duct, this ring also served as a diaphragm to prevent cold air from bypassing the burner. The exit end of the transition duct slipped into the inlet end of the cascade duct and the two sections were locked together by pins which passed through the top and bottom plates of the cascade duct and upstream of flanges on each side of the transition duct. A slip joint in the cylindrical section of the transition duct permitted unrestrained thermal expansion of the transition duct.

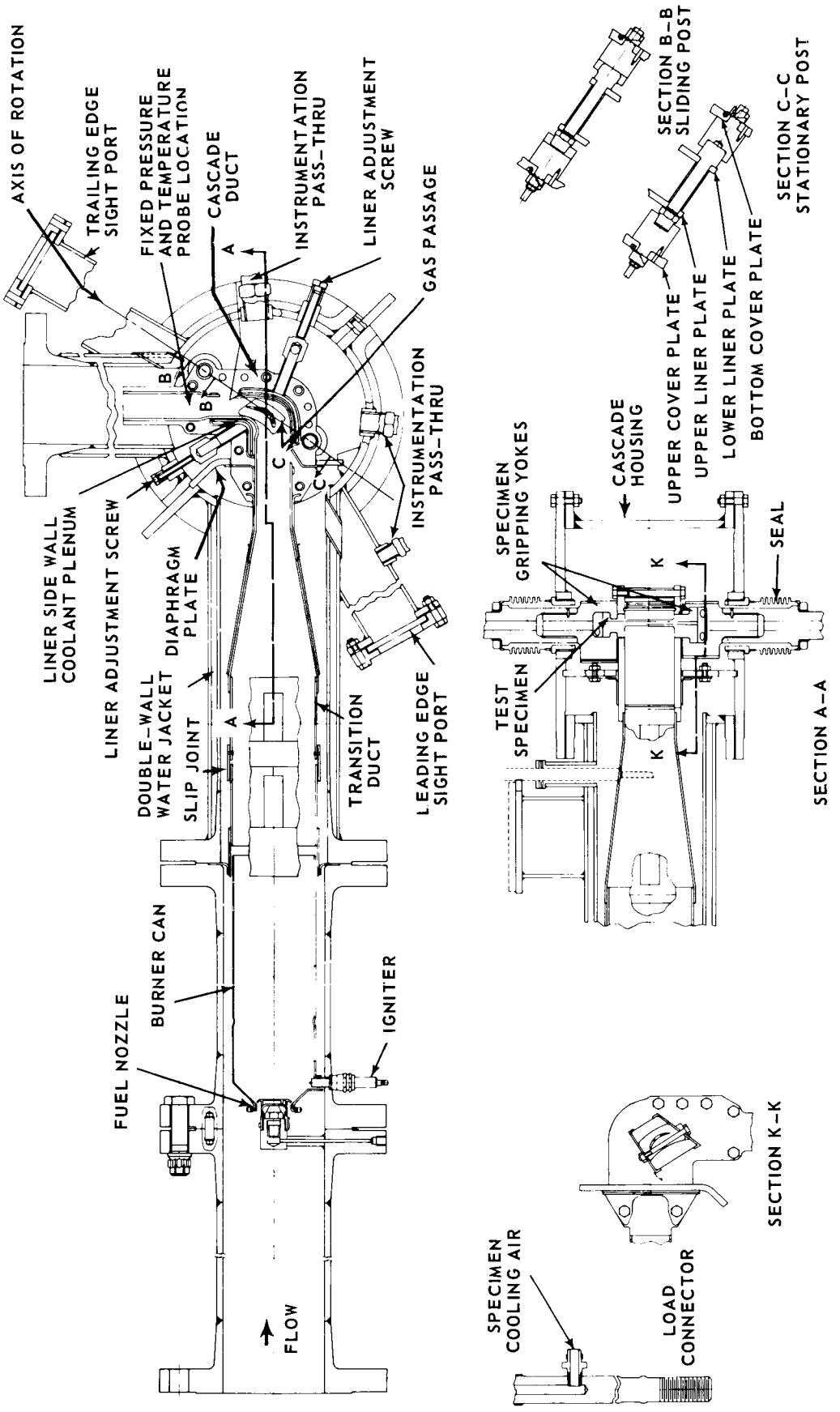


Figure 10 Thermal Mechanical Fatigue Cascade Rig Burner And Test Chamber

The cascade duct was a mechanical assembly of TD nickel consisting of a top and a bottom plate bolted together with spacers and sheet metal sides. These parts formed a wind tunnel about the test specimen which simulated the cascade channels formed by adjacent airfoils in an engine. The top and bottom plates were held apart by spacers around each bolt. The sheet metal sides fitted into grooves machined into the top and bottom plates and could expand freely as the gas temperature changed. Two of the tie bolts formed posts which were designed to locate the cascade duct with respect to the outer case and to transmit lateral reaction loads resulting from bowing of the specimen or misalignment between the loading mechanism and the cascade duct to the outer case. These posts were located in the plane of the minimum inertial axis of the airfoil section of the specimen. They engaged pedestals which bolted to the top and bottom covers of the cascade housing. The upstream post engaged close fitting holes in the pedestals and thereby was fixed in all lateral directions. The downstream post engaged slots in the pedestals which permitted movement along the axis through the two posts and restrained lateral movement in all other directions. The lower ends of these posts seated against the pedestals. The upper ends had sufficient clearance to permit vertical thermal growth.

The cascade duct was assembled in a rectangular hole in the diaphragm plate. The diaphragm plate served to minimize primary gas bypassing the specimen. The cascade was bolted to the diaphragm plate in a manner which minimized leakage across the plate. The edges of the diaphragm plate were fitted into grooves in the side walls and the top and bottom covers of the cascade housing.

Downstream of the diaphragm plate, the sides of the cascade duct were convectively cooled by air directed against them by the liner cooling nozzles. These nozzles were contoured to fit the side walls and were held in place by jack-screws which threaded through the outer case and provided additional structural support for the side walls.

The specimen was positioned in the cascade by openings in the top and bottom plates of the cascade duct. These openings were shaped to fit the contour of the lugs on the specimens closely, but allowed the smaller lug to pass through to permit replacement of the specimen.

The pull rods engaged the lugs at each end of the specimen and applied a tensile load to the specimen. These rods passed through bellow seals in the covers of the cascade housing and attached to the loading mechanism. Internal passages in the pull rods provided cooling air to the specimen. End covers bolted on the yoke-shaped end of the pull rods provided a seal between the pull rod and the end lugs of the test specimen and positioned the specimen relative to the pull rods. Approximately one inch outside of the bellows seals, the pull rods were necked down for about 1.5 inches and strain gaged to measure bending moments in the planes of the minimum and maximum inertial axes of the specimen airfoil section.

## Loading Mechanism

The loading mechanism consisted of a bearing block, two L-shaped load arms, a hydraulic cylinder, a load cell, and connecting linkage; as seen in Figure 11. The bearing block was supported by a steel framework mounted on a bed plate which was common with the test chamber support structure. Gusset plates tied the two support structures together at the upper ends to reduce relative movement between the loading mechanism and the test chamber. The bearing block was positioned relative to the test chamber such that the pivot axes of the load arms were in the vertical plane defined by the minimum inertial axis of the airfoil section of the specimen and at the same elevation as the axis of rotation of the ends of the blade specimen. The loading mechanism was designed to permit bowing of the specimen about the minimum inertial axis of the airfoil section with minimum restraint. The load arms pivoted about their bearing axes and maintained the direction of the applied load tangent to the line formed by the centroids of the airfoil at the ends of the airfoil. A mechanical load was applied to the specimen by the hydraulic cylinder located in the linkage between the lower load arm and specimen pull rod. The applied mechanical load was measured by a load cell which was installed in the linkage connecting the upper load arm to the specimen pull rod. Turnbuckles were provided in the upper and lower linkage to permit adjusting the length of the linkage and the vertical location of the specimen.

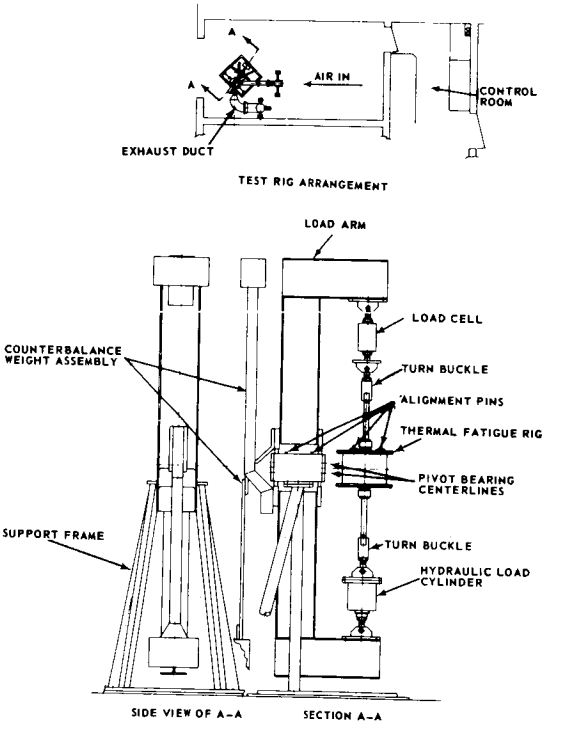


Figure 11 Thermal Mechanical Fatigue Cascade Rig Loading Mechanism

## Primary Air System

Primary air was supplied to the test rig from a shop air system at a nominal pressure of 100 psig. As shown in Figure 12, the primary air passed through a pressure regulating valve, a flow measuring orifice, a flow control valve and a preheater before entering the test rig. A water spray was used to cool the primary air at the exit of the test rig. The air then passed through a back pressure control valve and a silencer before exhausting to the atmosphere. The pressure regulating valve reduced the supply pressure to 95 psig and damped pressure fluctuations from the shop air system. The flow control and back pressure control valves were used to set the airflow and pressure conditions in the test rig at the maximum cycle temperature to 1.25 pounds per second and 65 psig static pressure at the cascade inlet. The settings of these valves remained fixed during temperature cycling and the airflow and back pressure were allowed to vary as a function of the primary air temperature. The preheater, which consisted of a two inch diameter burner installed in a section of four inch pipe, served to heat the primary air to 350-400°F before it entered the test rig. The water spray rate was adjusted to cool the primary air to 250 ±25°F after it exited from the test section of the rig at both the maximum and idle temperature conditions by using two groups of spray nozzles. One group was set to control the water spray rate at the idle temperature condition, while the other group supplemented the first at maximum temperature conditions and was turned on and off in phase with the fuel flow.

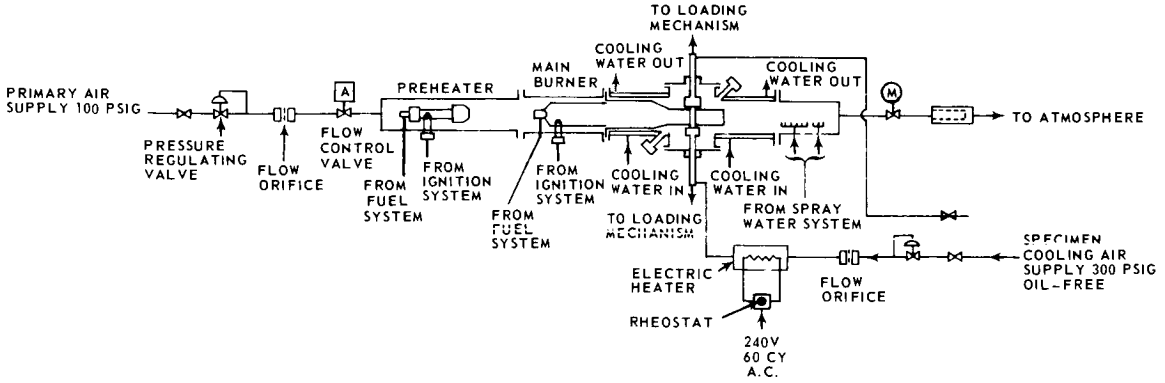


Figure 12 Primary And Specimen Cooling Air System Diagram

## Specimen Cooling Air System

Cooling air was supplied to the blade specimens from an oil-free 300 psig shop air system, as shown in Figure 12. The flow rate was controlled by setting the inlet pressure to the specimen using a pressure reducing valve. The flow was

measured by a sharp-edged orifice installed downstream of the pressure reducing valve. An electric heater with a variable voltage rheostat was provided to heat the cooling air to any required temperature up to 1200°F. After passing through the heater, the cooling air was supplied to the specimen through a short length of flexible tubing and the lower specimen pull rod. The chamber formed at the end of the specimen by the yoke and yoke end covers at the end of the pull rod distributed the air to the three spanwise cavities in the cooled specimens. After passing through the specimen the cooling air entered the chamber formed by the yoke and yoke end covers on the upper pull rod and was exhausted into the cascade housing through holes in the yoke end covers. Here, it mixed with the liner sidewall cooling air and the primary air and was then exhausted to the atmosphere. The end lugs of the uncooled specimens were cooled by unheated air which was supplied through both specimen pull rods and exhausted to the cascade housing through holes in the pull rod yoke covers. The lower pull rod was supplied in the normal manner, but the upper pull rod was supplied through a branch line which bypassed the pressure reducing valve, flow orifice, and heater as shown in Figure 12. Flow was controlled through this branch line by adjusting a manual valve to set approximately 100 psig inlet pressure to the pull rod.

Fuel System

The primary air preheater and the test rig burner were supplied from a common fuel header using independent fuel pumps, flow controls, and pressure controls as shown in Figure 13. Electric motor-driven gear pumps were used. The pump discharge pressure was controlled by recirculating fuel to the pump suction using the manual bypass valve between the pump discharge and suction lines. Fuel flow to the preheater was controlled by a manual control valve between the pump and the fuel nozzle. The preheater was operated at a constant fuel flow during the tests. The main burner fuel flow was controlled by a manual control valve and a pneumatically-operated control valve connected in parallel. The manual valve was used to set the primary air idle temperature at the cascade inlet. The pneumatically-operated valve was used to control the rate of temperature rise and the maximum and overshoot temperatures of the primary air at the cascade inlet by changing the fuel flow rate to the burner. This valve was automatically-operated by the cycle control system, as shown in Figures 14 and 15.

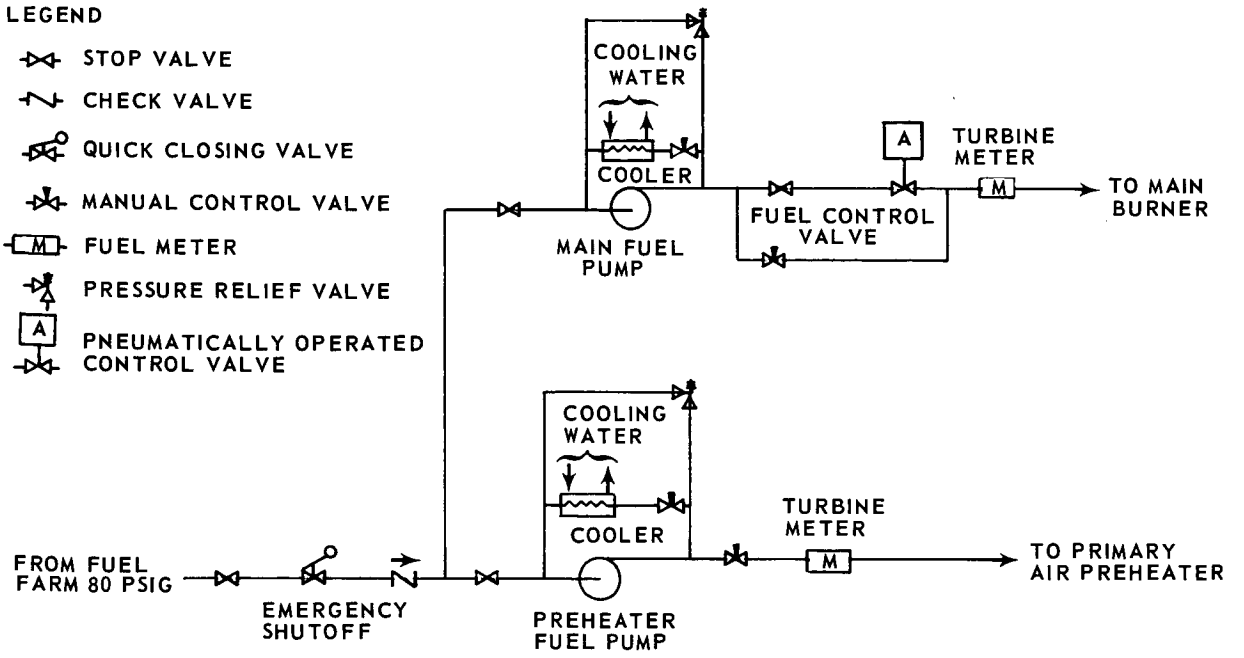


Figure 13 Fuel System Diagram

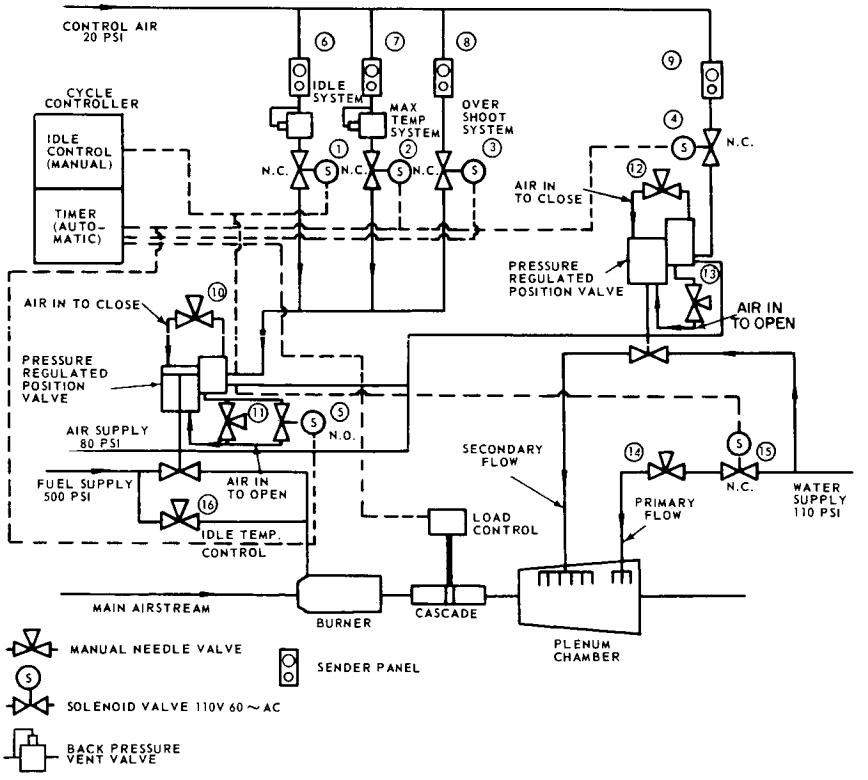


Figure 14 Fuel, Water Spray, and Load Cycling System Diagram

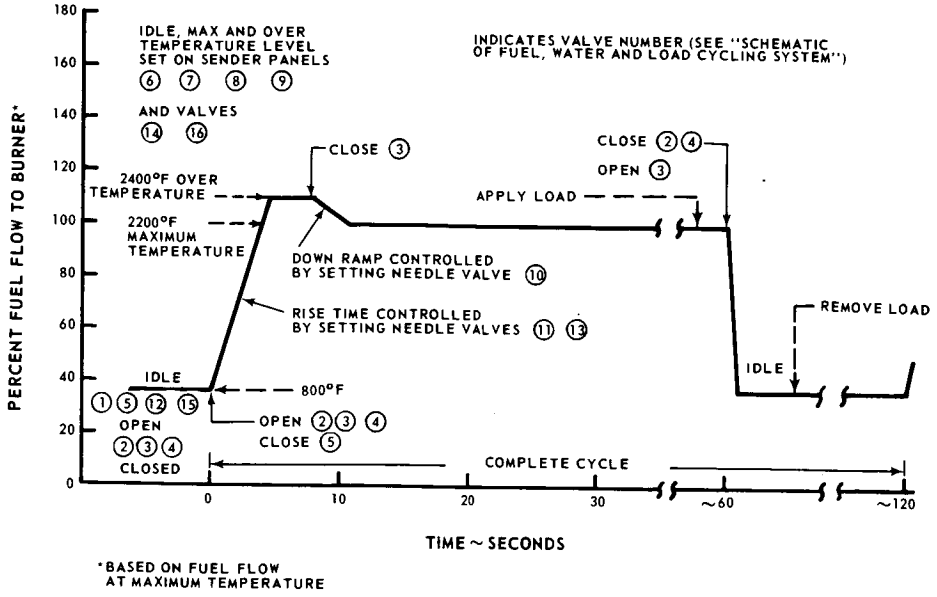


Figure 15 Typical Cycle Showing Fuel Flow and Load Application for a Four Second Rise to Maximum Temperature

## Hydraulic Load System

The mechanical load was applied to the test specimen by a hydraulic system which is shown schematically in Figure 16. This system included an integral pump and reservoir unit, a self-contained pilot actuated pressure regulator, a cycle control valve, and a hydraulic cylinder which was connected in the load mechanism linkage as previously described. The pressure regulator was adjusted manually to set the hydraulic pressure necessary to develop the required load on the specimen. Excess hydraulic fluid was recirculated to the reservoir. The cycle control valve consisted of a three-way solenoid-operated valve which connected and disconnected the hydraulic cylinder to the pressure regulator and vented the pressure side of the hydraulic cylinder to the reservoir when the load was off. The non-pressure side of the hydraulic cylinder was vented continuously to the reservoir. The cycle control valve was automatically-operated by the cycle control system.

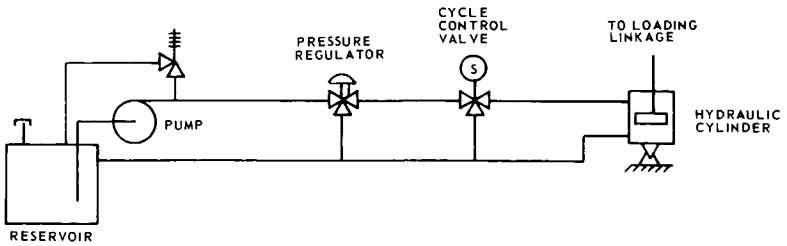


Figure 16 Hydraulic Load System Diagram

Instrumentation and Control System

The instrumentation and control system is shown schematically in Figure 17. Instrumentation was provided to:

- Measure the pressure, temperature, and flow rate of all specimen heating and cooling fluids,
- Measure the specimen metal surface temperature at mid-span,
- Measure the test rig metal temperature at several locations, and
- Measure the mechanical load and bending moments applied to the specimen.

The necessary variables were recorded during transient and steady state conditions on a punch tape recorder. Selected variables such as primary gas temperature, applied load, primary airflow, and pressures were recorded on strip charts to provide immediate visual records to aid in setting test conditions and in operating the test rig. Operation of the test rig was controlled by the cycle controller. Manual and automatic operating modes were provided. The programmer sequenced operation of the punch tape recorder, cable selector and transient and steady state scanners to record the test data in phase with the primary gas temperature cycle. Transient data was recorded at a nominal rate of ten points per second. The variables to be recorded during the transient portion of the cycle were arranged in cables containing groups of ten variables each. The cable selector was designed to sequence automatically from one cable to the next in a predetermined order on consecutive gas temperature cycles. The cable selector also had provisions to continuously monitor any selected cable. The transient scanner connected the data points in the selected cable to the punch tape recorder one at a time in a predetermined order. Steady state data was recorded at a nominal rate of four points per second through the steady-state scanner. Up to fifty steady-state data points could be recorded.

All temperatures were measured using chromel-alumel thermocouples, except for the primary gas temperature which was measured using a platinum-platinum/10% rhodium aspirated probe. This probe could be traversed across the gas stream in the spanwise direction of the specimen to measure the primary gas temperature profile entering the cascade. All chromel-alumel thermocouples were read on a Brown temperature indicator through a Lewis selector switch. The platinum-platinum/rhodium thermocouple was read on a separate Brown indicator through a Lewis selector switch and on a Honeywell strip chart recorder.

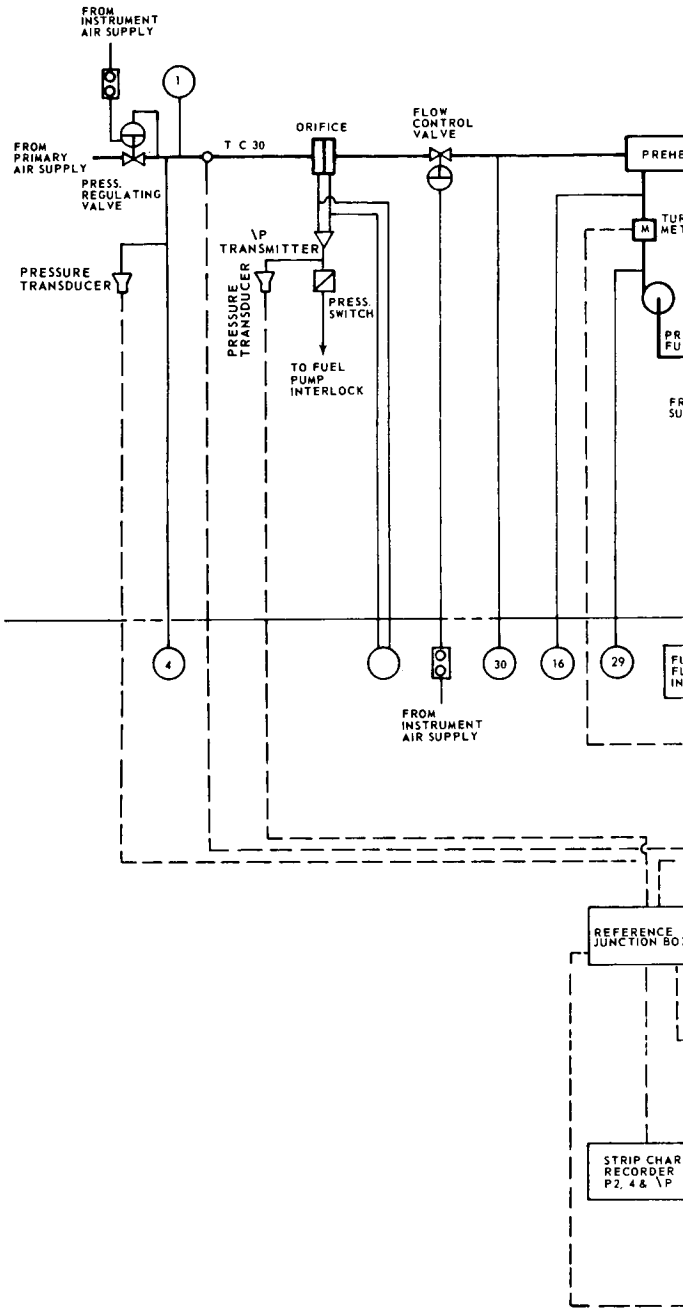
FROM INSTRUMENT AIR SUPPLY
1
FROM PRIMARY AIR SUPPLY
PRESS. REGULATING VALVE
T C 30
ORIFICE
FLOW CONTROL VALVE
PREHE
TUR
MET
M
ΔP TRANSMITTER
PRESSURE TRANSDUCER
PRESS. SWITCH
TO FUEL PUMP INTERLOCK
PRESSURE TRANSDUCER
PR
FU
FR
SU
4
30
16
29
FU
FL
IN
FROM INSTRUMENT AIR SUPPLY
REFERENCE JUNCTION BO
STRIP CHAR
RECORDER
P2, 4 & ΔP

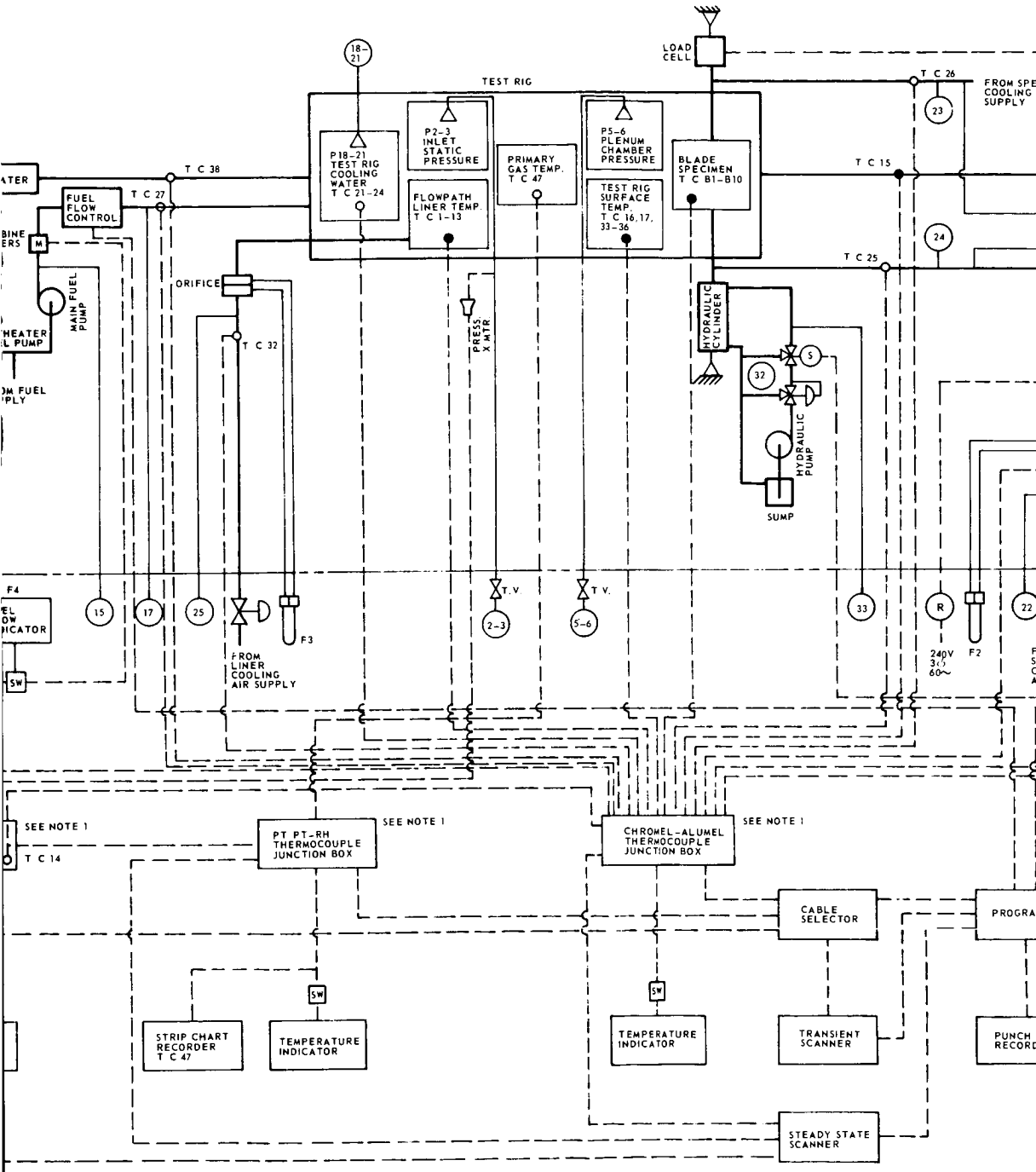
LOAD CELL
TEST RIG
18–21
P18–21 TEST RIG COOLING WATER T C 21–24
P2–3 INLET STATIC PRESSURE
FLOWPATH LINER TEMP. T C 1–13
PRIMARY GAS TEMP. T C 47
P5–6 PLENUM CHAMBER PRESSURE
TEST RIG SURFACE TEMP. T C 16, 17, 33–36
BLADE SPECIMEN T C B1–B10
T C 26
FROM SPE COOLING SUPPLY
T C 15
T C 25
T C 38
T C 27
FUEL FLOW CONTROL
MAIN FUEL PUMP
ORIFICE
T C 32
PRESS X MTR
HYDRAULIC CYLINDER
HYDRAULIC PUMP
SUMP
T.V. 2–3
T.V. 5–6
FROM LINER COOLING AIR SUPPLY
F3
F2
240V 3∅ 60~
SEE NOTE 1
T C 14
PT. PT–RH THERMOCOUPLE JUNCTION BOX
CHROMEL–ALUMEL THERMOCOUPLE JUNCTION BOX
CABLE SELECTOR
STRIP CHART RECORDER T C 47
TEMPERATURE INDICATOR
TRANSIENT SCANNER
STEADY STATE SCANNER

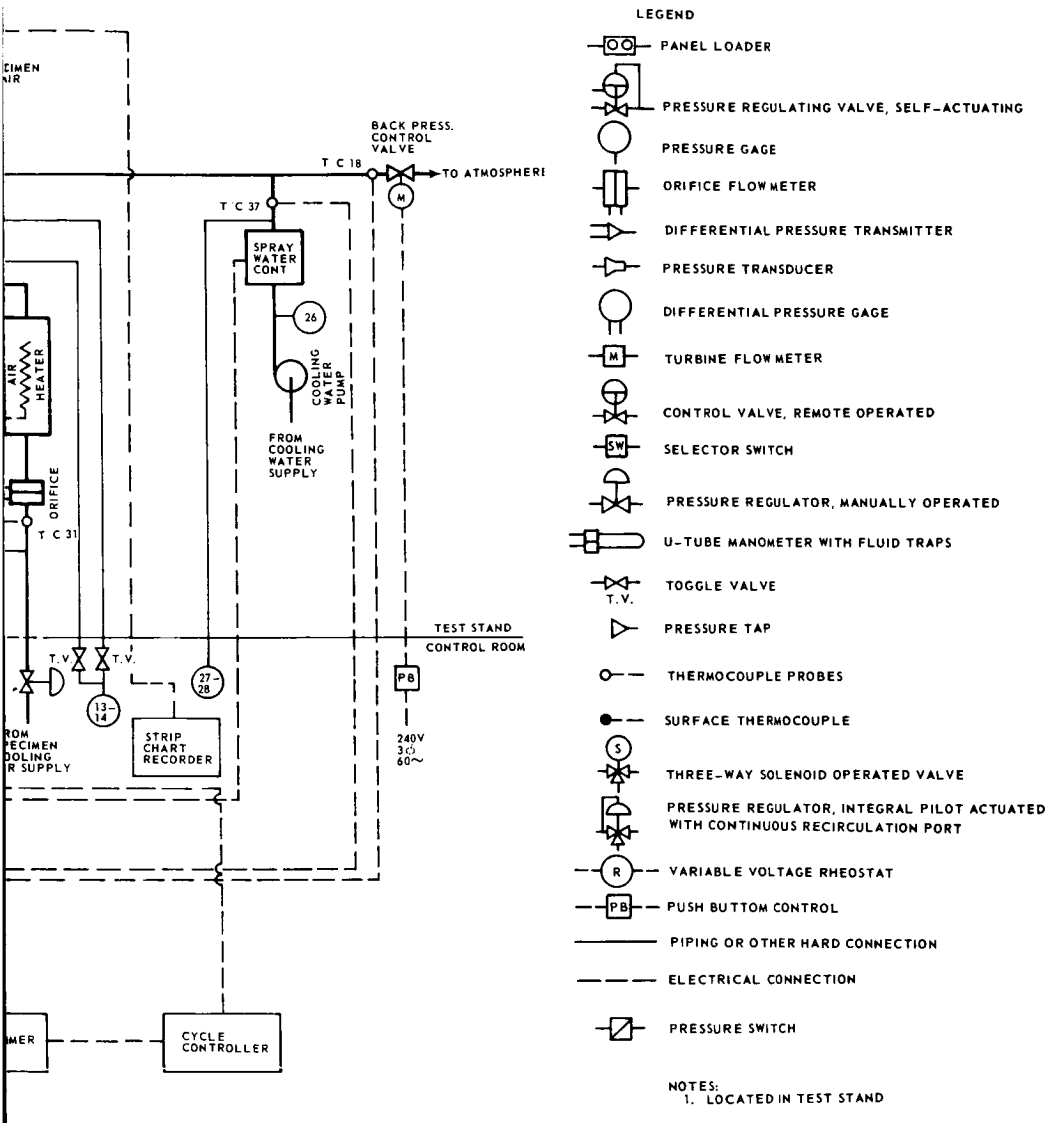


Figure 17 Instrumentation and Control System Diagram

T/C

1
2
3
4
5
6
7
8
9
10
11
12
13
14
15
16
17
18
19
20
21
22
23
24
25
26
27
28
29
30
31
32
33
34
35
36
37
38
39
47
48
B1

## Thermocouple List

| No. | Function |
|---|---|
| | Transition duct sidewall |
| | Transition duct sidewall |
| | Cascade duct bottom cover upstream of specimen |
| | Cascade duct top cover upstream of specimen |
| | Cascade duct bottom cover downstream of specimen |
| | Cascade duct top cover downstream of specimen |
| | Cascade duct ID sidewall - leading edge |
| | Cascade duct ID sidewall - mid-chord |
| | Cascade duct ID sidewall - trailing edge |
| | Cascade duct OD sidewall - leading edge |
| | Cascade duct OD sidewall - 1/3 chord |
| | Cascade duct OD sidewall - 2/3 chord |
| | Cascade duct OD sidewall - trailing edge |
| | Reference junction box |
| | Exhaust stack surface-upstream of water spray |
| | Test rig top cover surface |
| | Test rig bottom cover surface |
| | Exhaust gas |
| | Test rig jacket cooling water inlet |
| | Test rig gas temperature probe boss surface |
| | Test rig inlet section jacket water out |
| | Test rig exhaust section jacket water out |
| | Test rig upstream viewport cooling water out |
| | Test rig downstream viewport cooling water out |
| | Specimen cooling air in-bottom |
| | Specimen cooling air in-top |
| | Main fuel |
| | Spare |
| | Spare |
| | Primary air supply |
| | Specimen cooling air supply |
| | Liner cooling air supply |
| | Test rig inlet section water jacket surface |
| | Test rig exhaust section water jacket surface |
| | Test rig knuckle section surface - inlet |
| | Test rig knuckle section surface - exhaust |
| | Spray water inlet |
| | Preheater exhaust |
| - 46 | Spares |
| | Primary gas - cascade inlet |
| | Spare |
| - B10 | Specimen airfoil metal - mid-span |

| No. |
|---|
| 1 |
| 2 |
| 3 |
| 4 |
| 5 |
| 6 |
| 7 - 12 |
| 13 |
| 14 |
| 15 |
| 16 |
| 17 |
| 18 |
| 19 |
| 20 |
| 21 |
| 22 |
| 23 |
| 24 |
| 25 |
| 26 |
| 27 |
| 28 |
| 29 |
| 30 |
| 31 |
| 32 |
| 33 |
| 34 |

| No. |
|---|
| F 1 |
| F 2 |
| F 3 |
| F 4 |

## Pressure Gage List

| Function |
|---|
| Primary air supply pressure |
| Cascade inlet static pressure |
| Cascade inlet static pressure |
| Primary air supply pressure |
| Plenum chamber static pressure upstream of diaphragm |
| Plenum chamber static pressure downstream of diaphragm |
| Spares |
| Specimen cooling air inlet pressure - bottom (remote) |
| Specimen cooling air inlet pressure - top (remote) |
| Main fuel pump discharge pressure |
| Preheater fuel nozzle pressure |
| Main burner fuel nozzle pressure |
| Test rig inlet section jacket cooling water discharge pressure |
| Test rig exhaust section jacket cooling water discharge pressure |
| Test rig upstream viewport jacket cooling water discharge pressure |
| Test rig downstream viewport jacket cooling water discharge pressure |
| Specimen cooling air supply pressure |
| Specimen cooling air inlet pressure - top (local) |
| Specimen cooling air inlet pressure - bottom (local) |
| Liner cooling air supply pressure |
| Cooling water pump discharge pressure |
| Idle temperature spray water nozzle pressure |
| Maximum temperature spray water nozzle pressure |
| Preheater fuel pump discharge pressure |
| Preheater inlet air pressure |
| Exhaust stack jacket cooling water inlet pressure (not shown) |
| Hydraulic pump discharge pressure |
| Hydraulic cylinder pressure |
| Exhaust stack jacket cooling water outlet pressure (not shown) |

## Flow Indicator List

| Function |
|---|
| Primary air flow |
| Specimen cooling air flow |
| Liner cooling air flow |
| Fuel flow |

Bourdon tube type gages were used to indicate pressures. Those pressures used to establish the test conditions (i.e., primary air supply pressure and inlet static pressure) were measured on ten inch Heise gages for greater accuracy. Provisions were also made to record these pressures on a Bristol strip chart recorder by using pressure transducers to convert the pressure to electrical signals.

Airflows were measured using VDI orifice meters. A differential pressure gage was used to measure the pressure drop across the orifice in the primary air line. Mercury filled U-tube manometers were used to measure the pressure drop across the orifices in the liner and specimen cooling air lines. Fuel flows to the main and preheater burners were measured using Cox turbine flow meters.

The mechanical load applied to the specimen was measured with a 10,000-pound capacity Baldwin-Lima-Hamilton load cell which was read and recorded on a Bristol strip chart recorder. Bending moments applied to the ends of the specimens were measured as described later.

## TEMPERATURE SYNTHESIS

The temperature distributions in the simulated turbine blade specimens were calculated using the analytical method described in Appendix A. A design temperature distribution was calculated for each configuration and material for assumed gas temperature cycles and boundary conditions during design of the turbine blade specimens. Heat transfer coefficients for these design temperature distribution calculations were calculated for the coolant and gas side surfaces as described in Appendix A.

The mid-span airfoil surface metal temperature at several chordwise locations, the gas stream temperature, and the coolant temperature were measured during transient and steady state portions of the test cycle during instrumented specimen tests. The measured gas temperature cycles were significantly different from the assumed temperature cycles used for specimen design, as shown in Figures 18 through 21. The measured gas temperature cycles were substituted for the assumed temperature cycles and corrected metal temperature distributions were calculated using the same heat transfer coefficients used for the design calculations. The corrected metal temperature cycles were compared with the measured metal temperatures at the thermocouple locations. The measured metal temperatures differed significantly from the calculated temperatures. These differences were most pronounced in the trailing edge region of the airfoil and were attributed to high radiation losses, principally to the cooling water spray in the exhaust duct.

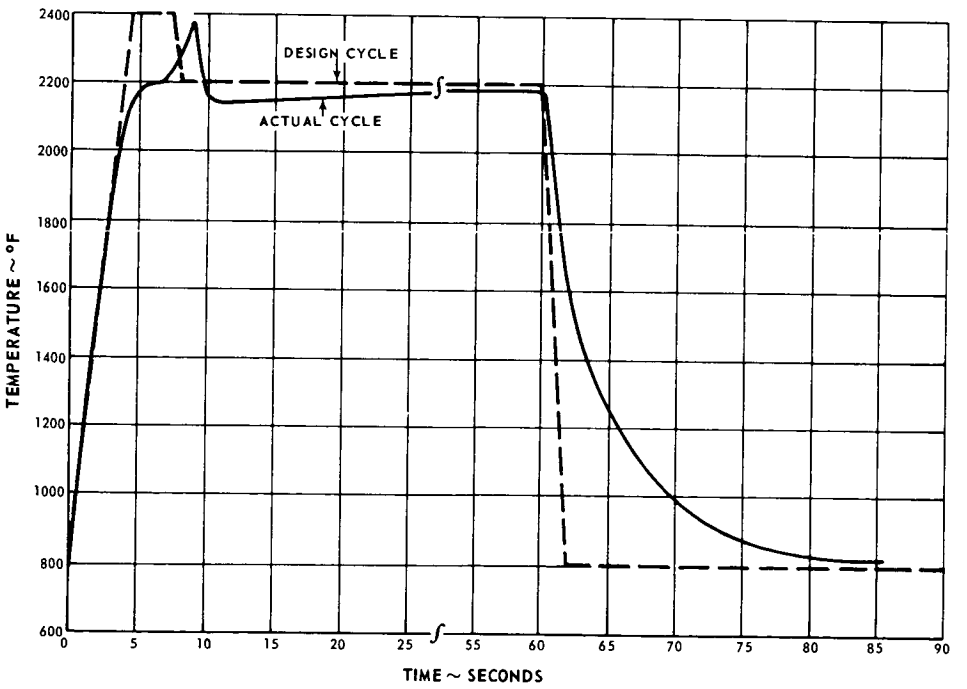


Figure 18 Comparison of Design and Actual Gas Temperature Cycles for Convectively Cooled and Film Cooled Specimens, Fast Acceleration Cycle

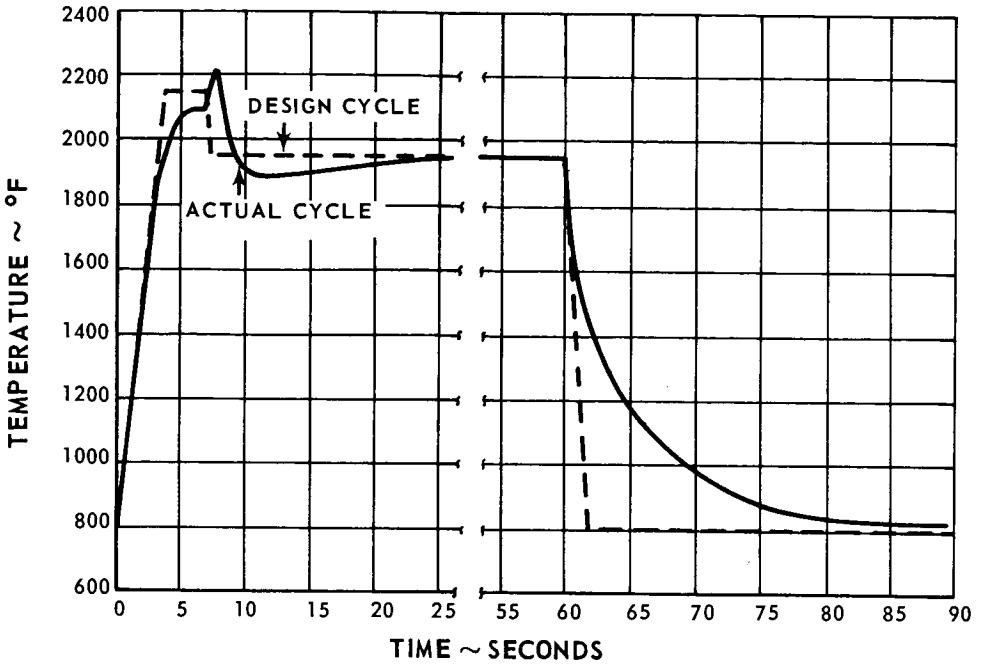


Figure 19 Comparison of Design and Actual Gas Temperature Cycles for Uncooled Solid Specimens, Fast Acceleration Cycle

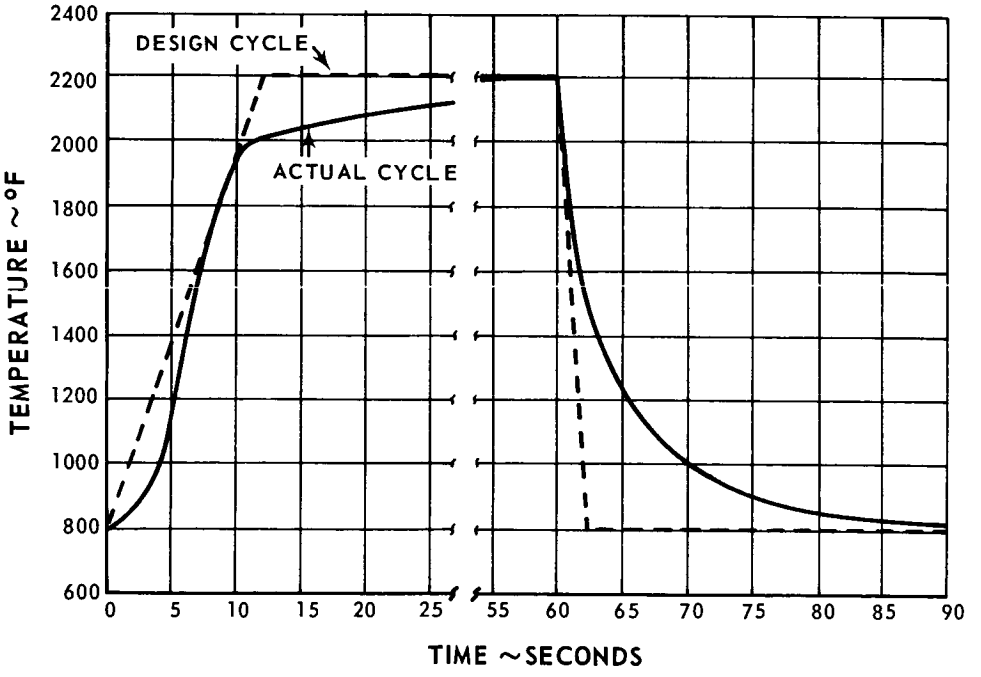


Figure 20 Comparison of Design and Actual Gas Temperature Cycles for Convectively Cooled and Film Cooled Specimens, Slow Acceleration Cycle

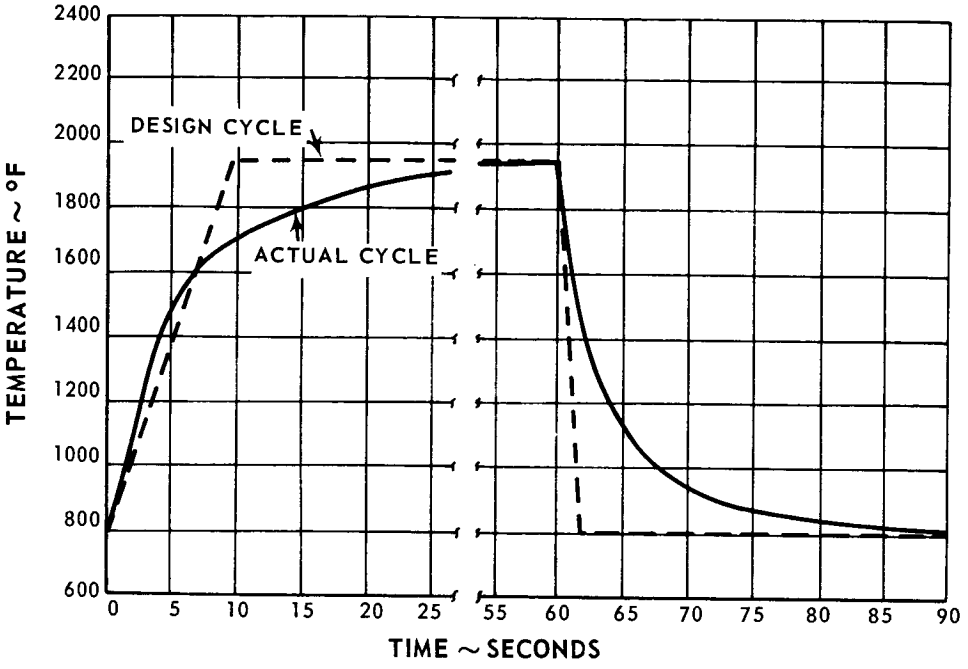


Figure 21 Comparison of Design and Actual Gas Temperature Cycles for Uncooled Solid Specimens, Slow Acceleration Cycle

To simulate the actual temperature distribution in the airfoil more closely, the boundary conditions were modified to produce closer agreement between the measured and calculated specimen metal temperatures at the thermocouple locations. The resulting temperature distributions calculated throughout the airfoil cross sections were used in the stress-strain analyses.

Temperature syntheses on the convectively cooled specimens were completed for the fast acceleration temperature cycle. Syntheses on the uncooled solid specimens were started for both the slow and fast acceleration temperature cycles and on the convectively cooled specimens for the slow acceleration temperature cycle. Final iterations to obtain closer agreement between measured and synthesized temperatures were not completed due to an uncertainty as to which temperature cycles were going to be used for the fatigue tests after the initial tests of the convectively cooled specimens. Measured and synthesized temperatures for the convectively cooled and uncooled specimens are shown in Figures 22 through 26. Measured temperatures for the film cooled specimens are shown in Figures 27 through 29. Actual temperatures at thermocouple locations which are not shown in Figures 22 through 29 were deduced from data measured at these locations for different gas temperature cycles or on different specimens relative to data measured at adjacent thermocouple locations. These additional data are too voluminous to be included herein.

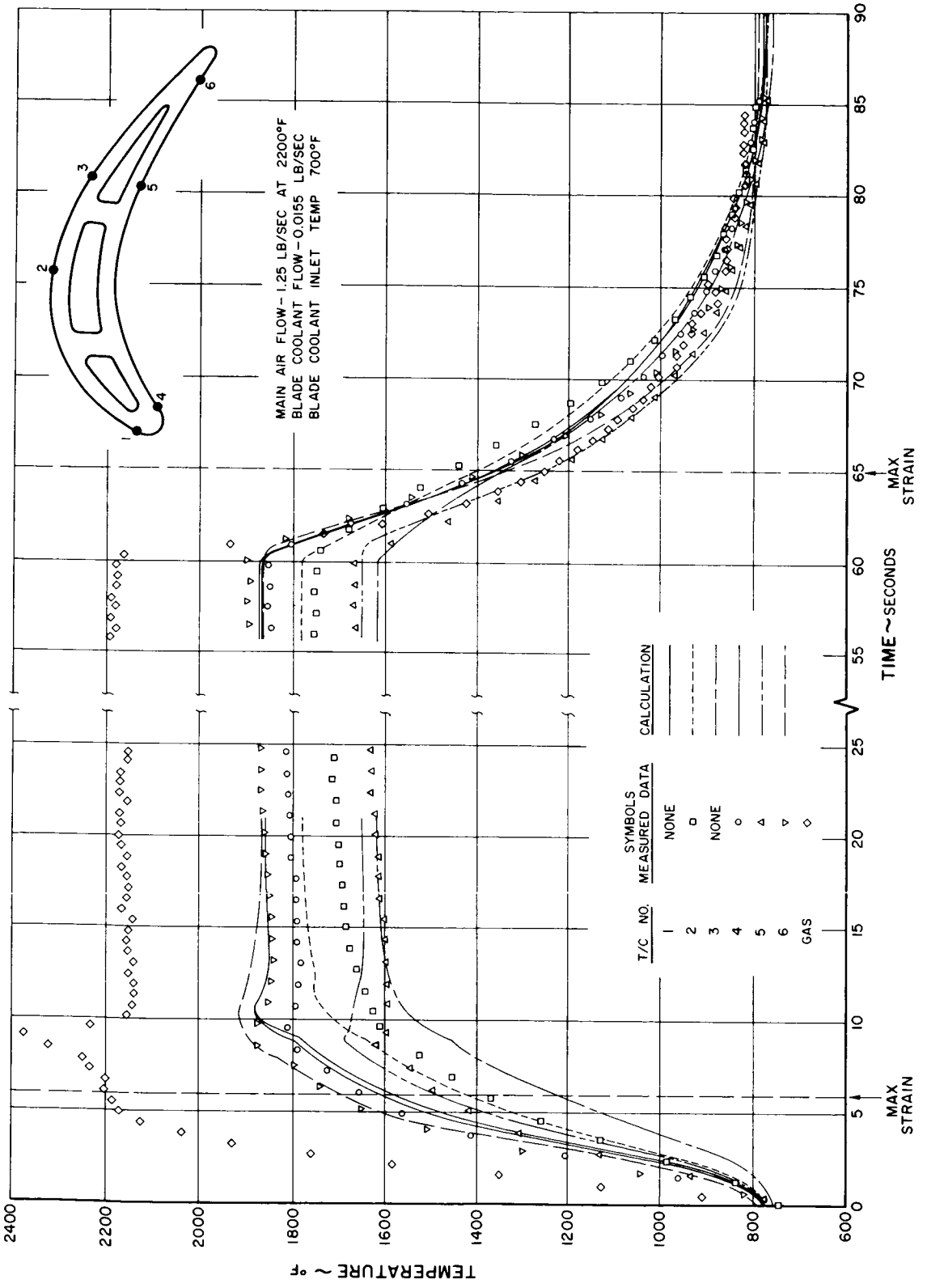


Figure 22 Measured and Calculated Temperatures for PWA 663 Convectively Cooled Specimen, Fast Acceleration Cycle

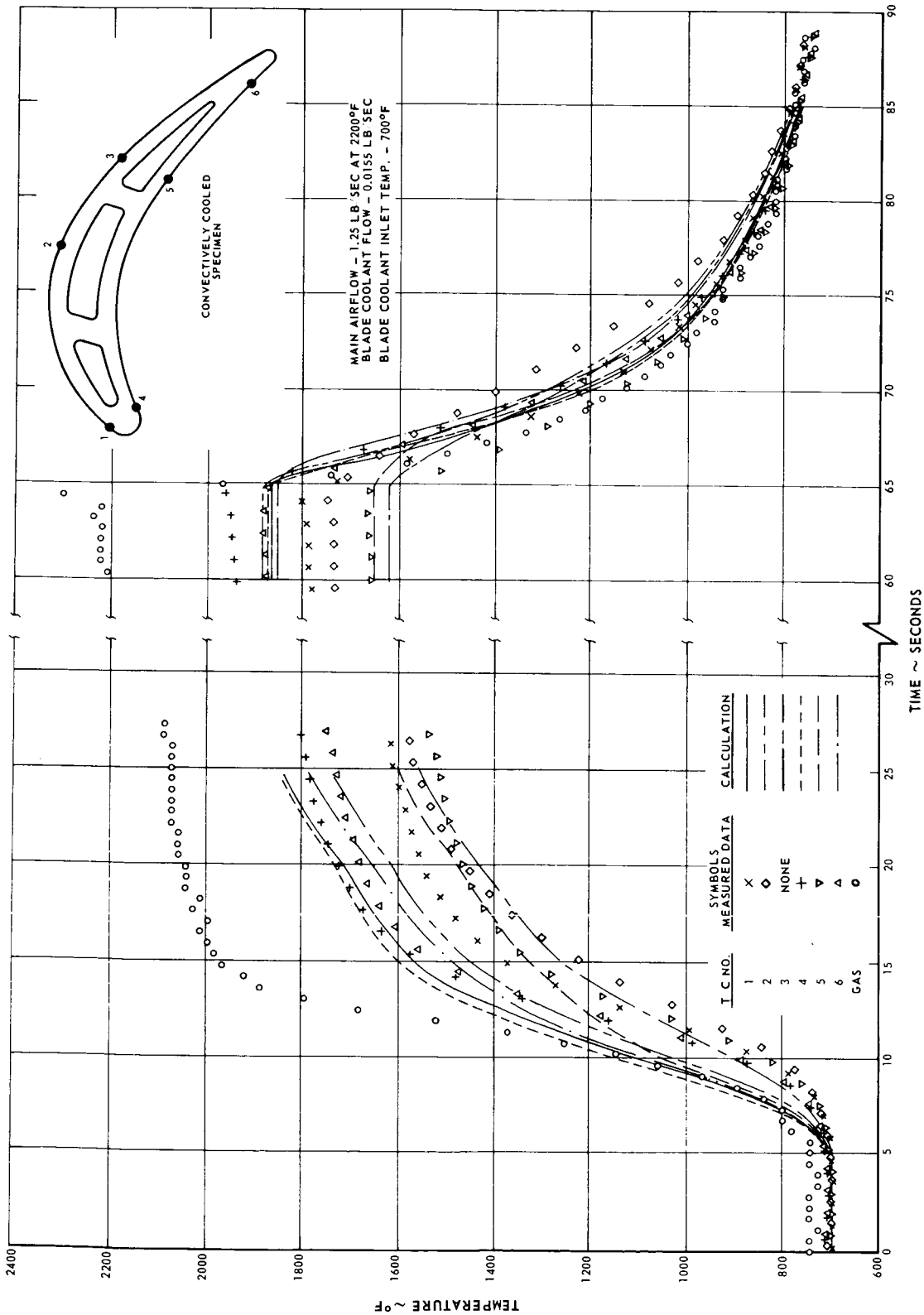


Figure 23 Measured and Calculated Temperatures for PWA 663 Convectively Cooled Specimen, Slow Acceleration Cycle

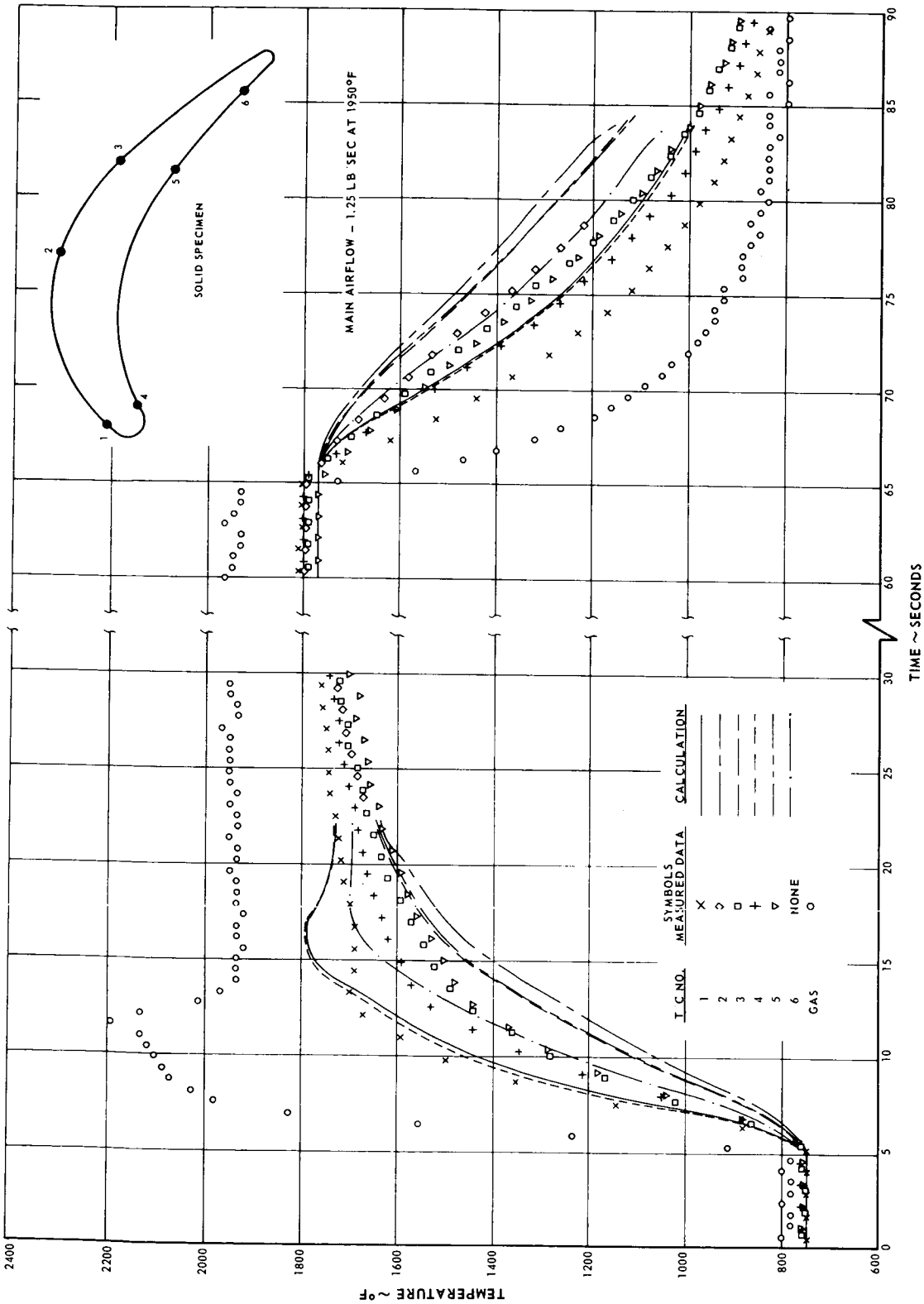


Figure 24 Measured and Calculated Temperatures for PWA 663 Uncooled Solid Specimen, Fast Acceleration Cycle

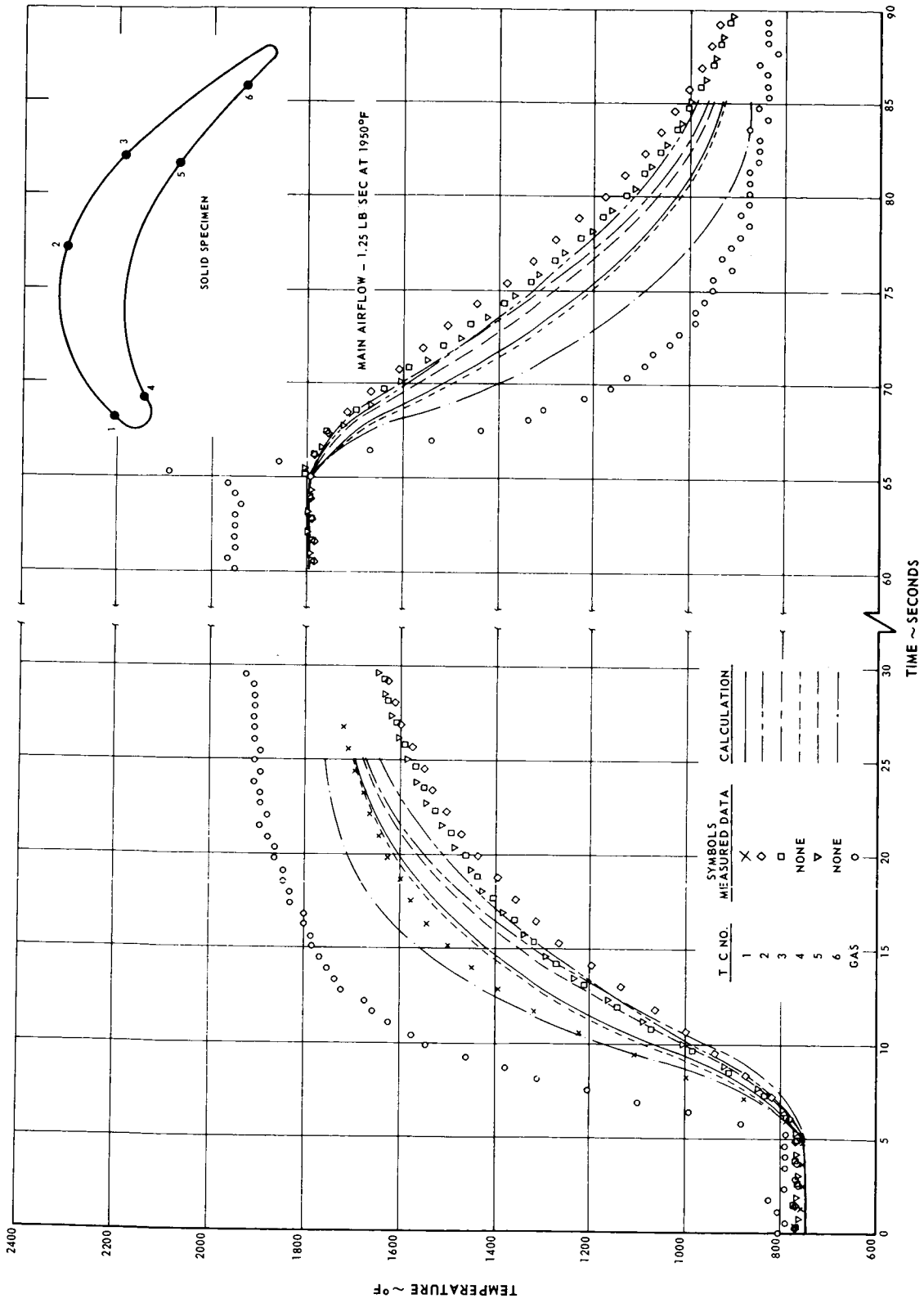


Figure 25 Measured and Calculated Temperatures for PWA 663 Uncooled Solid Specimen, Slow Acceleration Cycle

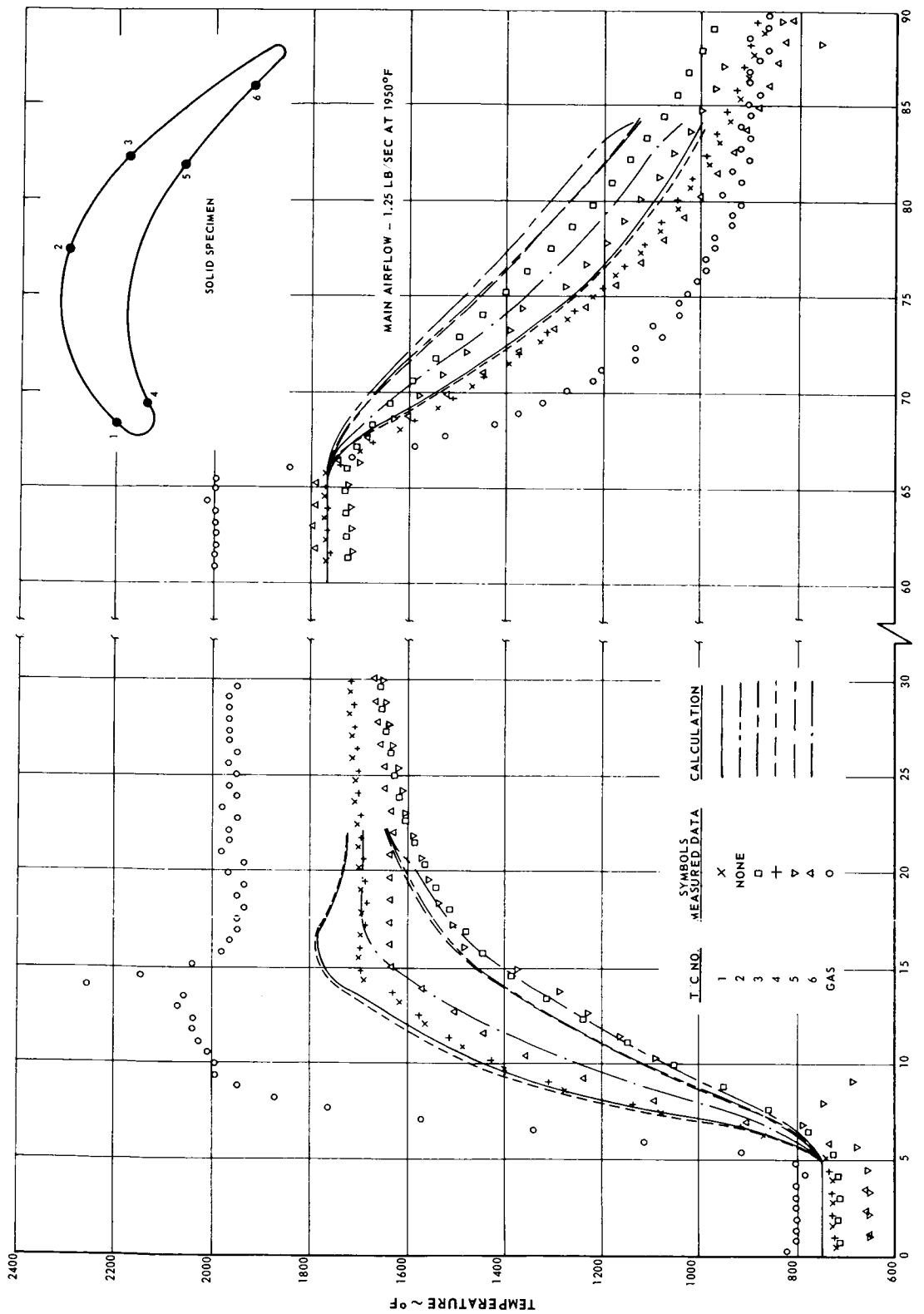


Figure 26 Measured and Calculated Temperatures for PWA 658 Uncooled Solid Specimen, Fast Acceleration Cycle

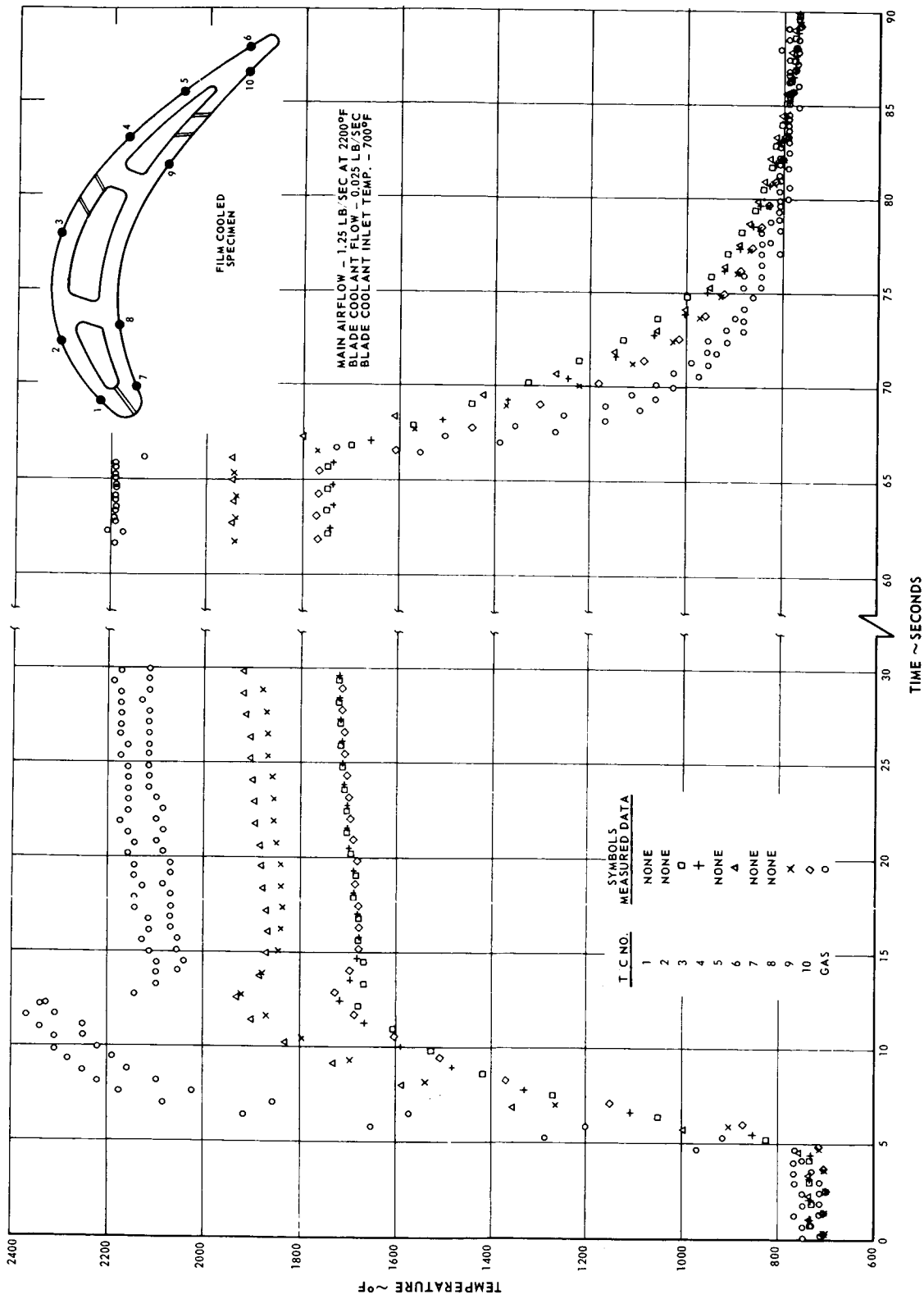


Figure 27 Measured Temperatures for PWA 663 Film Cooled Specimen, Fast Acceleration Cycle

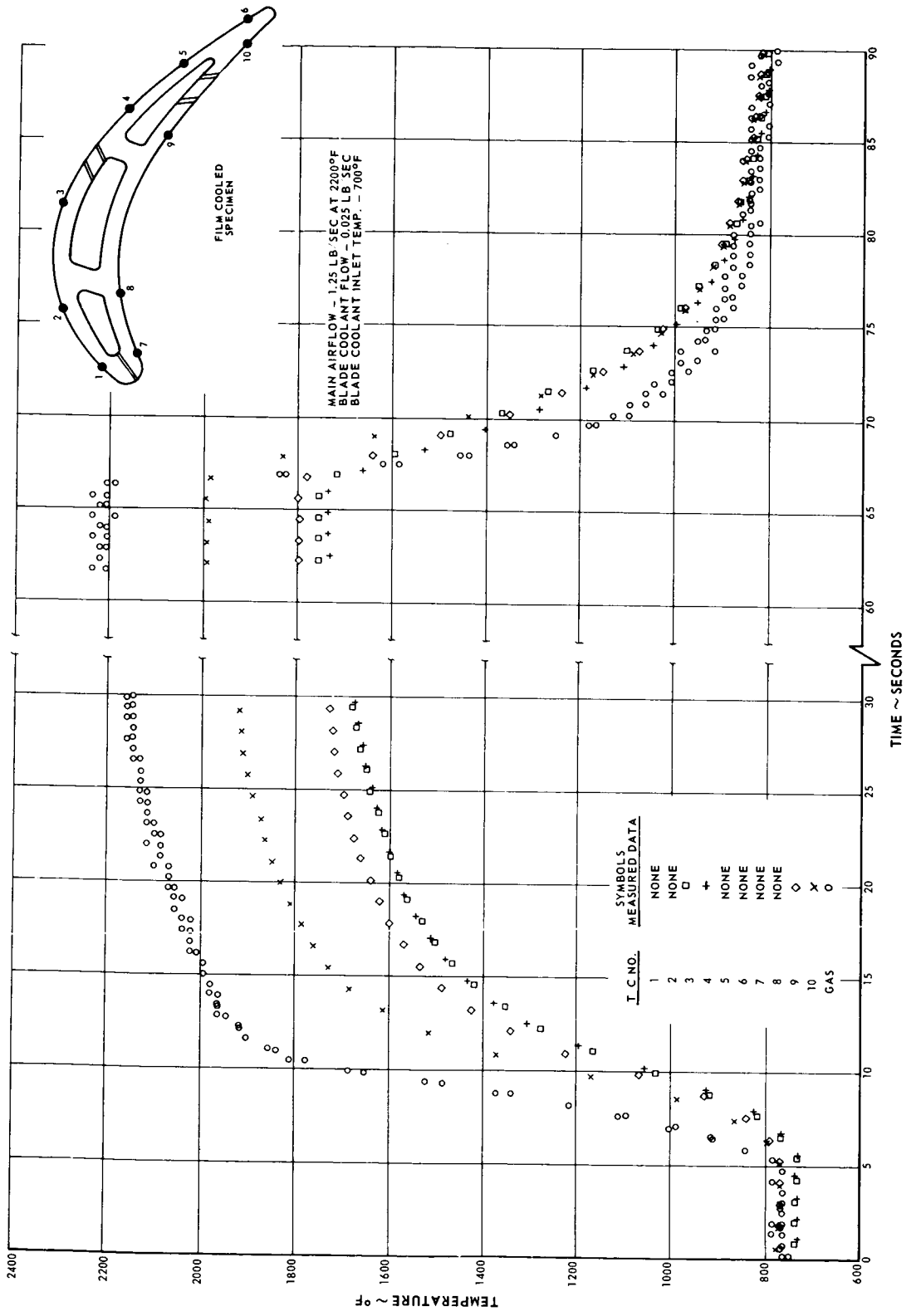


Figure 28 Measured Temperatures for PWA 663 Film Cooled Specimen, Slow Acceleration Cycle

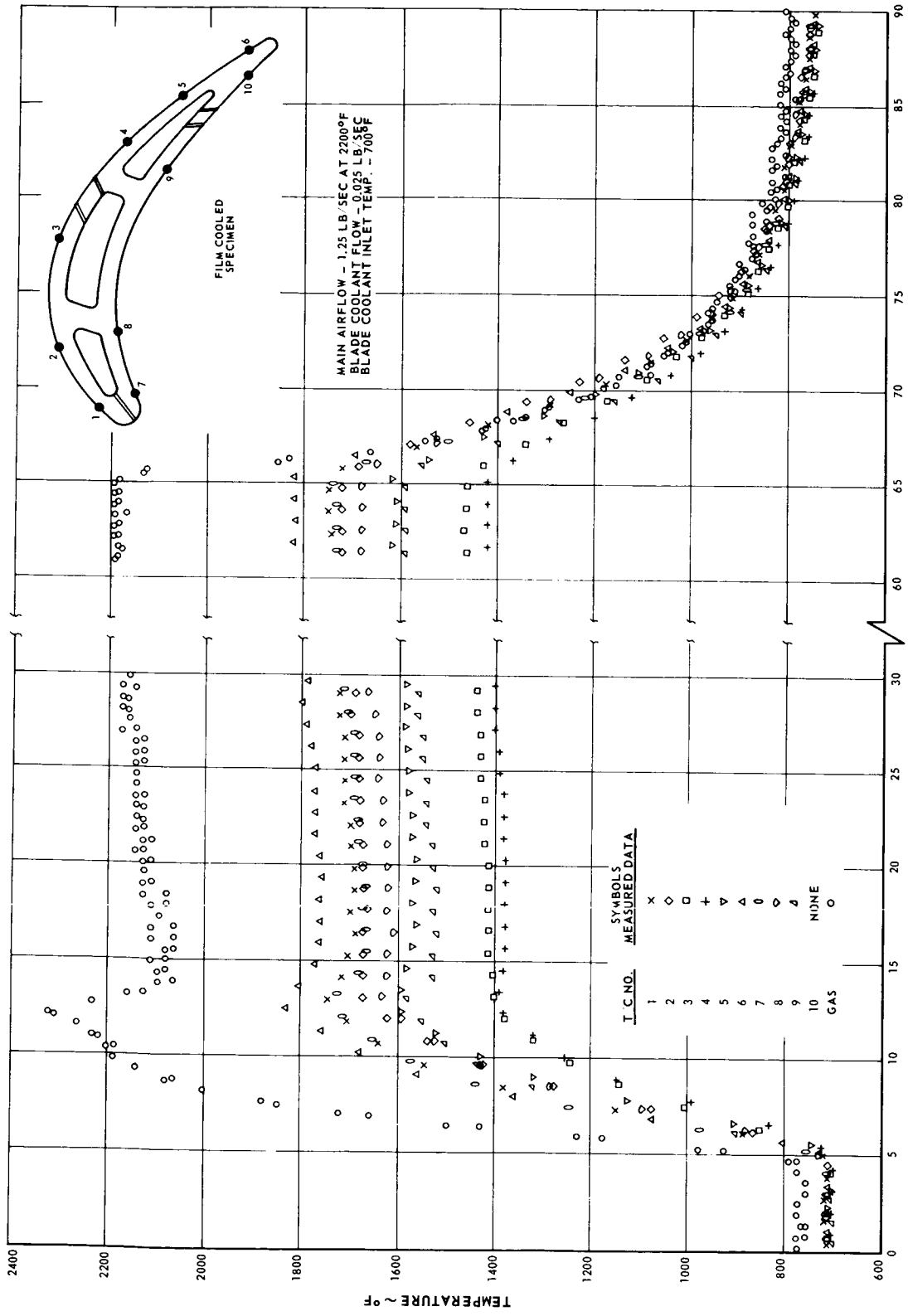


Figure 29 Measured Temperatures for PWA 658 Film Cooled Specimen, Fast Acceleration Cycle

## LIFE PREDICTION

The stress-strain history of the specimen was obtained through the use of the Turbine Airfoil Stress Analysis Computer Program described in Appendix B. The geometry of each specimen was idealized by partitioning the specimen into discrete elements. Each element was then represented in the program as an area with coordinates at the element centroid. The degree of fineness of the partitioning was increased in specimen areas which were deemed structurally critical in order to accomodate local effects.

The specimen's temperature history was obtained by using the procedure described in the previous section. This history was also oriented toward determining the maximum total strain range, in that temperatures were calculated at small intervals of time during the periods of maximum thermal gradient.

The state of stress and strain in the specimen was calculated approximately forty times during the two minute cycle with the mechanically-applied loads and estimated restraint included at pertinent times. The critical element, the element which experienced the greatest total strain, and the temperatures at which the maxima occurred were then determined. The strains in this element were then extrapolated to the specimen's surface, since crack initiation was under consideration and the strains calculated by the program were those at the element's centroid. This extrapolation was performed by considering the strains in the critical element and in the adjacent interior element. Taking the coordinates of these two elements and those of the specimen surface, a linear extrapolation was assummed which gave the surface strain. This strain valve generally yielded a strain four percent greater than the strain at the centroid of the critical element.

The total strain range versus cycles-to-failure at 1700°F for the appropriate material and configuration (See Appendix C) was used to obtain the predicted number of cycles to initiate cracking. For each set of test conditions a range of induced bending moments at the mid-span section of the specimen was considered. Separate stress analyses and life calculations were made for this range of assumed moments which gave cyclic life-to-crack initiation as a function of bending stress.

The IN-100 (PWA 658) strain cycling fatigue data used for this program was from the same heat of material used for the blade specimens. The strain cycling fatigue data for the B-1900 (PWA 663) material was partly from the same heat of material used for the blade specimen and partly from a different heat.

## BENDING STRESSES

Bending stresses in the mid-span section of the specimen were calculated from bending moments measured in the upper and lower specimen pull rods using the procedure described in Appendix D. Two strain gage bridges were installed on the necked section of each pull rod. These bridges were oriented to measure the bending moments in the pull rods in the planes of the minimum and the maximum inertial axes of the specimen airfoil section. Figure 30 presents a schematic of the strain gage installation. Gages in legs 1 and 3 of each bridge were installed on one side of the pull rod and gages in legs 2 and 4 were installed on the rod 180 degrees away. This arrangement resulted in strains due to pull rod elongation under load canceling out and bending strains in the plane of the gages being multiplied by a factor of four.

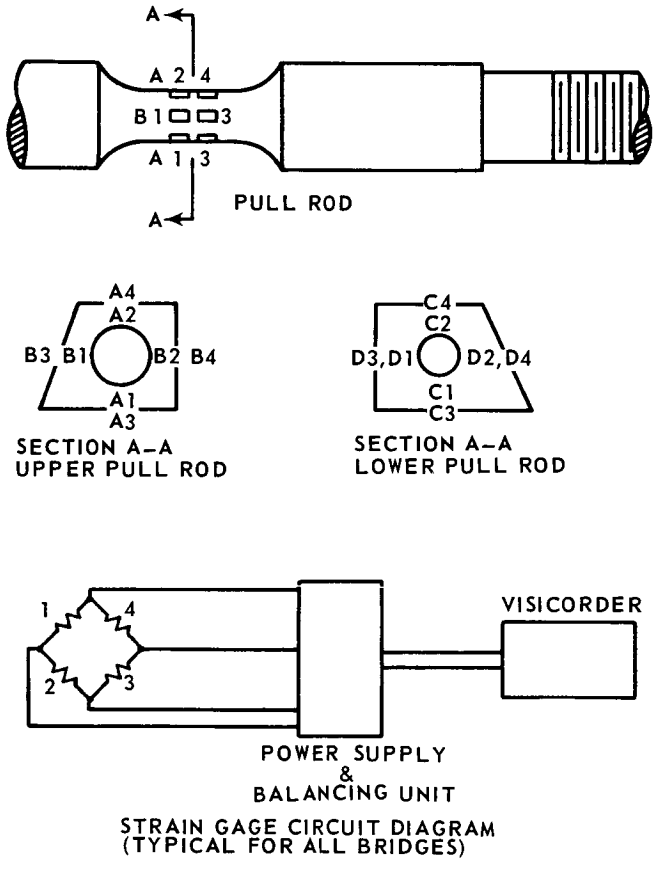


Figure 30 Strain Gage Installation On Specimen Pull Rods

Strain gages suitable for temperatures up to 800°F were used on the lower pull rod because specimen cooling air flowing in the rod was operated at temperatures up to 700°F. Strain gages suitable for temperatures up to only 500°F were used on the upper pull rod because high temperature air was not circulated through this rod. Also, a water-cooled chill block was bolted on the upper pull rod between the bellows seal and the strain gages to prevent excessive conduction heating at the strain gaged section.

Power was supplied to the strain gage bridges on the upper pull rod through a Honeywell 5KC Carrier-Amplifier Unit, Model 1124-5. Power was supplied to the strain gage bridges on the lower pull rod by a Pratt and Whitney Aircraft 2-12 volt DC Power Supply and Balancing Unit, Model 840-21. The strains were read and recorded on a Honeywell Visicorder, Model 899-1, using type M 1650 and M 100-120 galvonometers for the strain gages on the upper and lower pull rods, respectively. Two chromel-alumel thermocouples were installed on each pull rod 180 degrees apart at the level of the strain gages to measure the metal temperature of the pull rod. Each bridge was calibrated to indicate inch-pounds of bending moment and the indicated moments were manually-corrected for temperature effects.

## TESTS

### Instrumented Specimens

The instrumented specimens described in a previous section were tested to measure the temperature response of the airfoil metal at several chordwise locations at the mid-span section. These airfoil specimens were installed in the test rig and tested in the same manner as the non-instrumented (fatigue) specimens, except that external mechanical loads were not applied.

The thermocouples on each specimen were checked for continuity, secondary junctions, and resistance of the circuit (leg-to-leg and leg-to-ground) prior to installation in the test rig and subsequent to removal after testing. After installation in the rig, continuity and resistance checks were repeated on each specimen thermocouple.

Following the post installation check of all instrumentation, the test cycle conditions were set. Approximate specimen cooling airflow and temperature was established prior to lighting the preheater and main burner. Approximate flow rates and pressures also were set for the primary air, cooling air, and cooling water at the idle gas temperature condition. The maximum temperature controls were than manually-actuated and the nominal design flows, pressures, and temperatures of all cooling and heating fluids were set. This was necessary since all the parameters vary as a function of primary gas temperature, as previously discussed. The controls were then returned to the idle condition and the idle temperature was adjusted as necessary.

Automatic cycling of the primary gas temperature was started and the fuel control system was adjusted to set the required rate of temperature rise. The less severe slow acceleration cycle was run before the fast acceleration cycle to prolong specimen thermocouple life. After recording the slow acceleration data, the fuel control was readjusted to set the fast acceleration cycle temperature rise rate and to incorporate the overshoot temperature. Airfoil metal and primary gas temperatures were recorded for most of the cycles during adjustment to permit extrapolation of the data in the event of the specimen thermocouple failure. After recording at least three cycles of data at the proper acceleration rate on the punch tape recorder, automatic cycling was stopped and all pertinent flows, pressures, and additional temperatures were logged at maximum and idle temperature conditions.

Data recorded on the punch tape recorder was reduced to print-outs through a computer program. Selected data was further reduced to graphs of temperature vs. time. This data was reviewed prior to removing the specimen from the test rig. Any unsatisfactory data was immediately rerun if a sufficient number of

thermocouples on the specimen were still in good condition. Otherwise, a spare instrumented specimen was used or the specimen was reinstrumented. This data was then used as the basis for determining the temperature distribution in the specimens. Selected data from the program are presented in Figures 23 through 29.

## Fatigue Tests

A summary of the nine simulated turbine blade specimens which were tested is presented in Table III. Except for the first two specimens, these tests were directed toward developing a satisfactory test procedure and determining the loads which would produce fatigue cracks in the specimens in 10 to 1000 cycles. Spare and scrap specimens were used for these exploratory tests.

The appropriate fast acceleration temperature cycle, Figures 18 and 19, was used for these tests except for the fourth specimen tested. This specimen was tested with (a) radiation baffles installed over the viewports openings in the cascade duct and between the specimen and the exhaust water spray, and (b) a modified fuel control system which resulted in the gas temperature cycle shown in Figure 31. The radiation baffles caused the specimen to operate approximately 100°F hotter than specimens tested without the baffles. This was based on the results of an instrumented convectively cooled specimen test shown in Figure 32. The faster rates of temperature change, especially during cooldown, caused slightly higher thermal strains in the specimen.

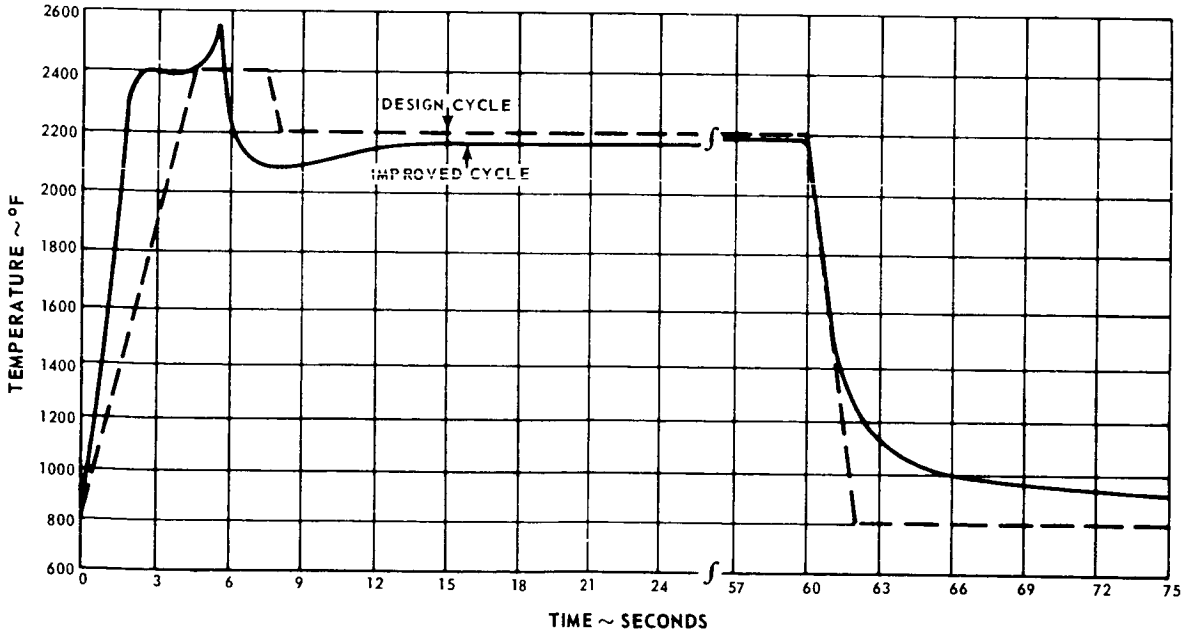


Figure 31 Imporved Gas Temperature Cycle

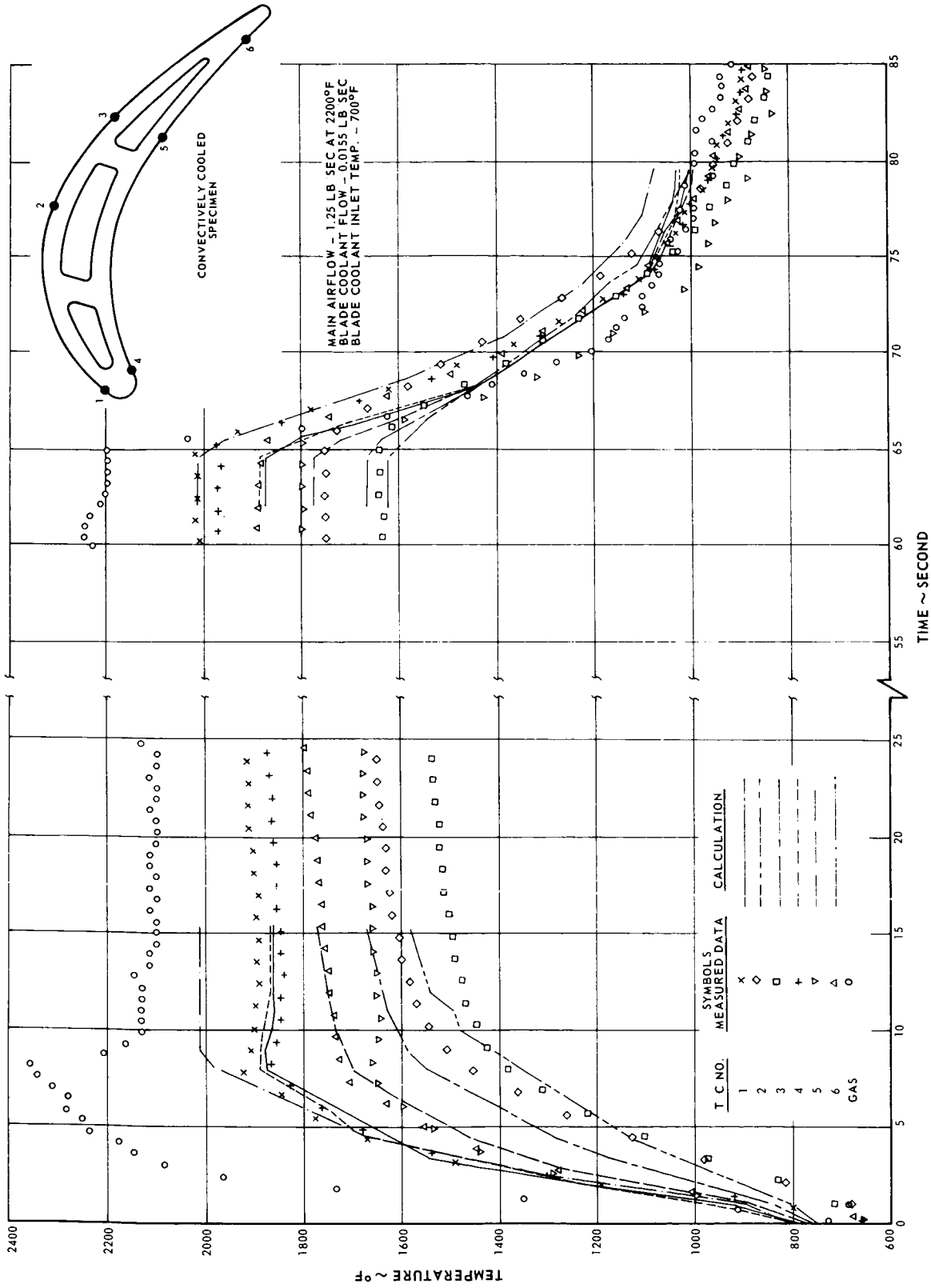


Figure 32 Measured And Calculated Temperatures for PWA 663 Convectively Cooled Specimen Tested With Radiation Baffles, Fast Acceleration Cycle

# TABLE III
## SUMMARY OF FATIGUE TEST RESULTS

| Test No. | Configuration PWA 663 Specimens | Test Results | Total Test Cycles | Test Conditions | Remarks |
|---|---|---|---|---|---|
| 1 | Convectively Cooled | Bowed | 37 | Load arms free<br>17 cycles at 5000-6000 lbs.<br>20 cycles at <5000 lbs. | High moments |
| 2 | Convectively Cooled | Fractured | 5 | Load arms locked<br>2 cycles at no load<br>1 cycle at 3000 lbs.<br>1 cycle at 5000 lbs.<br>1 cycle at 6900 lbs. | High moments |
| 4 | Cooled (scrap) | Cracked | 77 | Load arms free<br>20 cycles at no load<br>3 cycles at 1000 lbs.<br>54 cycles at 3000 lbs. | Minimized moments. Residual moments caused tension in LE. Radiation baffles installed. |
| 6 | Uncooled | Bowed | 246 | Load arms free<br>8000 lbs. load | Minimized moments. Residual moments caused tension in LE. |
| 7 | Uncooled | Bowed | None | Load arms free<br>8000 lbs. load | Excessive moment applied while adjusting load mechanism. |
| | PWA 658 Specimens | | | | |
| 3 | Cooled (scrap) | Fractured & cracked | 113 | Load arms free<br>100 cycles at no load<br>3 cycles at 1000 lbs.<br>9 cycles at 3000 lbs.<br>1 cycle at 4500 lb. | Minimized moment at 3000 lbs. |
| 5 | Uncooled | Cracked in fillet radius | 947 | Load arms free<br>5000 lbs. load | Minimized moments. Residual moments caused tension in LE. |
| 8 | Uncooled | Bowed & cracked | 238 | Load arms free<br>7000 lbs. load | Minimized moments. Residual moments caused tension in LE. |
| 9 | Uncooled | Cracked | 230 | Load arms locked<br>6500 lbs. load | Minimized moments at load and maximum temperature |

After installation in the test rig, the specimens were set above center in the cascade duct such that they would be centered when loaded at maximum temperature. The gas flows, pressures, and temperatures were set in the same manner used for the instrumented specimen tests.

Several methods of applying the load to the specimens were tried. The initial approach was to align the loading mechanism with the test chamber using a fixture which engaged the two pins on the top of the bearing block and the pins on the ends of the cascade duct locating pedestals which extend through the top cover of the test chamber. This fixture was designed to position the loading mechanism such that a line connecting the loading linkage attachments on the top and bottom load arms would pass through the centroids of the specimen airfoil sections with the arms positioned vertically and with a 5000 pound load applied to the specimen at maximum gas temperature (based on measured values of deflection in the load arms and relative movement between the loading mechanism and the test chamber). The load was set before lighting the burners or with the rig operating at idle gas temperature. The first two specimens were tested using this method, except the load arms were locked to prevent rotation about their bearing axes during testing of the second specimen.

For the remaining tests the loading mechanism was aligned with the test chamber using the bending moments measured in the specimen pull rods as the criteria for determining the correct alignment. The bearing block was adjusted laterally on its support plate as necessary to minimize the bending moments about both the minimum and maximum inertial axes of the specimen airfoil and to direct the residual moments such that they tended to put the leading edge in tension. Dial indicators were set up to measure the movement of the bearing block relative to its support plate. The load arms were left free to rotate except for the last specimen tested. For this specimen the load arms were locked to prevent rotation and positioned with the load arm stops at approximately zero inch pounds bending moment about the minimum inertial axis with the load applied at maximum gas temperature.

The first two specimens were to be tested at 8000 pounds load. The hydraulic cylinder piston stroke was short and resulted in the maximum load applied to the first specimen being 5600 pounds. The piston stroke was adjusted after 17 cycles and the load was raised in steps to 5000 pounds to obtain a record of the bending moment variation as a function of load. At this point the load arms were seen hitting against their stops. The stops were adjusted to permit about ten degrees rotation of the load arms. The load was again raised in steps to 5000 pounds while observing operation of the loading mechanism. On the second cycle at 5000 pounds the load arms again rotated against their stops. The specimen was badly bowed and cracked near the end lugs, as shown in Figure 33, and the test was discontinued. The second specimen was being loaded in steps to

8000 pounds with the load arms locked. It fractured, as shown in Figure 34, at 6900 pounds while applying a 7000 pound cycle. Noticeable necking at the leading edge and secondary cracking in the vicinity of the fracture indicated a stress rupture failure.

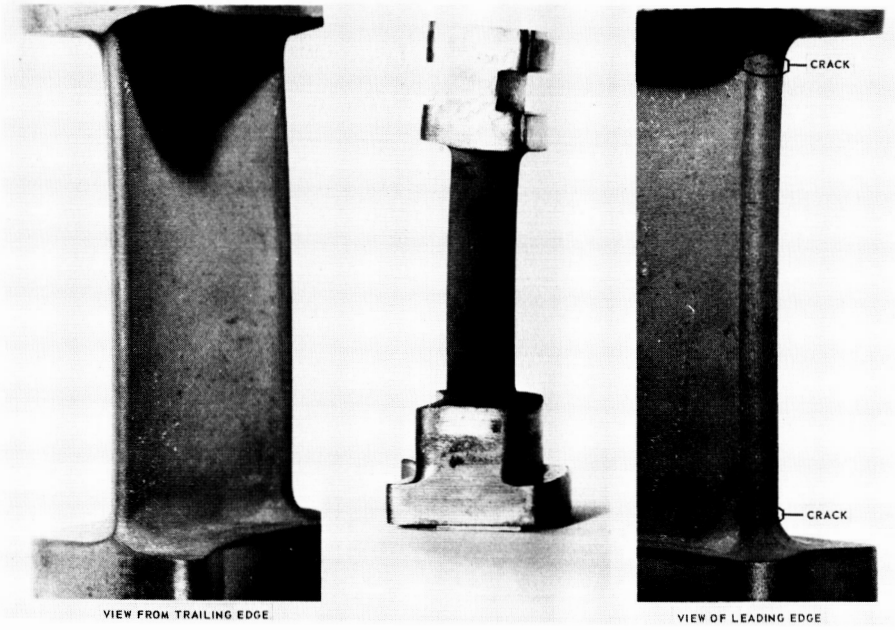


Figure 33 PWA 663 Convectively Cooled Blade Specimen After Test No. 1 (XP-72777)

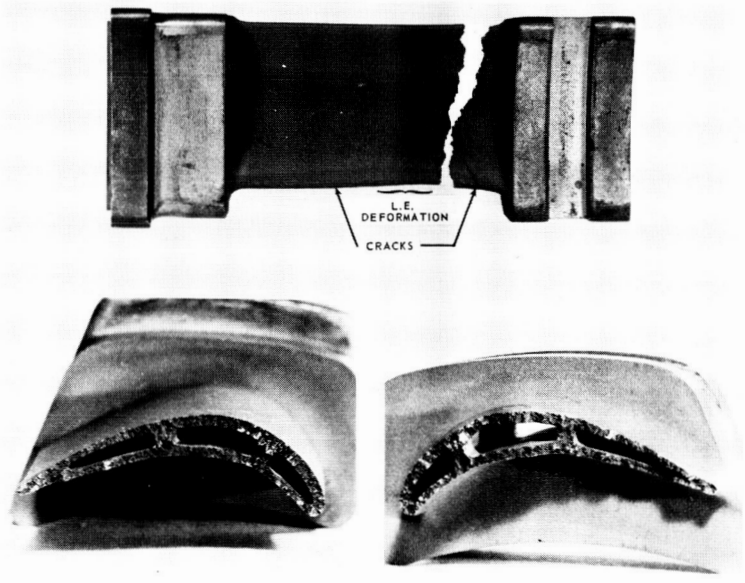


Figure 34 PWA 663 Convectively Cooled Blade Specimen After Test No. 2 (XP-72584)

Subsequent analysis of the results from these first two tests indicated high local loading of the specimen on the suction (convex) surface near the trailing edge due to the combination of high bending moments and applied load. Consequently, the method of minimizing the bending moments and controlling the direction of the residual moments previously described was developed. Efforts were also made to improve the gas temperature cycle to more closely approximate the design cycle to increase the thermal strain and reduce the mechanical load. By adding a manual needle valve and a solenoid valve in parallel with the fuel control and idle temperature control valves and by operating with a higher fuel pressure using the fuel control valve to control the overshoot temperature and the needle valve-solenoid valve combination to control the maximum temperature, the improvements in gas temperature shown in Figure 31 were obtained. This temperature cycle was not used, however, because the amount of improvement in the temperature cycle was not sufficient to warrant the additional expense and delay that would have been incurred due to the necessity of rerunning the instrumented specimen tests.

The third specimen tested was used for the improved gas temperature cycle investigations described above and then was fatigue tested. A scrap film cooled instrumented specimen with the holes and thermocouple grooves filled with Allen P-1 cement was used. Cooling air metering plates were not installed on this specimen, although the total cooling airflow and inlet temperature was set for the conditions specified for the convectively cooled speciments. It was planned to cycle this specimen at 5000 pound load. The load was increased in steps to 3000 pounds where the bending moments about the minimum inertial axis were minimized. The specimen fractured, as shown in Figure 35, at 4500 pounds while loading the specimen to 5000 pounds. The absence of secondary cracking and any noticeable necking indicated the fracture was probably due to propagation of a fatigue crack. The three leading edge cracks and one trailing edge crack also support this conclusion. One of the leading edge cracks was near mid-span and was about 5/16 inch long to either side of the leading edge. The other cracks were located near the ends of the airfoil.

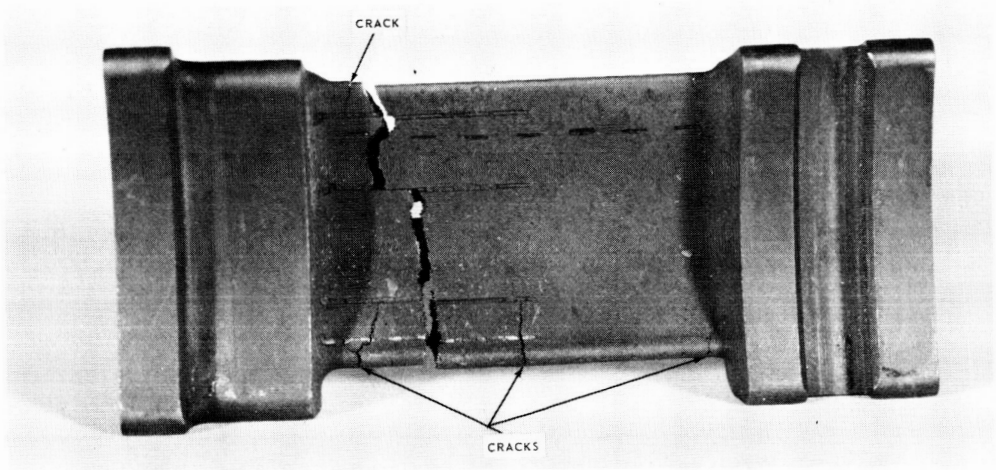


Figure 35 Scrap PWA 658 Film Cooled Blade Specimen After Test No. 3 (XP-74261)

The fourth specimen tested was also a scrap film cooled instrumented specimen with the holes and thermocouple grooves filled with Allen P-1 cement similar to the previous specimen. The gas temperature cycle was slightly different and radiation baffles were installed during this test as previously described. The bending moments were minimized about both axes at 3000 pounds load and then the specimen was cycled at 3000 pounds load. The measured bending moments started to change noticeably during the last few test cycles and the specimen was removed for visual inspection. There were five cracks in the leading edge ranging up to 1/4 inch long, as shown in Figure 36. The three longest cracks were located in the 25 to 75 percent span region.

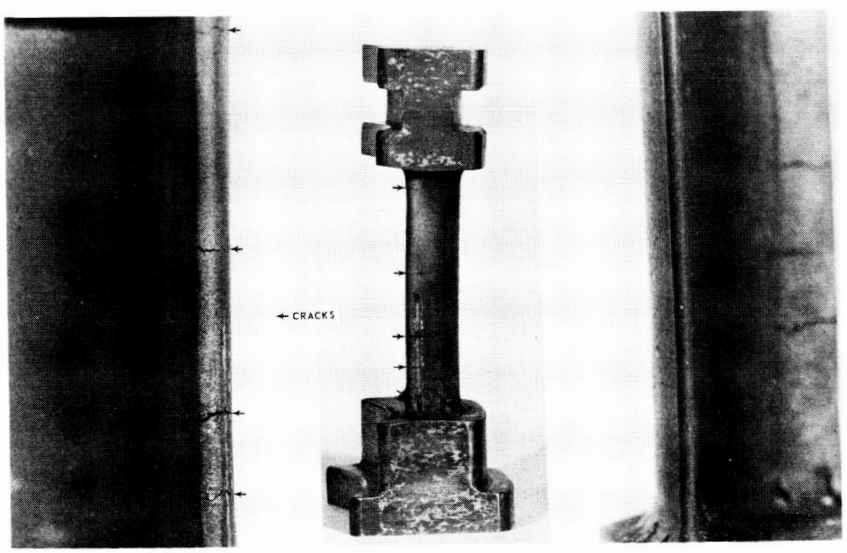


Figure 36 Scrap PWA 663 Film Cooled Blade Specimen After Test No. 4 (XP-74260)

It appeared that a satisfactory method of testing the specimens had been developed at this point and additional tests were planned to dtermine the load range necessary to develop fatigue cracks in the specimens in 10 to 1000 cycles. Spare specimens were used for these tests. Due to the scarcity of spare convectively cooled specimens, uncooled specimens were used. The fifth specimen was tested for 947 cycles at 5000 pounds load without any signs of distress other than a small crack in the leading edge fillet radius near the large end lug, as shown in Figure 37. Analyses indicated that these specimens should have a life greater than 5000 cycles at 8000 pounds load. Therefore, the next specimen was tested at 8000 pounds load. This specimen bowed, as shown in Figure 38, in 246 cycles.

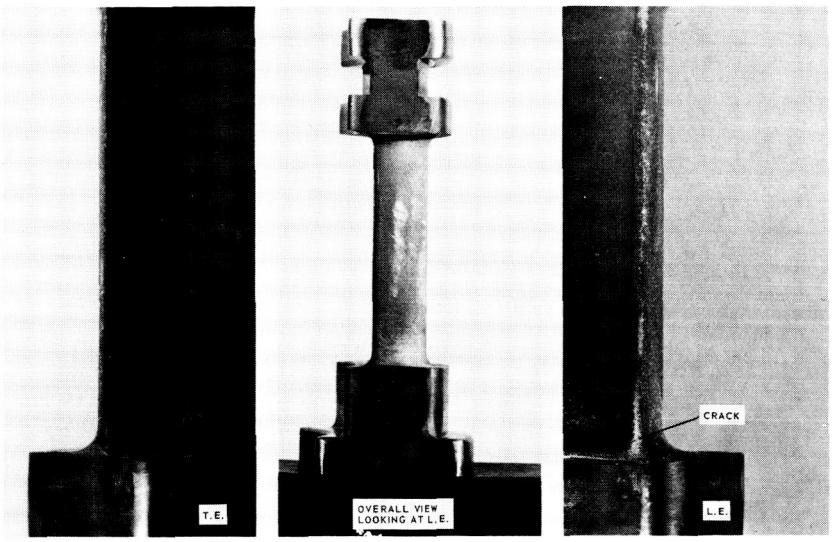


Figure 37 PWA 658 Uncooled Solid Blade Specimen After Test No. 5 (XP-75624)

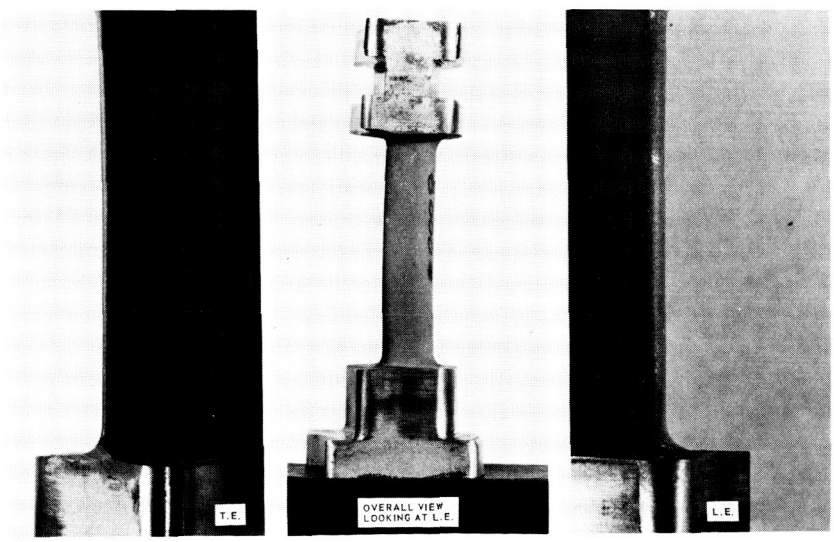


Figure 38 PWA 663 Uncooled Solid Blade Specimen After Test No. 6 (XP-75623)

The eighth specimen was tested at 7000 pounds load and visually inspected after 180 cycles. Slight bowing was observed which increased as testing was continued. Testing was stopped after 238 cycles due to the load arms hitting the stops and the measured moments changing noticeably. The specimen was bowed and cracked on the leading edge, as shown in Figure 39.

Since operation of the loading mechanism was stable and responding to gas temperature changes as would be expected due to thermal bowing of the specimens, strain ratcheting of the leading and trailing edges is believed to be the primary cause of the bowing. Therefore, the last specimen was tested at 6500 pounds load with the load arms locked. This resulted in higher bending moments being induced at the ends of the specimen due to restraint of specimen thermal bowing. Figures 40 and 41 show typical moments with the load arms locked and unlocked. This specimen developed a leading edge crack near mid-span, as shown in Figure 42, without any noticeable bowing after 230 cycles.

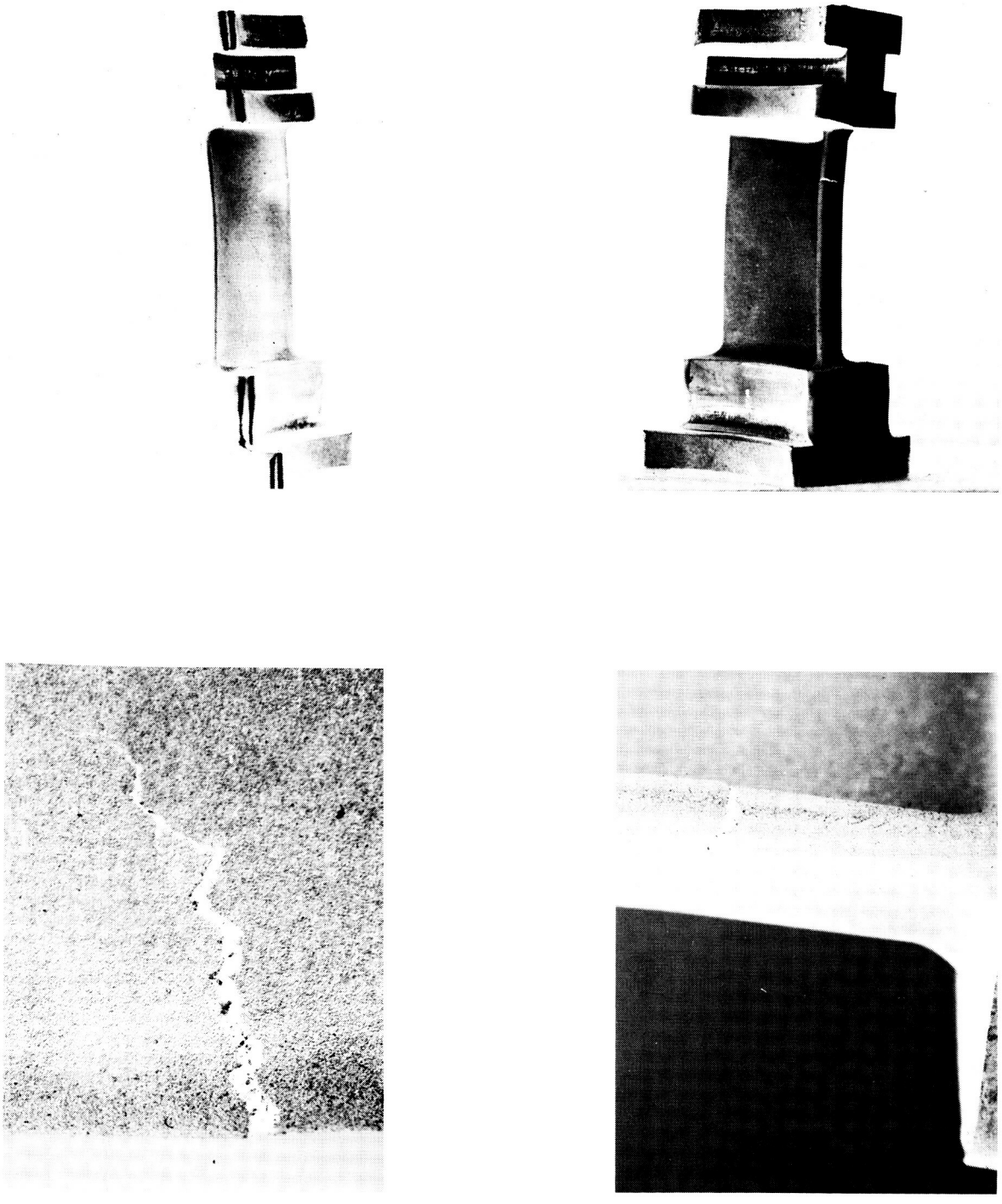

Figure 39 PWA 658 Uncooled Solid Blade Specimen After Test No. 8

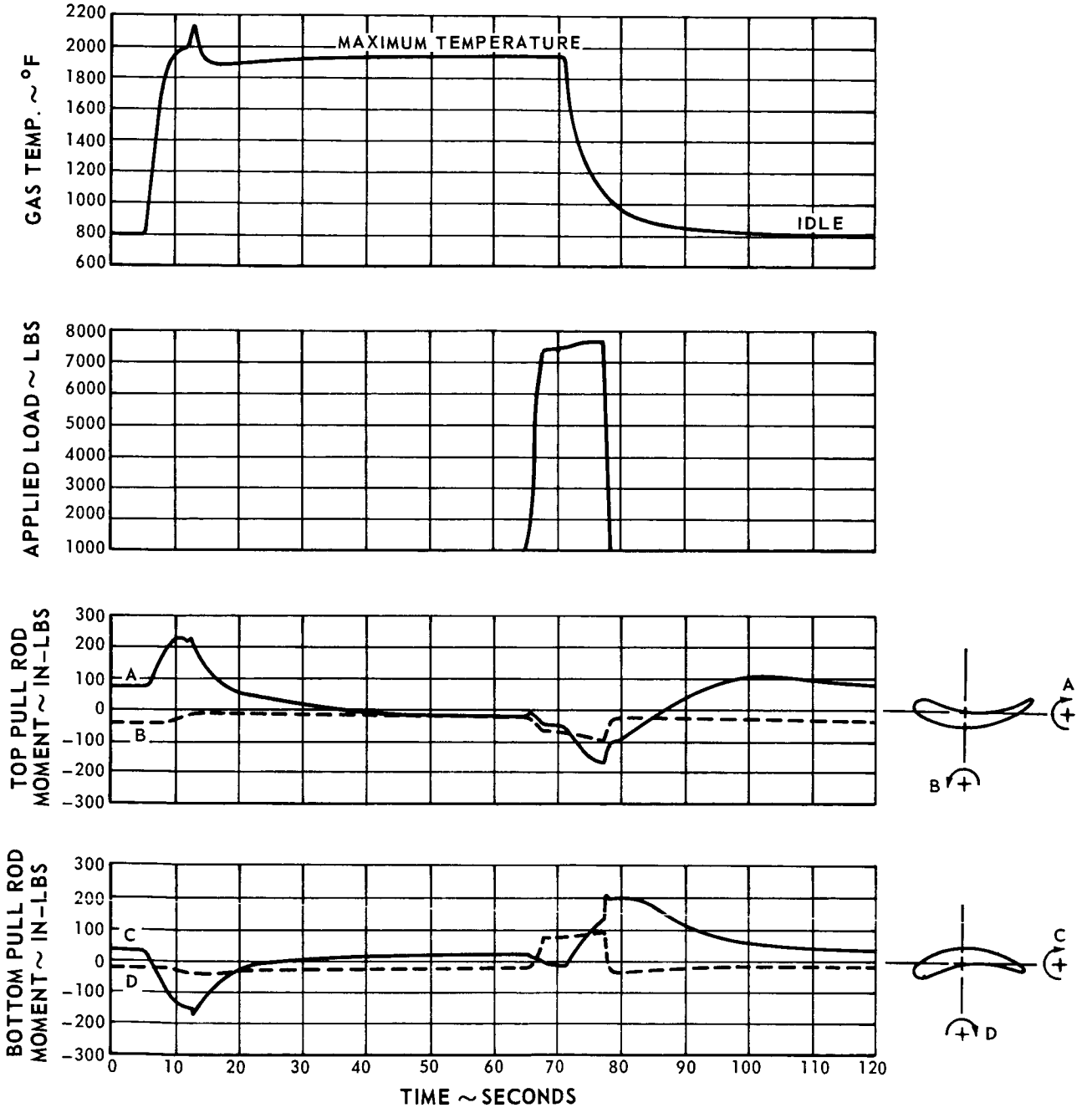


Figure 40 Typical Gas Temperature, Applied Load, And Bending Moment Cycles For An Uncooled Specimen With Load Arms Locked In Fixed Position

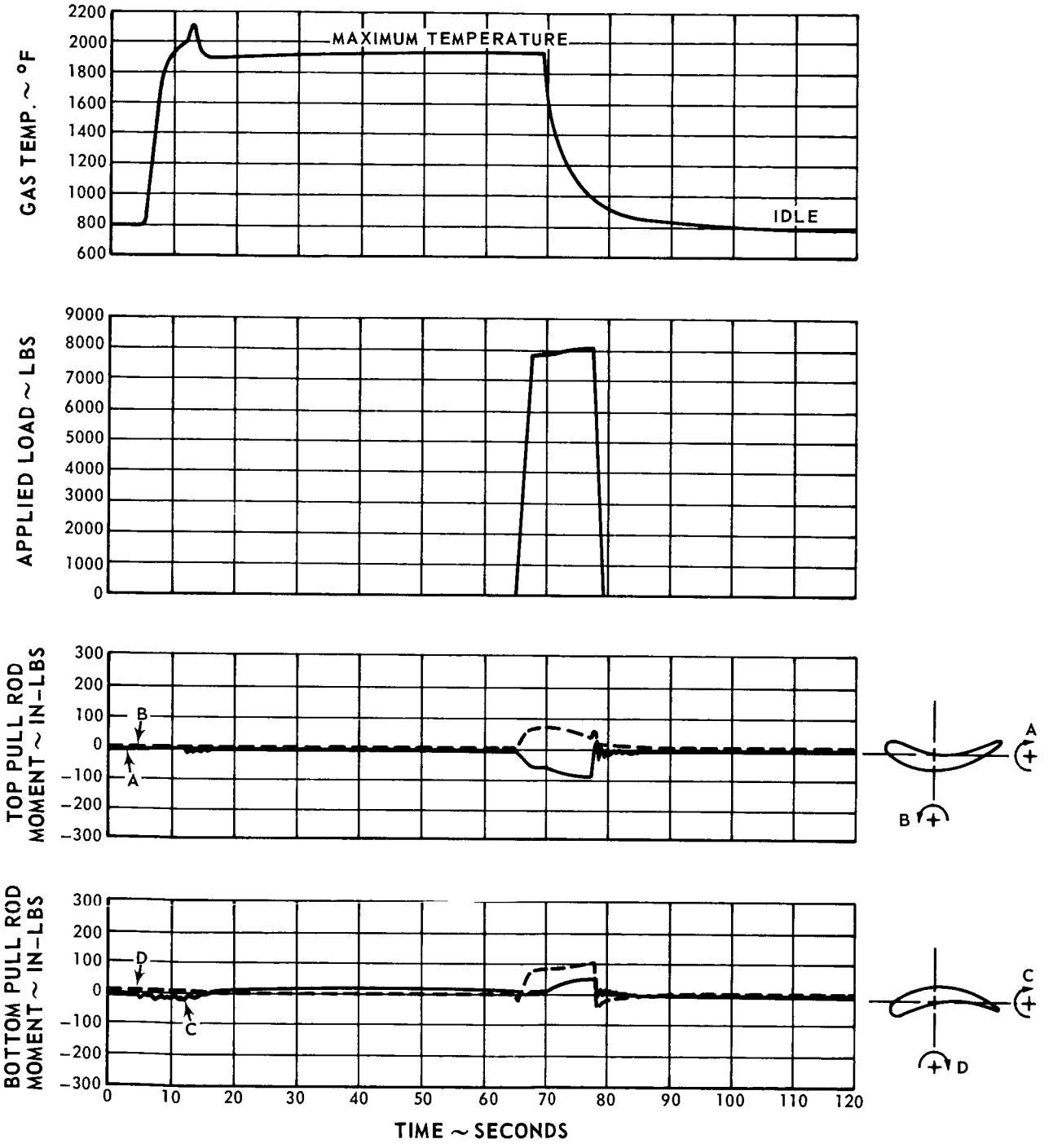


Figure 41 Typical Gas Temperature, Applied Load, And Bending Moment Cycles For An Uncooled Specimen With Load Arms Free To Rotate

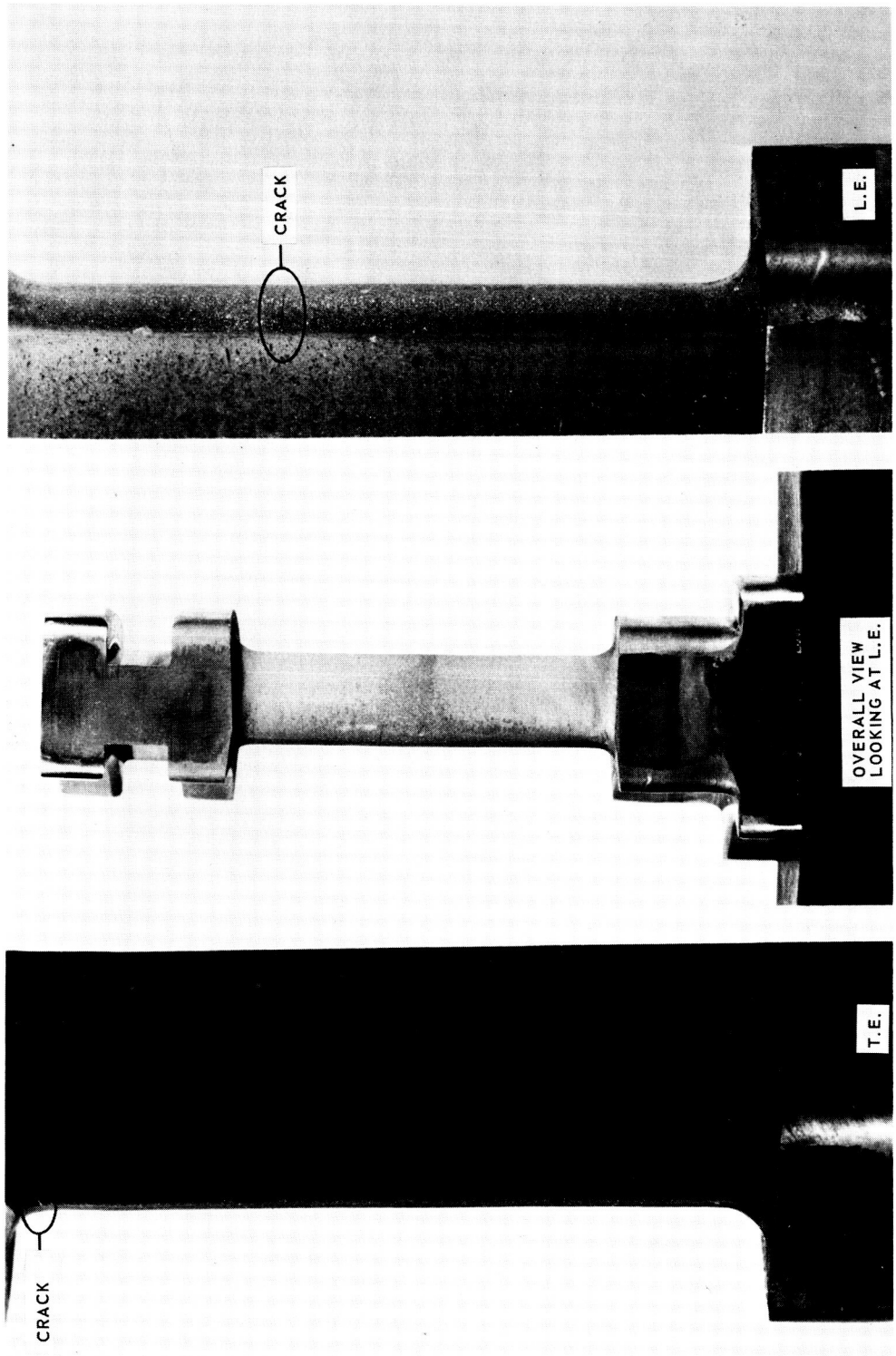


Figure 42 PWA 658 Uncooled Solid Blade Specimen After Test No. 9
(XP-75621)

## DISCUSSION

The transient gas and specimen metal temperature response was considerably less severe than anticipated during design, as shown in Figures 20 and 43. This resulted in less severe thermal stresses, especially during the cool down portion of the cycle. Operating characteristics of the fuel control system and radiation losses through the viewports and to the exhaust cooling water spray were considered the primary causes of the differences in the design and actual temperature cycles. Experimental investigations showed that some improvements could be attained in the gas temperature cycle by modifying the fuel control system. However, the desired cool down rate could only be obtained by shutting off the fuel entirely. Development of a satisfactory method of relighting the burners at test conditions would have been required. Installing radiation baffles to screen the specimen from the viewports and the exhaust cooling water spray raised the convectively cooled specimen temperature approximately 100°F as can be seen by comparing Figures 22 and 32. However, the improvements immediately available were not considered sufficient to justify the increased cost and delay that would have been incurred due to the necessity of reinstrumenting and rerunning the instrumented specimen tests.

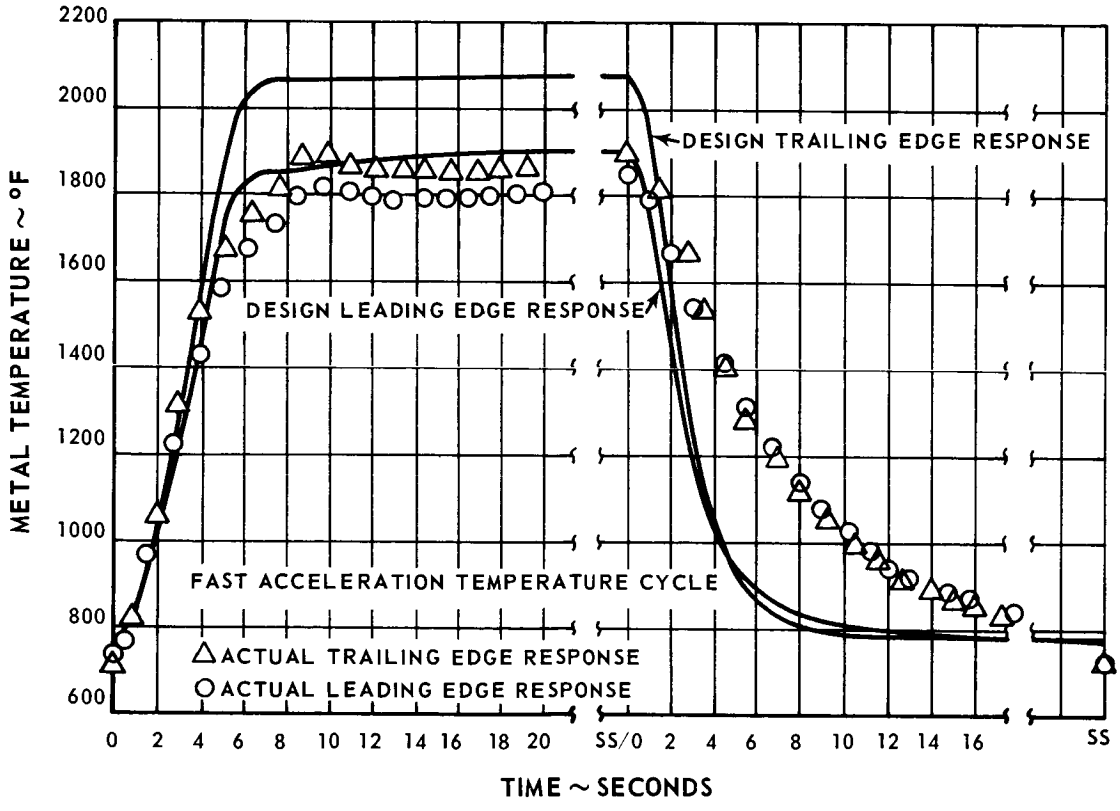


Figure 43 Comparison of Actual And Design Specimen Metal Temperature Response for PWA 663 Convectively Cooled Specimen, Fast Acceleration Temperature Cycle

Although analysis indicated that an increase in mechanical load was necessary to compensate for the lower thermal stresses, the first two specimens failed in relatively few cycles at loads well below that indicated analytically. Post-test analysis of the first two tests indicated (1) the maximum safe load from stress rupture considerations was approximately 5500 pounds for the convectively cooled specimen configuration and (2) the need to minimize bending moments and control residual moments to cause tension in the leading edge of the airfoil. Stress-rupture data on thin wall flat specimens cut from cast airfoils and coated with PWA47-14L on both sides were used for this analysis instead of data from 1/4 inch diameter tensile specimens. This data was used because the stress-rupture life of the thin wall flat specimens was considerably less than the life obtained from 1/4 inch tensile specimen tests. Also, the thin wall flat specimens were considered more representative of the convectively-cooled specimen geometry. This thin wall flat specimen stress-rupture data was not available for earlier analyses. Bending moments induced in the specimen, calculated from the measured moments in the upper pull rod, were also included in the analysis. These moments were very high and caused tension in the trailing edge of the specimen. They also contributed significantly to the fracture of the second sepcimen tested. Bowing of the first specimen was initially attributed to the high binding moments. Subsequent tests indicated bowing was probably due to strain ratcheting in the leading and trailing edges.

The "hot" alignment procedure was developed and subsequent tests indicated that convectively-cooled specimens could be cracked without bowing the specimens.

However, tests on the uncooled specimens indicated that they could not be cracked without bowing using this procedure. Consequently, the last specimen was tested with the load arms locked. This procedure resulted in cracking the uncooled specimen in 230 cycles at 6500 pounds load without any noticeable bowing, although the bending moments induced in the specimen increased significantly as evidenced by comparison of Figures 40 and 41.

The life prediction method was applied to the last test, using the mean life moment trace shown in Figure 44. The calculated strain and temperature histories at the centroid of the critical leading edge element are shown in Figures 45 and 46. The critical strains were extrapolated to the airfoil surface in order to predict crack initiation. A life of 750 cycles was predicted by entering the 1700°F low cycle fatigue curve for PWA 658, Figure C-24 in Appendix C, with the total strain range at the surface of the critical element, 0.0065 in/in, and reading the number of cycles to failure. This is in reasonable agreement with the test results of 230 cycles. Similar analyses on the convectively cooled specimens tested with the load arms free to rotate, however, predicted that the specimens would not fail.

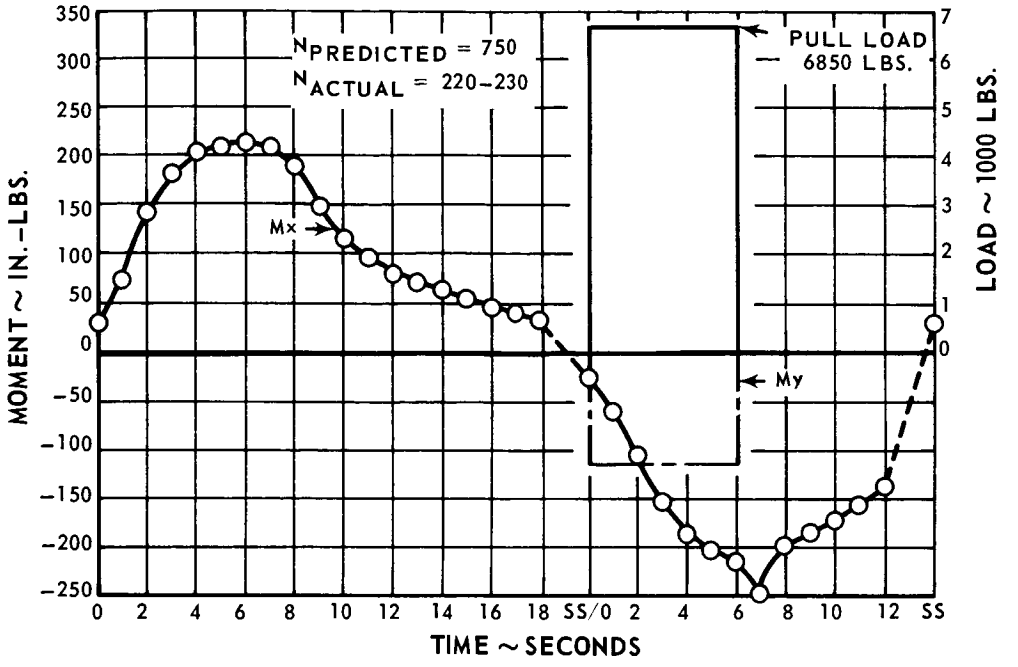


Figure 44 Mean Life Moment and Load for PWA 658 Uncooled Solid Specimen With Load Arms Locked

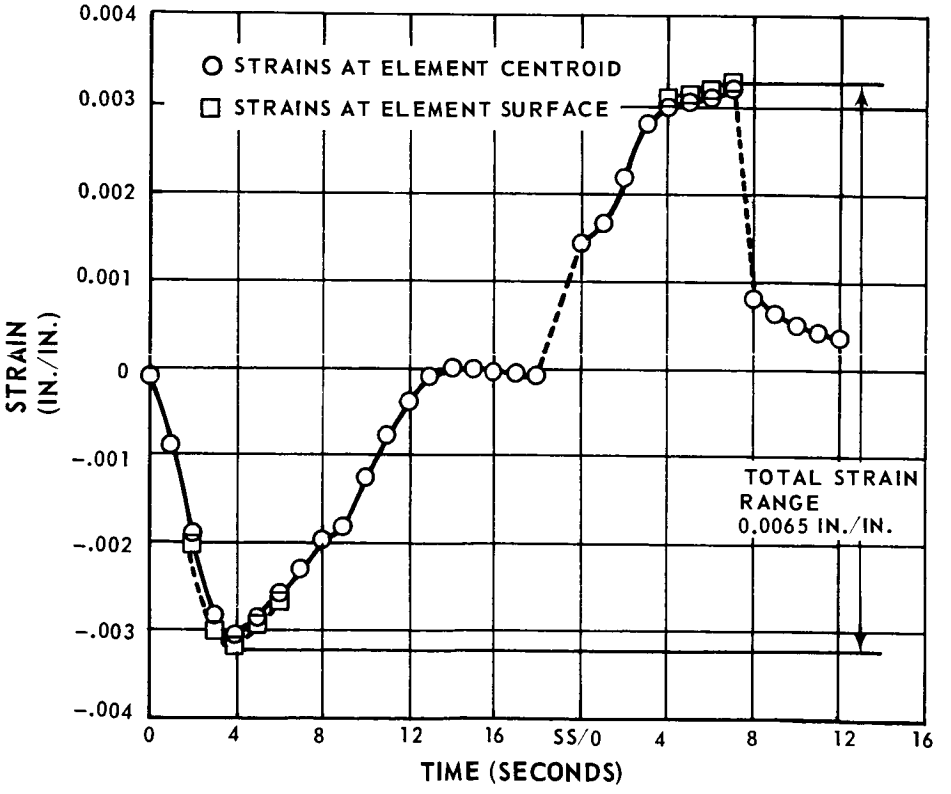


Figure 45 Critical Leading Edge Element Strain vs. Time for Uncooled PWA 658 Specimen With Load Arms Locked

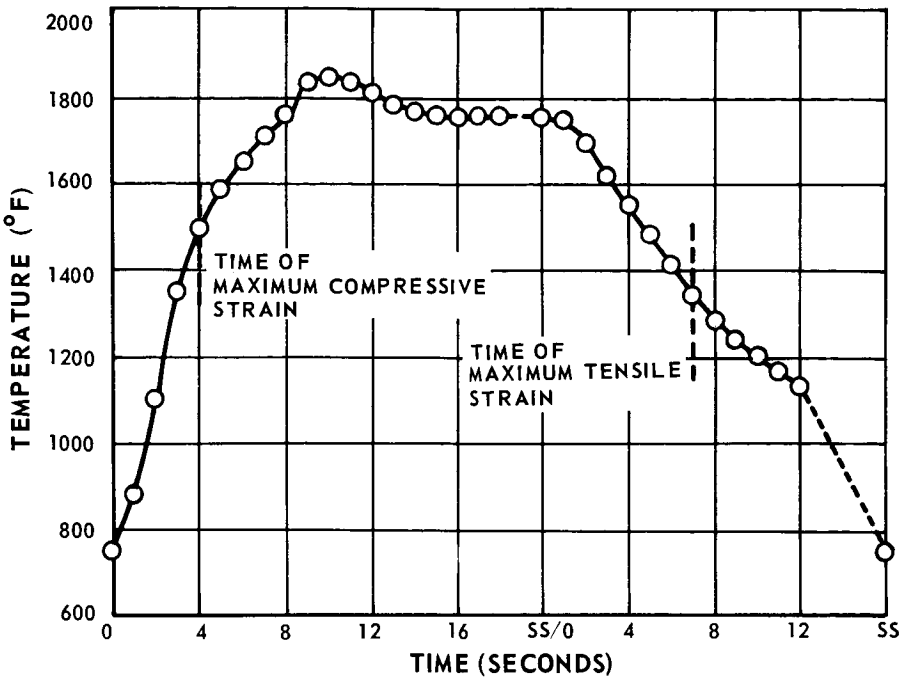


Figure 46 Critical Leading Edge Element Temperature vs. Time for Uncooled PWA 658 Specimen With Load Arms Locked

It should be noted that although the maximum compressive and tensile strains occur at 1497 and 1342°F, respectively, it was decided to base the life prediction on the 1700°F isothermal data based on the findings of Franklin et al[1]. They found in their work on the thermal fatigue of nickel base alloys that failure occurred at or near the maximum temperatures and correlated with yield strength at maximum temperature and elongations at 180°F below maximum temperature. At this point, it is deemed appropriate to use the 1700°F data without modification, as it falls within the range of criticality defined by the above authors and any possible modification would be speculative.

A revised test program using one thermal cycle and three load levels with the load arms adjusted and locked in position was recommended. The original program consisted of two thermal cycles and one load level with the load arms free to rotate. The revised program is outlined in Table IV. Prediction of the number of cycles to initiate cracking with the load arms locked is made difficult by the lack of precise information on the induced bending moments prior to actual testing. However, using the same degree of restraint as found in the last uncooled specimen test, predictions indicated nominal lives between 100 and 1000 cycles for the uncooled specimens and 3000 to 20,000 cycles for the convectively cooled specimens for the recommended test conditions. It is believed that the cooled specimens would actually fatigue in less than 1000 cycles. This is based on stress-rupture analysis and experience with the convectively cooled specimens tested.

(1) A. W. Franklin, J. Heslop, and R. A. Smith, "Some Metallurgical Factors Influencing the Thermal-Fatigue Resistance of Wrought Nickel-Chromium Base High Temperature Alloys", Journal of the Institute of Metals, Vol. 92, 1963-64

TABLE IV

RECOMMENDED REVISED TEST PROGRAM*

| Material | Configuration | No. of Specimens at Each Load | Load (lbs) |
|---|---|---|---|
| PWA 663 | Uncooled | 2 | 6850, 5850, 4850 |
| PWA 663 | Cooled (1) | 2 | 5500, 4750, 4000 |
| PWA 658 | Uncooled | 3 | 5850 |
| PWA 658 | Cooled (2) | 3 | 4750 |

Notes:

1. Flim and convectively cooled
2. Film cooled only

*Fast acceleration temperature cycle with load arms locked in position

A study of the sensitivity of the strain range calculations to the accuracy of the bending moments over the load ranges which were recommended indicated a high degree of sensitivity. It also indicated that it was necessary to know the applied bending moments within ±50 inch-pounds to yield significant results. Figures 47 and 48 present the results of this study. Restraint of 50 percent of the calculated thermal bowing was assumed to establish the nominal moment vs. load curves. A tolerance analysis indicated that the bending moments could be determined to at least this degree of accuracy and probably much better if (1) the moments in the load arms and the angular positions of the load arms were measured as a function of time during the test, (2) the eccentricities of the specimens and pull rod loading surfaces were determined by dimensional inspection before testing, and (3) the relative eccentricities between the specimens and the pull rods were prevented from changing during test by shimming.

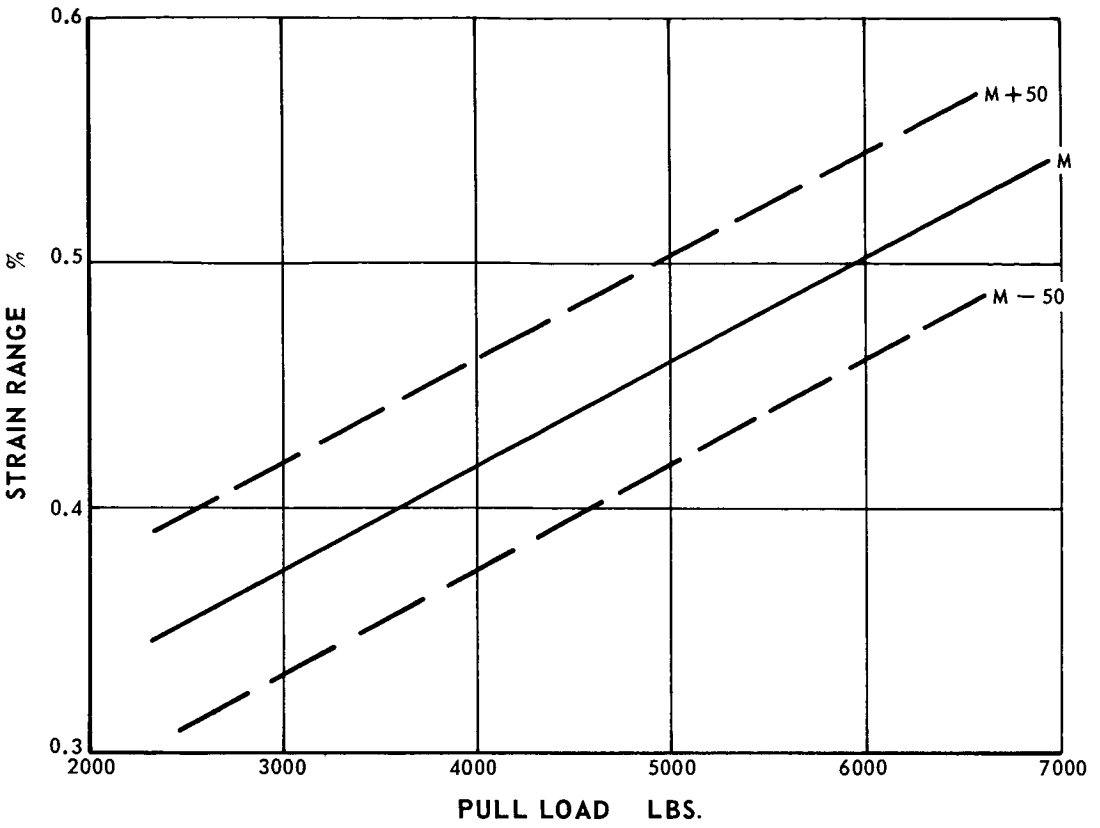


Figure 47 Convectively Cooled Specimen Moment - Load Sensitivity

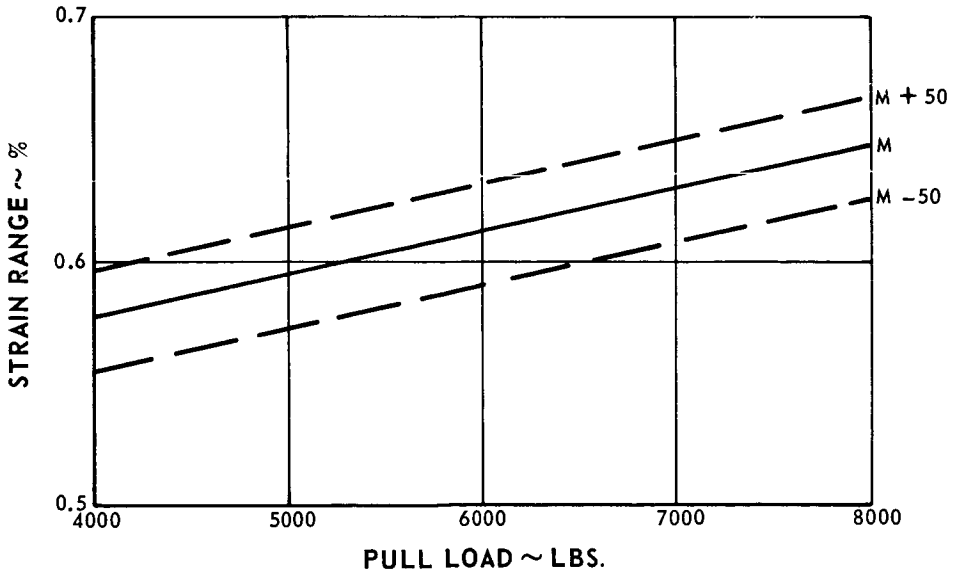


Figure 48 Uncooled Specimen Moment - Load Sensitivity

# CONCLUSIONS

Fatigue cracks can be initiated in the specimens in less than 1000 cycles in the present test rig using the fast acceleration temperature cycle and the "hot" alignment procedure.

With the load arms free to rotate, the uncooled specimens will bow at loads necessary to cause fatigue cracking in less than 1000 cycles. The probability of terminating the test because of severe bowing before developing a crack is high.

Locking the load arms to prevent rotation after minimizing the moments in the pull rods will produce cracks in the uncooled specimens in less than 1000 cycles without any noticeable bow. The magnitude of the induced moments is increased significantly and acts to oppose thermal bowing of the specimen.

The restraining moments induced in the specimen by locking the load arms are a significant factor in determining the life of the specimens. Consequently, the bending moments in the top and bottom pull rods and the angularity of the pull rods as a function of time, as well as the measured eccentricities of the specimens and the pull rods, must be known to determine the moment in the specimen.

Post-test life analysis of the PWA 658 uncooled specimen tested with the load arms locked gave encouraging correlation with the observed number of cycles to the first crack.

The test rig is satisfactory to perform tests to verify the fatigue life prediction method if:

- Provisions to accurately measure the angularity of the pull rods as a function of time are added, and
- Calibration tests to relate axial load and bending moments in the test section to axial load and bending moments measured in the pull rods are conducted.

Several areas such as the temperature control system, radiation losses from the specimen, provisions for changing the specimens, relative movement between the test chamber and loading mechanism, deflections of the load arms, and internal and external air leakage in the test chamber could be improved, but this is not necessary to initiate cracking of the specimens under known conditions of temperature and load.

The test program initially planned involving two gas temperature cycles could not be performed with the present test rig and specimen designs because the most severe temperature transients obtainable were required to assure cracking the specimens in a reasonable number of cycles.

## RECOMMENDATIONS

It is recommended that the fatigue tests be completed in accordance with the revised test program. Since no experimental verification of the load range recommended for the cooled specimen tests was obtained with the load arms locked in position, the loads may require adjustment. Testing the first cooled specimen at the lowest load is recommended to permit calibration of the actual life relative to the predicted life. The recommended load range could then be adjusted as necessary.

APPENDIX A



# METHOD OF CALCULATING THE TEMPERATURE DISTRIBUTIONS IN THE SPECIMEN AIRFOILS

Prepared by: F. L. Bruno

## Nomenclature

| | | |
|---|---|---|
| $Q_g$ | = | Rate of heat transferred to node 1 by convection (BTU/hr) |
| $h_g$ | = | Gas heat transfer coefficient at surface of node (BTU/hr-ft$^2$-°F) |
| $A_L$ | = | Surface area of element in contact with gas (ft$^2$) |
| $Q_{r-s}$ | = | Rate of heat transferred from node r to node s (BTU/hr) |
| $A_{r-s}$ | = | Contact surface area between adjacent nodes (ft$^2$) |
| $L_{r-s}$ | = | Distance between centroids of adjacent nodes r and s (ft) |
| k | = | Thermal conductivity of material between centroids (BTU/hr-ft-°F) |
| r & s | = | Arbitrary identification numbers of nodes |
| $T_g$ | = | Gas temperature (°F) |
| $T_r$ | = | Temperature at centroid of node r(°F) |
| m | = | Mass of node (lbs) |
| $c_p$ | = | Specific heat of node material (BTU/lb-°F) |
| $T_N$ | = | Average temperature of node at time $\theta$ (°F) |
| $T_{N'}$ | = | Average temperature of node at time $\theta + \Delta\theta$ (°F) |
| $\theta$ | = | Time (hrs) |
| $\Delta\theta$ | = | Time increment (hrs) |
| $h_c$ | = | Coolant heat transfer coefficient at surface of node (BTU/hr-ft$^2$-°F) |
| $T_c$ | = | Bulk coolant temperature (°F) |
| h | = | Local heat transfer coefficient (BTU/hr-ft$^2$-°F) |
| D | = | Diameter of cylinder (ft) |
| $k_f$ | = | Gas stream thermal conductivity at reference temperature $T_f$ (BUT/hr-ft-°F) |

$\rho_f$ = Density of gas stream at reference temperature $T_f$ (lbs/ft$^3$)

V = Free stream gas velocity (ft/sec)

$\mu_f$ = Dynamic viscosity of gas stream at reference temperature $T_f$ (lb/ft-sec)

$Pr_f$ = Prandtl number of gas at reference temperature $T_f$, dimensionless

$\phi$ = Angle from stagnation point (deg)

X = Distance along a flat plate (ft)

$F_{LAM}$ = Pressure gradient correction factor

$T_f$ = Film temperature (°F)

$T_\infty$ = Free stream temperature (°F)

$T_{aw}$ = Adiabatic wall temperature, recovery temperature (°F)

$T_w$ = Airfoil surface temperature (°F)

$T_s$ = Static temperature of gas stream (°F)

$\rho_o$ = Density of coolant at bulk temperature (lbs/ft$^3$)

$d_o$ = Hydraulic diameter of channel (ft)

$V_c$ = Coolant velocity (ft/sec)

$\mu_o$ = Dynamic viscosity at bulk temperature (lb/ft-sec)

$Pr_o$ = Prandtl number of coolant at bulk temperature (dimensionless)

$T_m$ = Metal temperature (°F)

$T_{c1}, T_{c2}$ = Coolant temperatures at locations 1 and 2 respectively (°F)

M = Coolant mass flow rate (lbs/hr)

x = Distance from slot (ft)

s = Slot dimension (ft)

## General Approach

The temperature distribution in the simulated turbine blade specimens was calculated using the analytical method described below. First, the temperature distribution was calculated for each test condition and airfoil configuration based on estimated boundary conditions. These estimated conditions were obtained using an airfoil pressure profile similar to the one shown in Figure A-1. The velocity profile, flow conditions, and gas side heat transfer coefficients were obtained from the pressure profile. Figure A-2 showns typical gas side heat transfer coefficients obtained in this manner.

After measuring the specimen airfoil surface temperatures in the test rig, the boundary conditions were adjusted as necessary to obtain agreement between measured and calculated surface temperatures. These corrected temperature distributions were used in the strain analysis to predict the number of cycles required to initiate thermal fatigue cracking in each airfoil.

## Analytical Method

The transient and steady-state temperature distributions within an airfoil were calculated using a digital computer program which incorporates classical heat transfer solutions. The geometry was defined by a nodal system as shown in Figure A-3. The system of detail "A" in Figure A-3 was mathematically represented in the solution as shown in Figure A-4.

The steady-state temperature distribution was found by solving the steady-state heat balance at each node

$$\Sigma Q_N = 0 \qquad (1)$$

for N equations simultaneously. At Node 1 of Figure A-4,

$$Q_g - Q_{1-3} - Q_{1-2} = 0$$

where:

$$Q_g = h_g A_L (T_g - T_1)$$

$$Q_{1-3} = \frac{k A_{1-3}}{L_{1-3}} (T_1 - T_3)$$

$$Q_{1-2} = \frac{k A_{1-2}}{L_{1-2}} (T_1 - T_2)$$

The transient temperature distribution was found by solving the following equation:

$$Q_N = \frac{m\, c_p\, (T_{N'} - T_N)}{\Delta\theta} \qquad (2)$$

At Node 1 of Figure A-4,

$$Q_g - Q_{1-3} - Q_{1-2} = \frac{m_1\, c_p\, (T_{1'} - T_1)}{\Delta\theta}$$

It can be shown that equation (2) is stable and a good solution when:

$$\Delta\theta \leq \frac{m\, c_p}{\sum\left(\frac{k\, A}{L} + h\, A\right)} \qquad (3)$$

In the region near the leading edge of the airfoil, an equation for the heat transfer coefficients on a cylinder in cross flow was used:

$$\frac{h\, D}{k_f} = 1.14 \left(\frac{\rho_f\, V_\infty\, D}{\mu_f}\right)^{0.5} (Pr_f)^{0.4} \left[1 - \left(\frac{\phi}{90}\right)^3\right] \qquad (4)$$

$$\infty \leq \phi \leq 80°$$

In the region of laminar flow, the following equation was used:

$$\frac{h\, X}{k_f} = 0.332 \left(\frac{\rho_f\, V_\infty\, X}{\mu_f}\right)^{0.5} (Pr_f)^{0.333}\, F_{LAM} \qquad (5)$$

In the region of turbulent flow, the following equation was used:

$$\frac{h\, X}{k_f} = 0.0296 \left(\frac{\rho_f\, V_\infty X}{\mu_f}\right)^{0.8} (Pr_f)^{0.333} \qquad (6)$$

Temperature dependent fluid properties were evaluated in equation (4) at a reference temperature defined by:

$$T_f = 0.5 \ (T_\infty + T_w)$$

and were evaluated in equations (5) and (6) at a reference temperature defined by:

$$T_f = 0.5 \ (T_s + T_w) + 0.22 \ (T_{aw} - T_s)$$

The gas temperature, $T_g$, used in the heat transfer equations was $T_{aw}$.

## $h_{coolant}$ & $T_{coolant}$

The coolant side heat transfer coefficient was calculated using the fully developed pipe flow equation:

$$\frac{h \ d_o}{k_o} = 0.024 \left( \frac{\rho_o \ V_c \ d_o}{\mu_o} \right)^{0.8} (Pr_o)^{0.4} \qquad (7)$$

The coolant temperature was calculated using the simple heat balance:

$$h_c A_c \ (T_m - T_{c1}) = M \ c_p \ (T_{c2} - T_{c1}) \qquad (8)$$

Equation (8) was solved on a computer for the coolant temperature, $T_c$, along the length of the cooling passage.

## Film Temperatures

When film cooling was used, the film temperatures were calculated using a film correlation presented by Hartnett, Birkebak and Eckert in Ref. 1:

$$\eta = T_g - T_f = K \ (x/ \ s)^{-y}$$

where:

$$\eta = 1.32 \ (x/u \ s)^{-0.167} \qquad 10 < x/u \ s < 30$$

$$\eta = 2.65\ (x/u\ \ s)^{-0.372} \qquad 30 < x/u\ \ s < 100$$

$$\eta = 9.16\ (x/u\ \ s)^{-0.640} \qquad 100 < x/u\ \ s < 1000$$

and:

$$u = \frac{\rho_o V_{coolant}}{\rho_f V_{gas}}$$

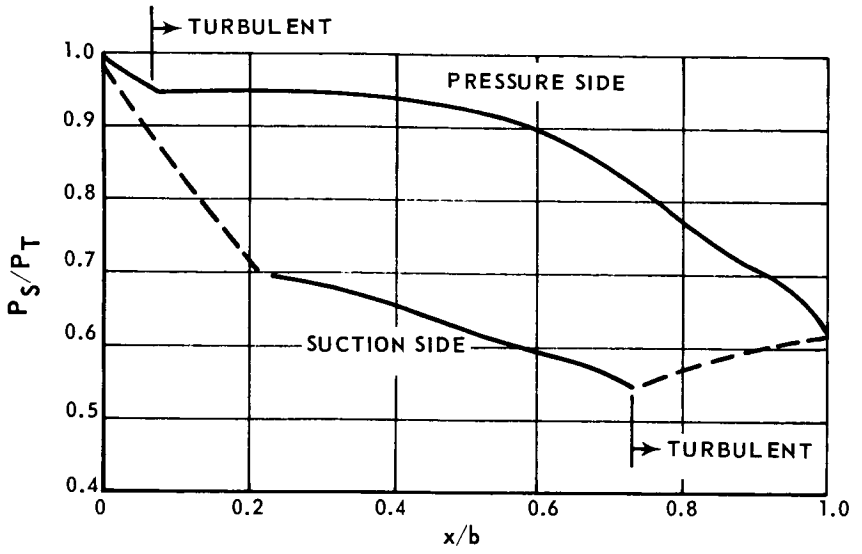


Figure A-1 Typical Pressure Distribution

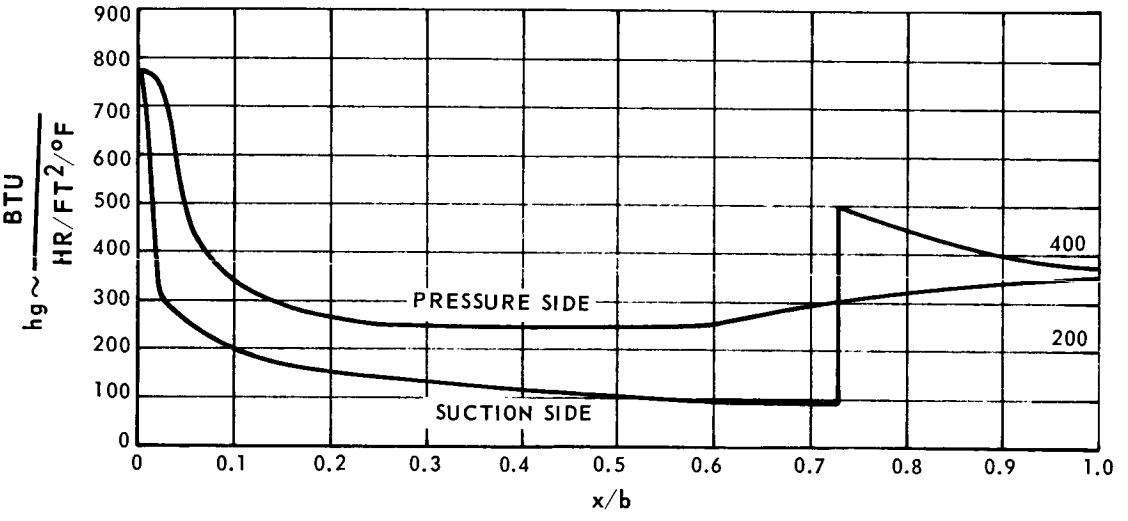


Figure A-2 Typical Heat Transfer Coefficients

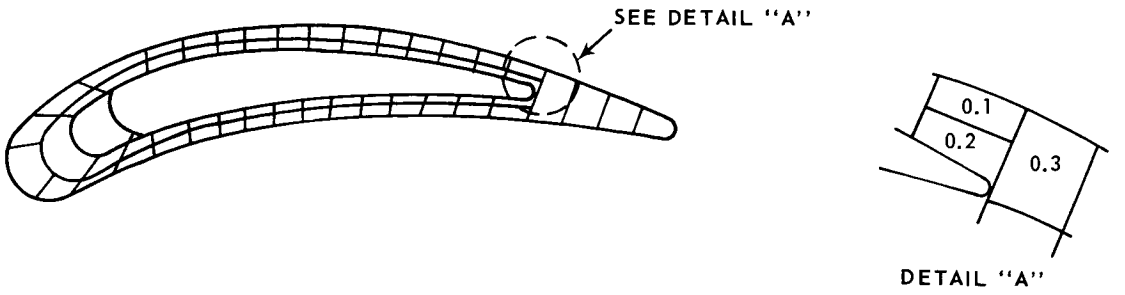


Figure A-3 Typical Nodal System

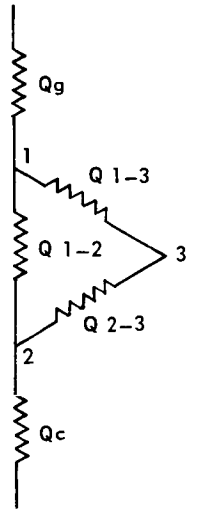


Figure A-4 Typical Mathematical Representation of Nodal System

## Reference

1. Hartnett, Birkebak and Eckert, "Velocity Distribution, Temperature Distributions, Effectiveness and Heat Transfer for Air Injected Through a Tangential Slot into a Turbulent Boundary Layer", ASME Paper No. 60-HT-31.

APPENDIX B



# TURBINE AIRFOIL STRESS ANALYSIS COMPUTER PROGRAM

Prepared by: W. H. Vogel

## Nomenclature

| | | |
|---|---|---|
| $\sigma_z$ | = | Normal stress on the plane of the cross section (psi) |
| $\epsilon_z$ | = | Normal strain on the plane of the cross section (in/in) |
| $\epsilon_p$ | = | Plastic strain component (in/in) |
| $E$ | = | Modulus of elasticity (psi) |
| $\alpha$ | = | Thermal expansion coefficient (in/°F) |
| $x, y$ | = | Axes in plane of cross section |
| $z$ | = | Axis perpendicular to cross section |
| $w$ | = | Displacement in z direction (in) |
| $\delta_k$ | = | Free thermal expansion (in) |
| $\Delta T$ | = | Temperature - 70°F |
| $F$ | = | Axial applied force (lb.) |
| $M_x$ | = | Applied bending moments about x-axis (in-lb.) |
| $M_y$ | = | Applied bending moments about y-axis (in-lb.) |
| $\sigma_p$ | = | Virgin material proportional limit (psi) |

| | | |
|---|---|---|
| 0.2% yield strength | = | Stress when virgin plastic strain is 0.2% (psi) |
| 0.02% yield strength | = | Stress when virgin plastic strain is 0.02% (psi) |
| $R_1, R_2, R_3$ | = | constants |
| a, b, c, d, B, K | = | constants |

## CAPABILITIES

The program can be summarized by stating that it:

- Applies to any geometric shape which was basically prismatic.
- Calculates the normal stress, $\sigma_Z$, and strain $\epsilon_Z$, on planes perpendicular to the prism axis.
- Calculates the stress and strain due to arbitrary temperature distributions on planes which are normal to the prism axis.
- Includes the effect of an arbitrary applied axial force and bending moments about the two coordinate axes in the plane normal to the axis.
- Calculates the stress and strain in the elastic plastic range.
- Includes hysteresis effects.

## ASSUMPTIONS

The basic assumptions for this program were that:

- The body is a prism - i.e.: the cross section is constant with length.
- The temperature varies over the cross section but is constant with length.
- The cross section examined is a reasonable distance from the free end, i.e. one-third the largest lateral dimension of the cross section, so that end effects can be neglected.
- Poisson's Ratio effects can be neglected.
- Initially plane cross sections remain plane after heating and loading and the consequent bending and elongation.
- Externally-applied loads were not so large that the body yields grossly.
- The stress-strain curve can be represented by a logarithmic curve tangent at the proportional limit to the elastic portion of the actual stress-strain curve and passing throught two more points in the plastic portion of the actual stress-strain curve.

Then, upon substituting equation (4) into equation (3):

$$\sigma_{Z_k} = E_k \left\{ - \alpha_k \Delta T_k + R_1 + R_2 x_k + R_3 y_k - \epsilon_{p_k} \right\} \quad (5)$$

The stress must satisfy the equilibrium equations:

$$\sum_{k=1}^{n} \sigma_{Z_k} \Delta A_k = F \quad (6)$$

$$\sum_{k=1}^{n} \sigma_{Z_k} X_k \Delta A_k = M_y$$

$$\sum_{k=1}^{n} \sigma_{Z_k} Y_k \Delta A_k = M_x$$

where F, $M_y$, and $M_x$ are the applied load and moments. The stress from equation (5) is substituted into these equations and the system is solved from the unknown constants $R_1$, $R_2$, and $R_3$.

The resulting equations feature the explicit appearance of the unknown plastic strain components and can be solved by an iterative technique. The first iteration involves solving the system of equations (6) for $R_1$, $R_2$, and $R_3$, assuming values of $\epsilon_p$ derived from the previous history. Equation (5) then gives the iterative stress values. Using this stress and the material stress-strain curves, the corresponding first iterative plastic strain components are obtained. From these plastic strains a new assumed set of plastic strains are derived and substituted into equation (6) which are again solved for $R_1$, $R_2$, and $R_3$. This procedure was continued until the set of plastic strains calculated upon the $r^{th}$ and $(r-1)^{st}$ iteration satisfy the following convengence criterion:

$$\sum_{k=1}^{n} \left[ \epsilon_{p_k}(r) - \epsilon_{p_k}(r-1) \right]^2 \Big/ \sum_{k=1}^{n} \epsilon_{p_k}^{\,2}(r-1) < \text{Tolerance} \quad (7)$$

## ANALYSES

### Stress Analysis

Coordinate axes (x, y) are set up in the plane of the cross-section under investigation as shown in Figure B-1. The area was split into n elements of area $\Delta A_k$ with centroid locations given by $x_k$, $y_k$.

The axial normal stress, $\sigma_Z$, and strain, $\epsilon_Z$, is calculated for each centroid location. The temperature and material properties at each location must be specified.

Under the assumed compatibility condition that plane sections remain plane, the axial extension per unit length of element k at the section was

$$\frac{dw}{dz} = R_1 + R_2 x_k + R_3 y_k \tag{1}$$

If it was free, the thermal expansion per unit length of element k would be

$$\delta_k = \alpha_k \Delta T_k \tag{2}$$

The difference between the actual displacement and the free thermal expansion per unit length is the total strain due to stress.

$$\epsilon_{Z_k} = -\alpha_k \Delta T_k + R_1 + R_2 x_k + R_3 y_k \tag{3}$$

The total strain in any element corresponding to any loading condition and previous history is composed of an elastic component and a plastic component, Figure B-2:

$$\epsilon_{Z_k} = \sigma_{Z_k}/E_k + \epsilon_{p_k} \tag{4}$$

## Material Stress-Strain Analysis

a. Constant Temperature

The plastic strain component at any point is determined by the plastic hysteresis loop developed during the previous history. This loop is defined by the minimum and maximum plastic strains in the history, the yield stresses at these strains, and the range defining curves connecting the minimum and maximum plastic strains, as shown in Figure B-3.

These curves are:

- Virgin curve - $\sigma_Z$ - proportional limit = $B\epsilon_p^k$
- Positive stress - $\sigma_Z - a = B(\epsilon_p - \epsilon_{pmin})^k$
- Negative stress - $\sigma_Z + c = B(-\epsilon_p - \epsilon_{pmax})^k$

where B and k are constants. The second and third statements are merely shiftings of the virgin curve.

The plastic strain corresponding to a new stress depends on the relationship of the previous strain to this loop.

Referring to Figure B-2, if the previous condition is given by point 1, a new condition can be given e.g. by:

- Point 2 - if the stress increases,
- Point 3 - if the stress decreases but compressive yielding does not occur.
- Point 4 or 5 - if compressive yielding occurs.

From Point 3 a new condition can be:

- on the same $\epsilon_p$ line - if no yielding occurs,
- Points 4 or 5 - if compressive yielding occurs, or
- Point 2 - if tensile yielding occurs

From Point 5 a new condition can be:

- Point 10 - if the stress increases but no yielding occurs,
- Point 8 - if tensile yielding occurs, or
- Point 11 - if the stress becomes more compressive.

Similarly from Point 10 the next condition could be on the same $\epsilon_p$ line, Point 11, or Point 8 depending on whether yielding occurs or not and whether the yielding is tensile or compressive.

From Point 8 the next condition could be Point 12, Point 9, or Points 4, 5, etc.

b. Varying Temperature

When a new load case involves introduction of a new temperature distribution, all the material properties in the calculation are immediately changed to those at the new temperatures. These quantities, proportional limit, 0.2% yield strength, 0.02% yield strength, E , and $\alpha$ do not involve the history.

New range defining curves are calculated using the new properties before the new plastic strain components are evaluated.

The minimum and maximum plastic strains in the history are carried over to define the new plastic hysteresis loops and the first new iteration is based on assumed plastic strain values derived from the previous plastic strain values.

## Computer Program

The following describes the input and the output of the computer program.

a. Input

1. General

A. Title card: Assign any desired title. Cite the materials from which the part is made.

B. Enter the number of materials used in Column 10. Up to through (3) materials are permissible.

2. Materials Tables

For each material enter the following properties from 100°F to 2500°F in steps of 100°F in fields of 14 and five to a card.

C. $\sigma_p$ = proportional stress limit (psi)

D. $\sigma_{0.02} - \sigma_p$ (psi)

E. $\sigma_{0.2} - \sigma_p$ (psi)

F. Elasticity modulus (psi)

G. Coefficient of thermal expansion (in/in/°F)

C* - G* Materials properties for other materials

H. Put in Columns 1-14: 0.0002, and in Columns 14-28: 0.002

3. Specific

J. Put between Columns 41-44 the sum of elements (up to 200 are permissible).
Columns 45-48 sum of temperature - load cases.
Columns 53-62 tolerance for plastic strain check (recommended $10^{-3}$ or $10^{-4}$)

Note: the number for the sum of points must end in Column 44 and the number for the temperature-load cases in Column 48.

4. Geometry (in fields of 14 and 5 to a card)

K. Areas of the elements ($in^2$)

L. X coordinate to the center of each element (in)

M. Y coordinate to the center of each element (in)

N. (In fields of 2 and 5 to a card)
Number of the material of which the specific element consists (1, 2, or 3). The number for the material is defined by the order in which the materials are cited in the title card and compiled under the Materials Tables.

5. Temperature and Load (in fields of 10)

O. Temperature for each element (° F)

P. Columns 1-10 external force (lbs)
Columns 11-20 external moment $M_y$ (in-lbs)
Columns 21-30 external moment $M_x$ (in-lbs)

O*-P* Repeat for further load cases (a card with the external load must follow each temperature case.)

Note:

1. The moment $M_y = PX$ ($M_x = PY$) was positive if increasing X (Y) coordinate gives an increasing positive bending stress, Figure B-1. The positive stress direction coincides with the direction of Force P.

2. The origin of the X-Y coordinate system ought to coincide with the point where the Force P acts. If this is not the case, counter-balancing moments must be put in.

b. Output

The program prints out:

- Title
- Geometry input
- Temperature, stress, plastic strain, and total strain for each element.
- $R_1$ the average extension of the analyzed part (in/in)
  $R_2$ the slope of the cross section in the z-x plane
  $R_3$ the slope of the cross section in the z-y plane
- Load (pull, moment $M_y$, moment $M_x$)

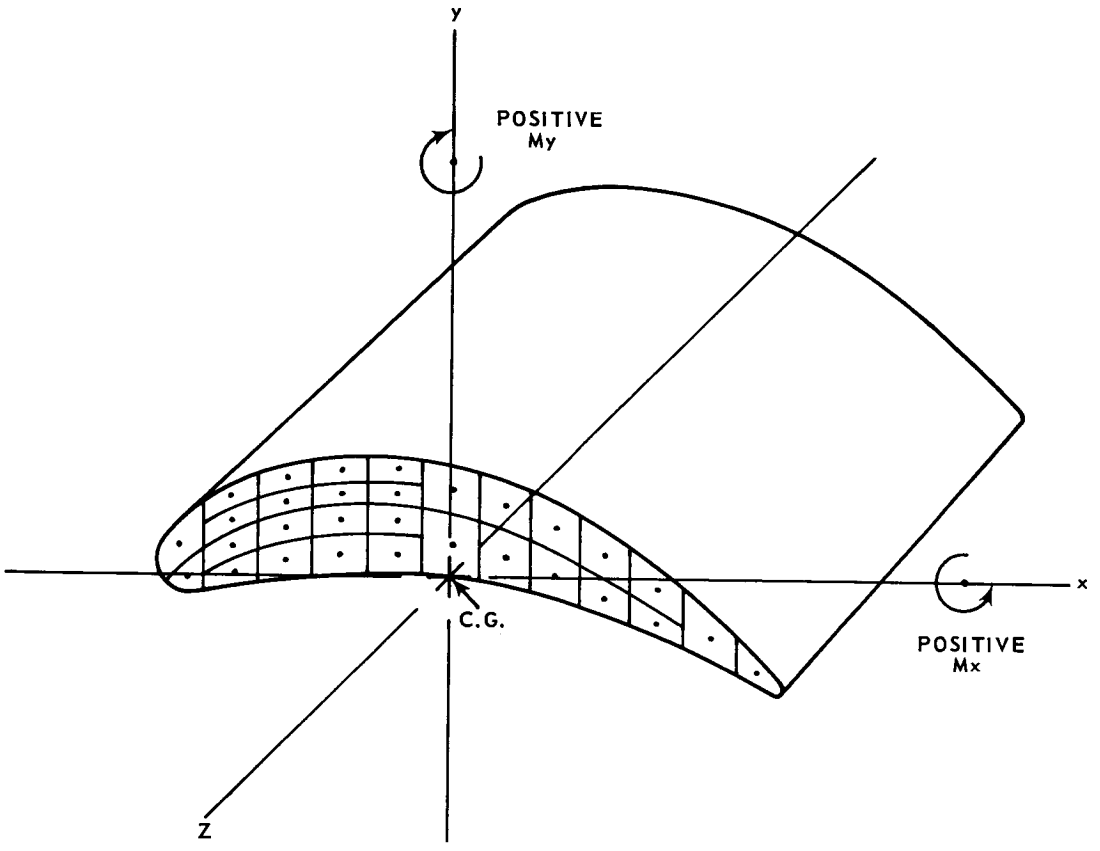


Figure B-1 Typical System of Coordinate Axes

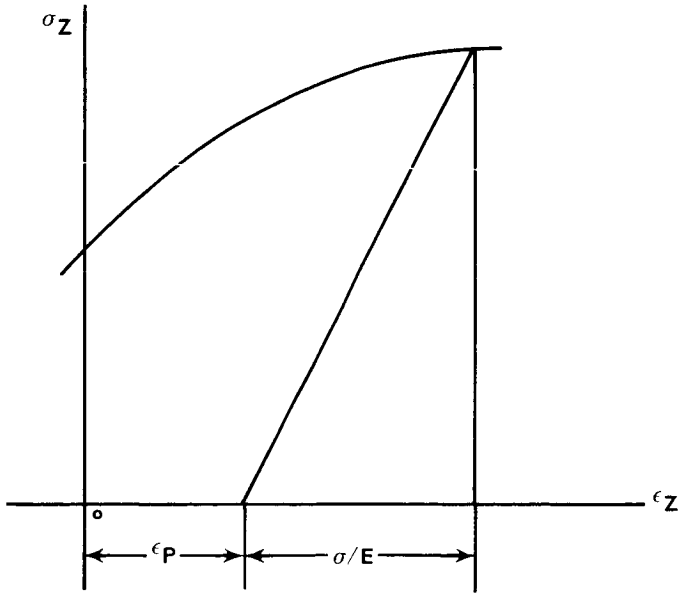


Figure B-2 Stress-Strain Curve

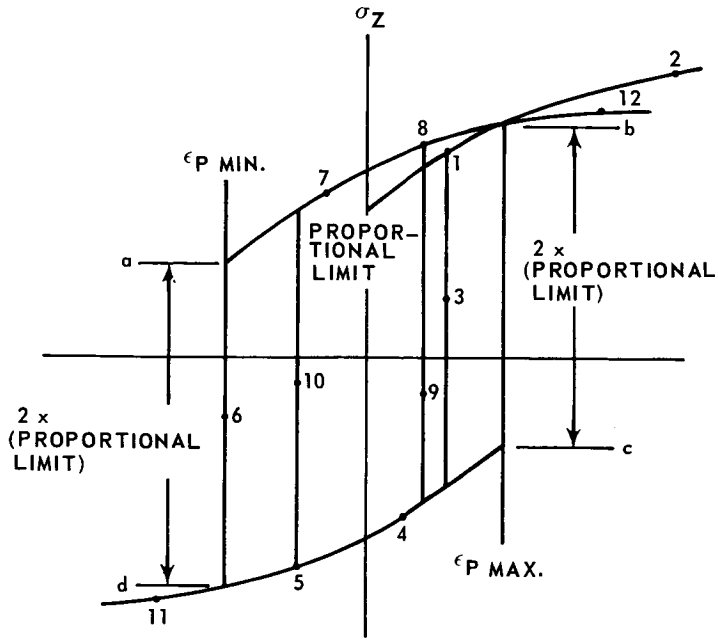


Figure B-3 Stress-Plastic Strain Curve

# APPENDIX C

## TURBINE BLADE SPECIMEN

## MATERIAL PROPERTIES

Figures C-1 through C-12 and C-16 through C-32 present the properties of the two specimen materials used to predict the life of the blade specimens tested under this program. Figures C-13 through C-15 show the specimen configurations used to obtain the constant temperature strain cycling fatigue data.

The density of the two test materials is 0.297 lb/cu-in for PWA 663 (B-1900) and 0.0280 lb/cu-in for PWA 658 (IN-100).

Tensile and strain cycling fatigue properties for PWA 658 material was obtained from the same material heat (C-650) as the turbine blade specimens. Tensile data was obtained for aged and unaged material. The blade specimens were aged.

Limited tensile and smooth specimen strain cycling fatigue properties for PWA 663 material were obtained from the same material heat (54V4123) as the turbine blade specimens to verify existing data. Notched specimen strain cycling fatigue data for PWA 663 material was obtained from the heat of material used for the turbine blade specimens. Where there was a significant difference between the properties of the material heat being used for the blade specimens and existing data, such as found in the tensile properties, the curves were drawn based on data from material heat 54V4123.

Other properties of the materials included were obtained from existing handbook data for these materials.

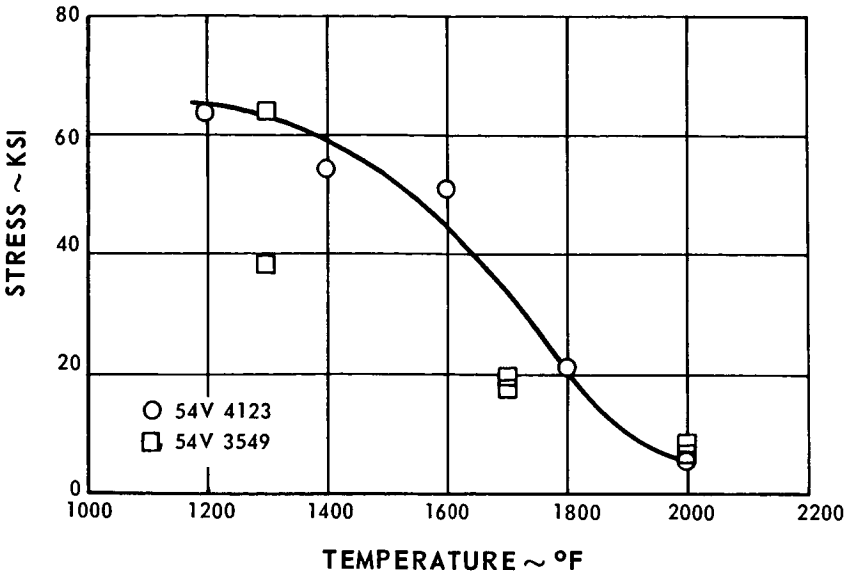


Figure C-1 Proportional Limit vs. Temperature, PWA 663 Specimen Coated per PWA 47-14L and Aged at 1650°F (10 hours)

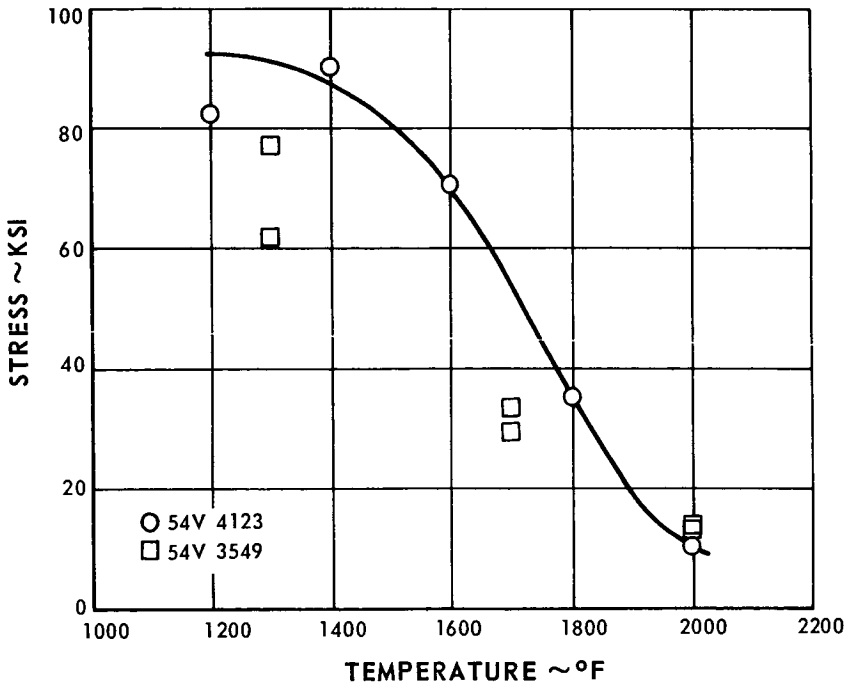


Figure C-2 0.02% Yield Strength vs. Temperature, PWA 663 Specimen Coated per PWA 47-14L and Aged at 1650°F (10 hours)

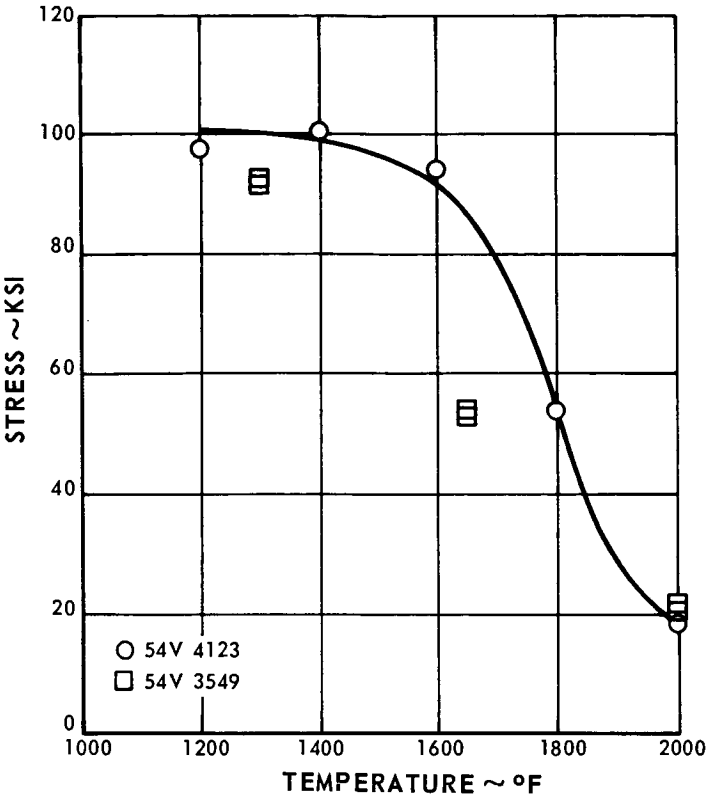


Figure C-3 0.2% Yield Strength vs. Temperature, PWA 663 Specimen Coated per PWA 47-14L and Aged at 1650°F (10 hours)

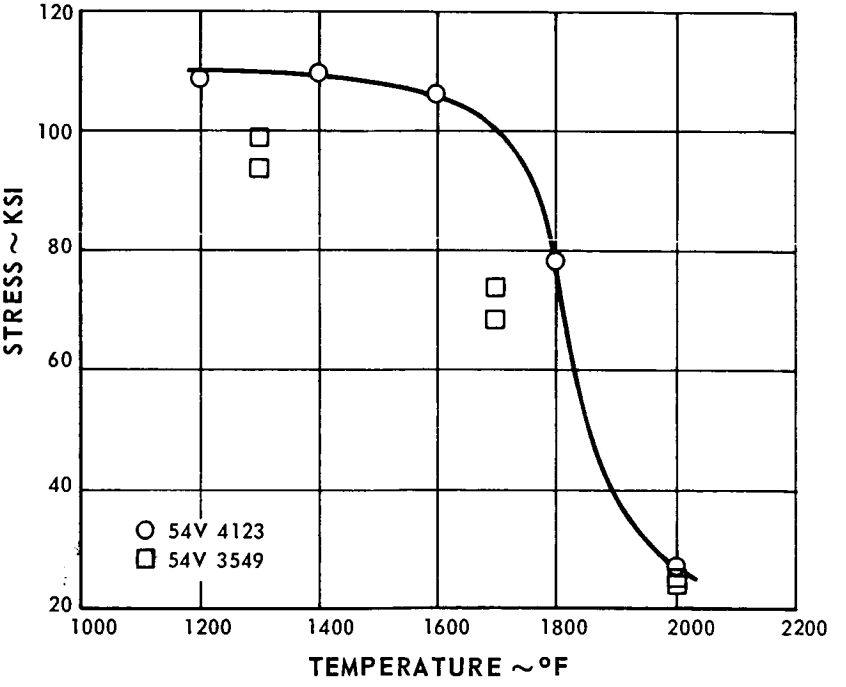


Figure C-4 Ultimate Tensile Strength vs. Temperature, PWA 633 Specimen Coated per PWA 47-14L and Aged at 1650°F (10 hours)

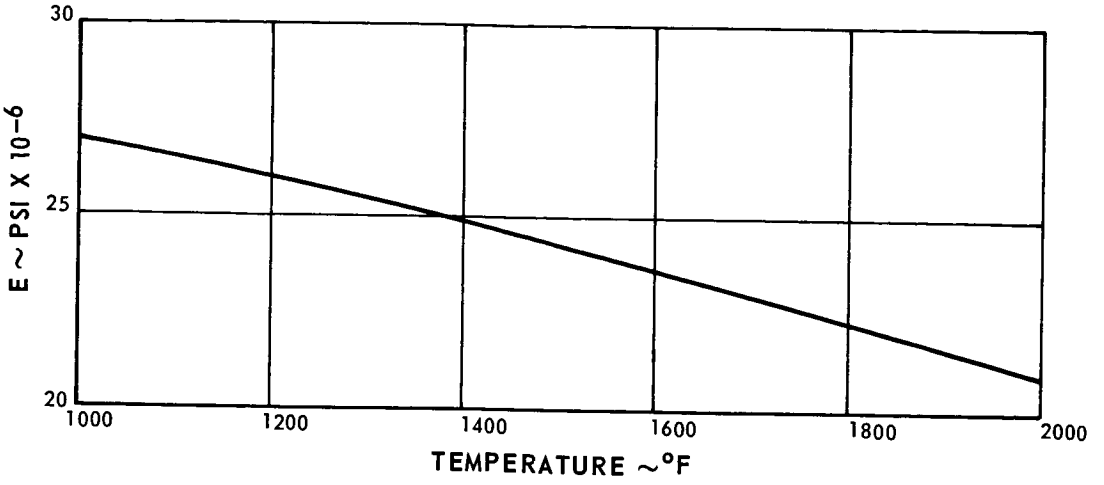


Figure C-5 Dynamic Young's Modulus vs. Temperature, PWA 663 Specimen (As Cast)

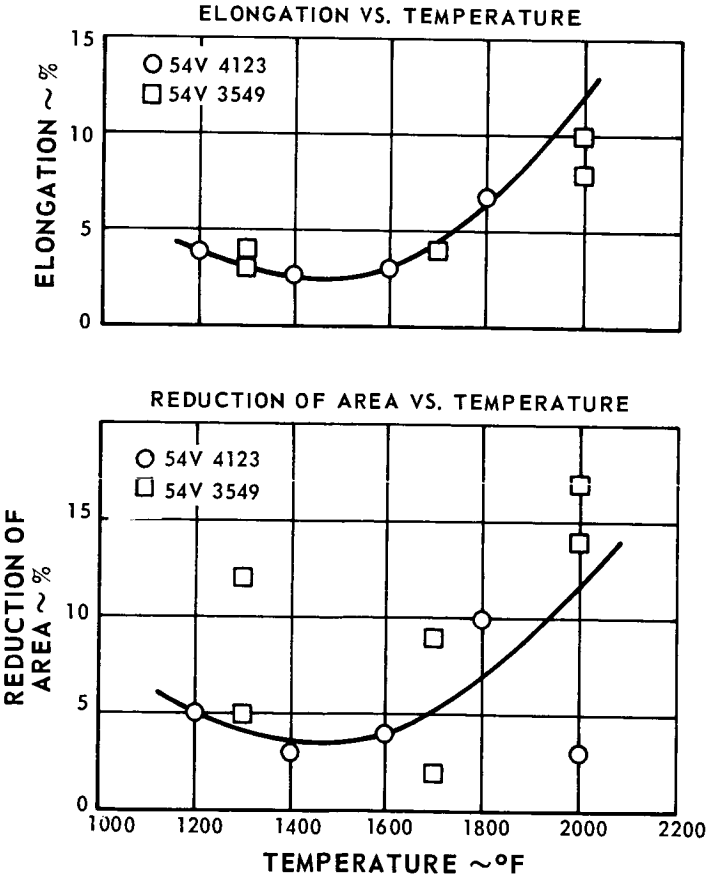


Figure C-6 Elongation and Reduction of Area vs. Temperature, PWA 663 Specimen Coated per PWA 47-14L and Aged at 1650°F (10 hours)

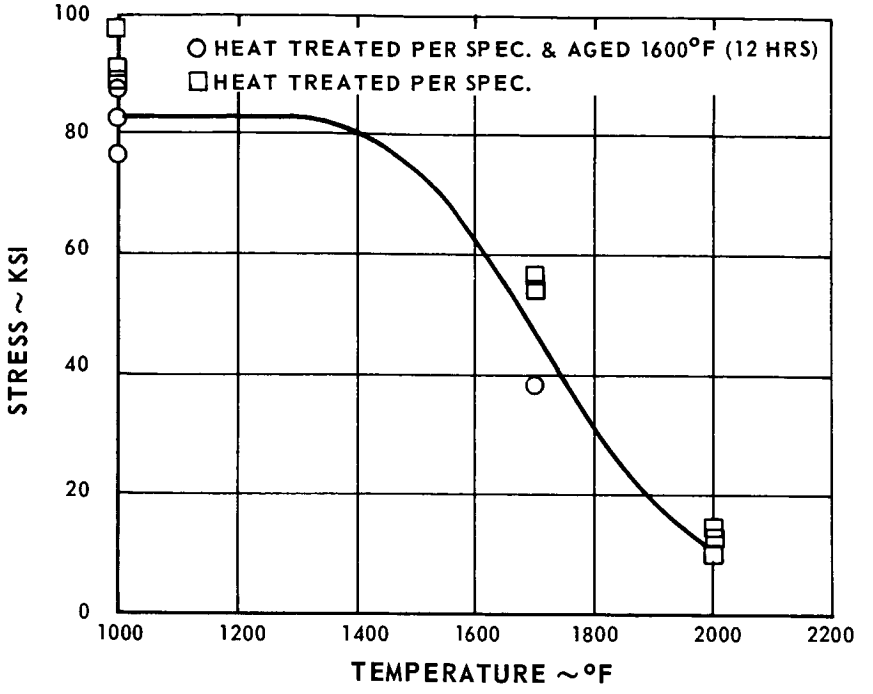


Figure C-7 Proportional Limit vs. Temperature, PWA 658 Specimen Coated per PWA 47-14L

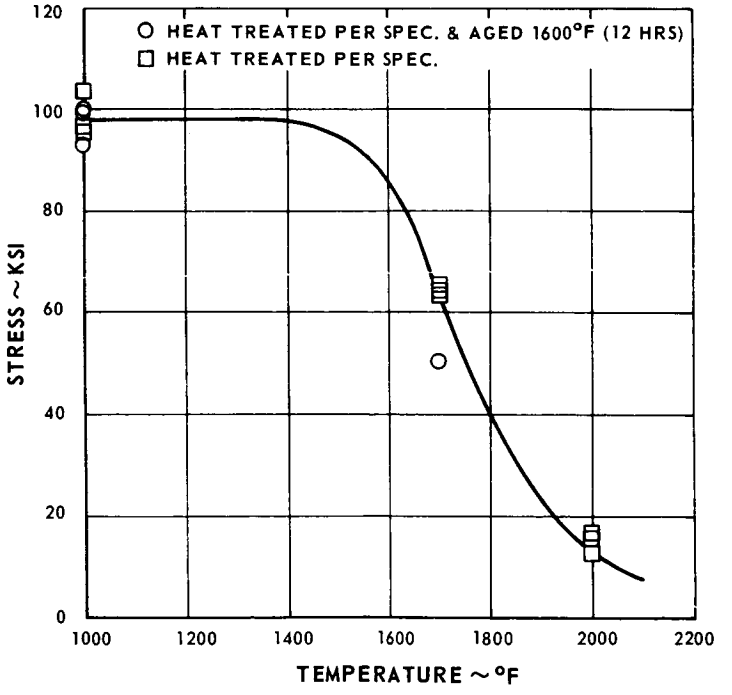


Figure C-8 0.02% Yield Strength vs. Temperature, PWA 658 Specimen Coated per PWA 47-14L

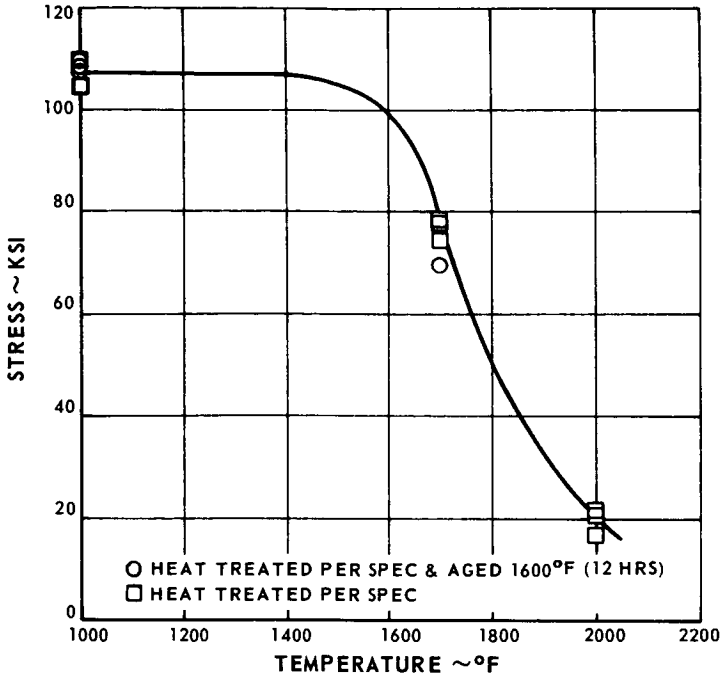


Figure C-9 0.2% Yield Strength vs. Temperature, PWA 658 Specimen Coated per PWA 47-14L

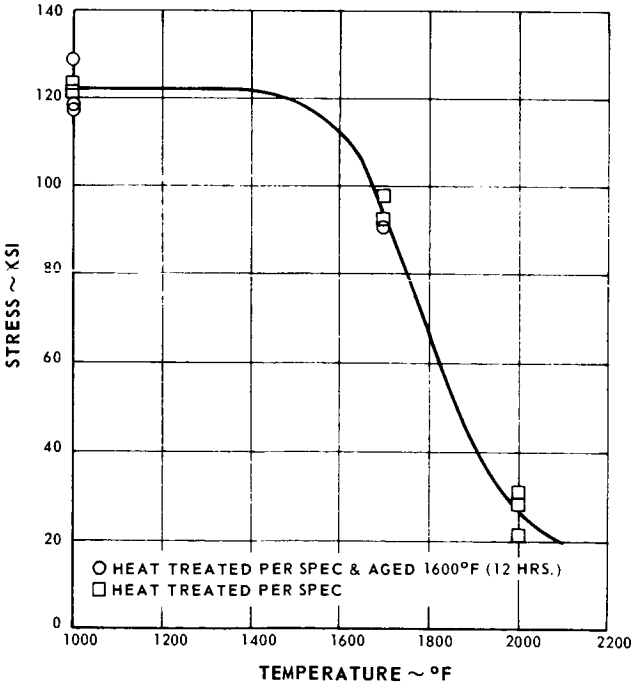


Figure C-10 Ultimate Tensile Strength vs. Temperature, PWA 658 Specimen Coated per PWA 47-14L

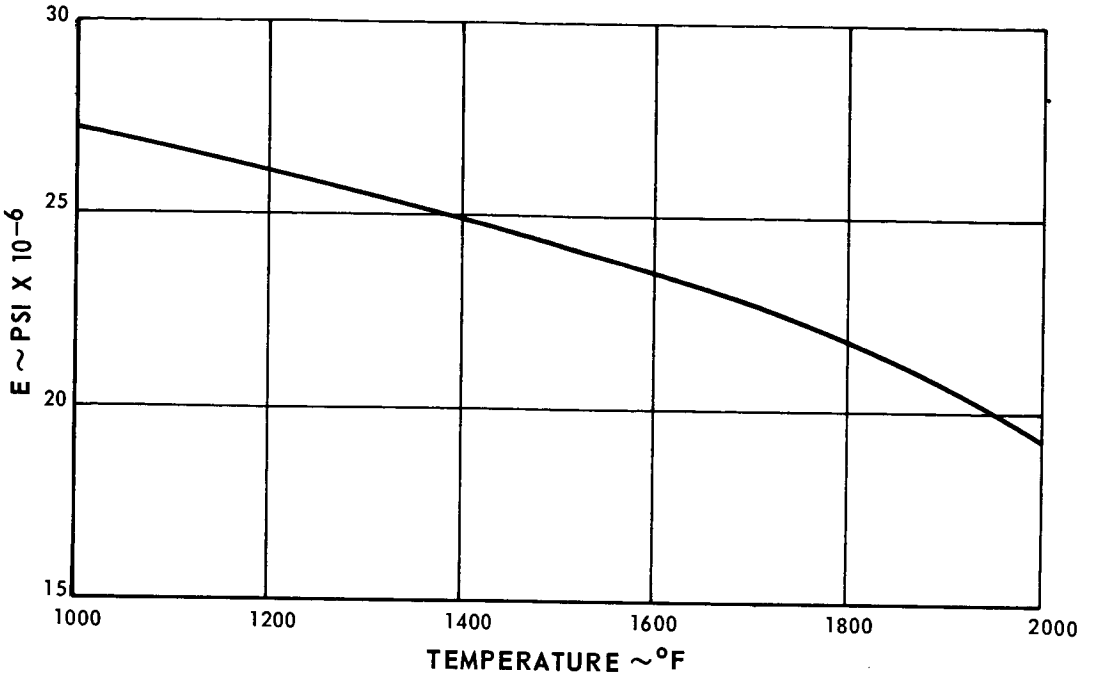


Figure C-11 Dynamic Young's Modulus vs. Temperature, PWA 658 Specimen (As Cast)

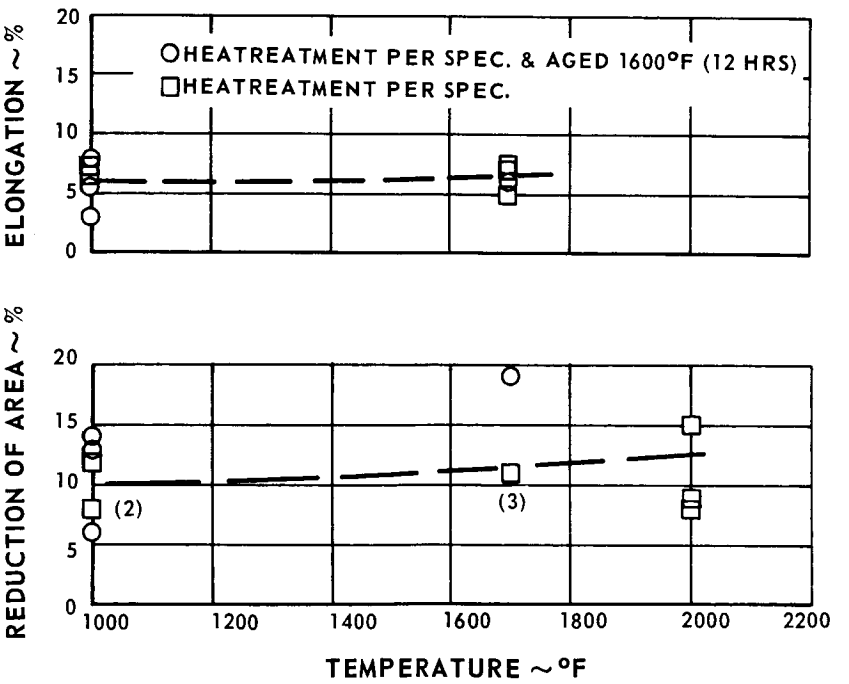


Figure C-12 Elongation and Reduction of Area vs. Temperature, PWA 658 Specimen Coated per PWA 47-14L

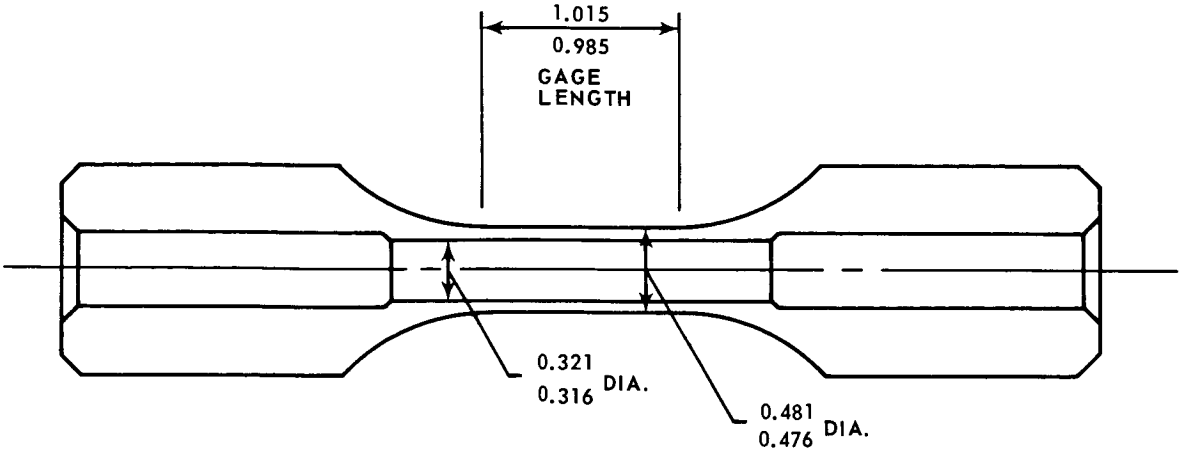


Figure C-13 Strain Specimen

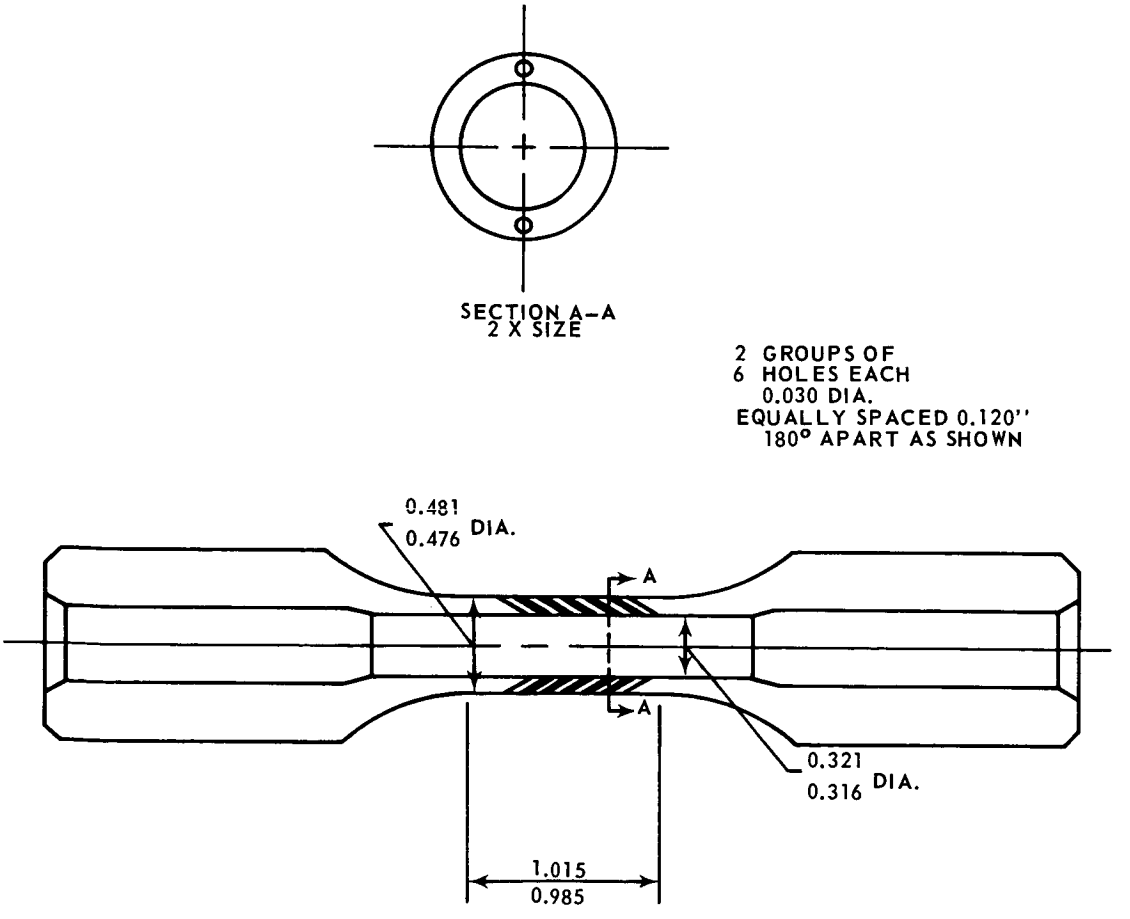


Figure C-14 Strain Specimen With Holes

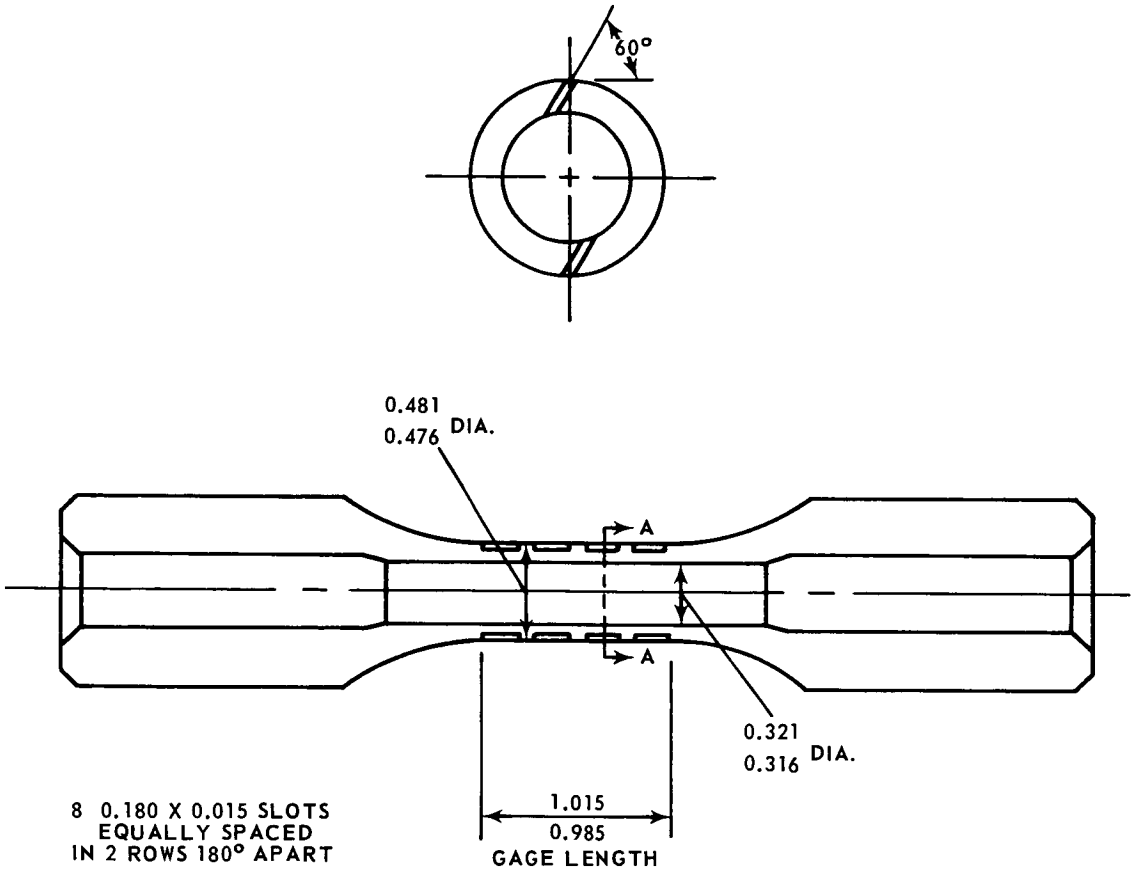


Figure C-15 Strain Specimen With Slots

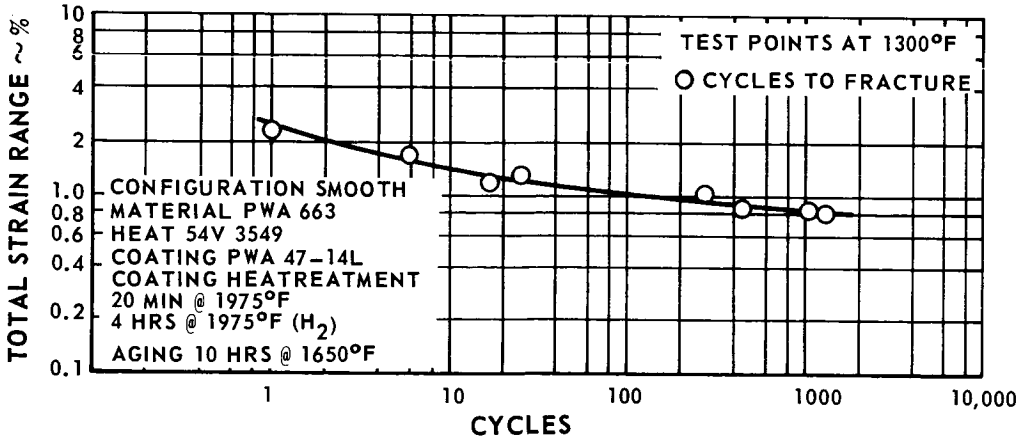


Figure C-16 Total Strain Range vs. Cycles. Constant Temperature Strain Cycling Fatigue Test of PWA 663 Smooth, 1300°F

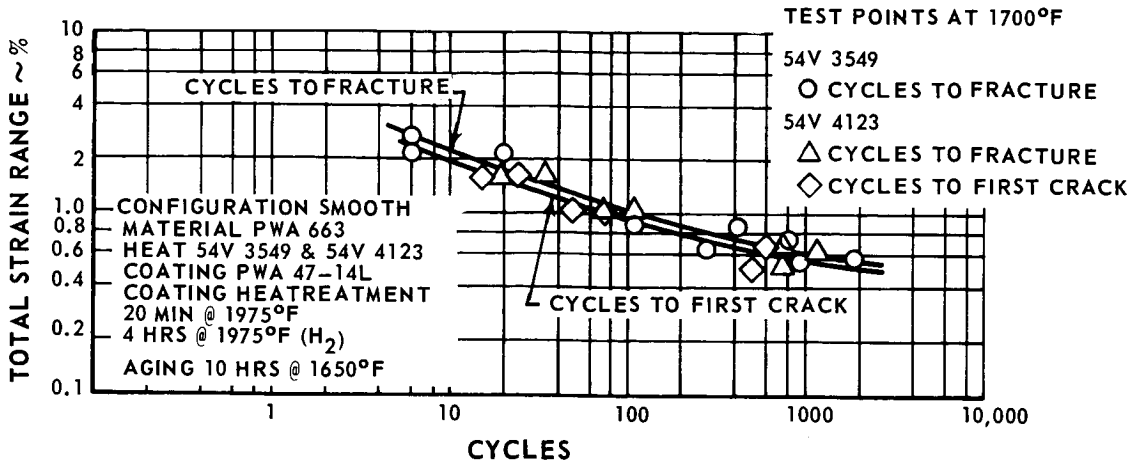


Figure C-17 Total Strain Range vs. Cycles. Constant Temperature Strain Cycling Fatigue Test of PWA 663 Smooth, 1700°F

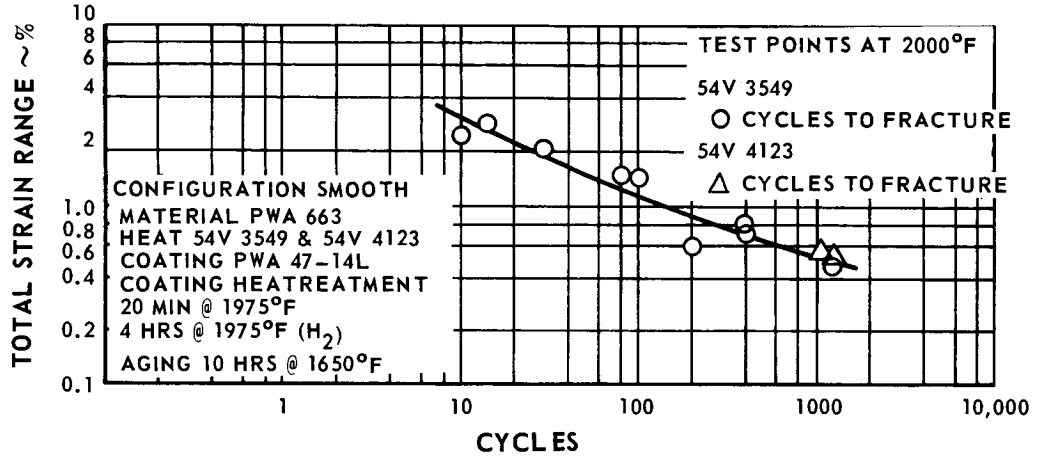


Figure C-18 Total Strain Range vs. Cycles. Constant Temperature Strain Cycling Fatigue Test of PWA 663 Smooth, 2000°F

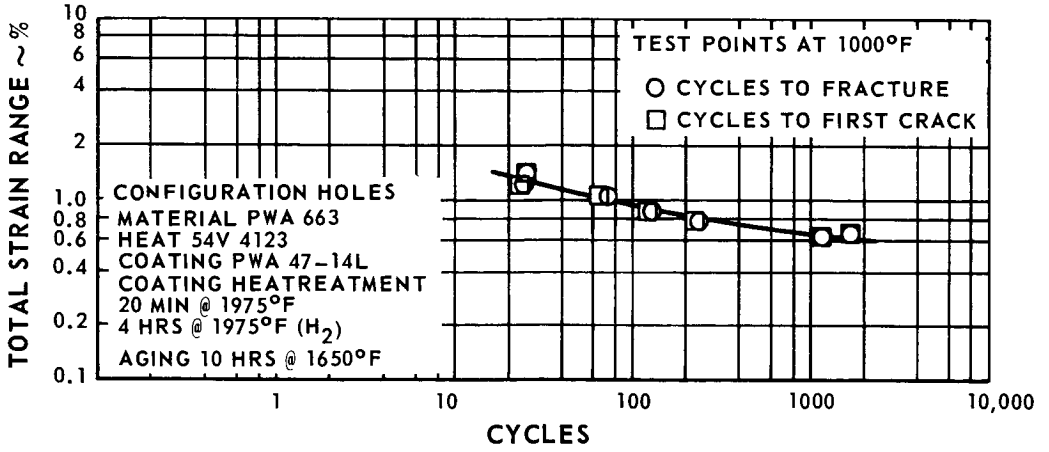


Figure C-19 Total Strain Range vs. Cycles. Constant Temperature Strain Cycling Fatigue Test of PWA 663 Holes, 1000°F

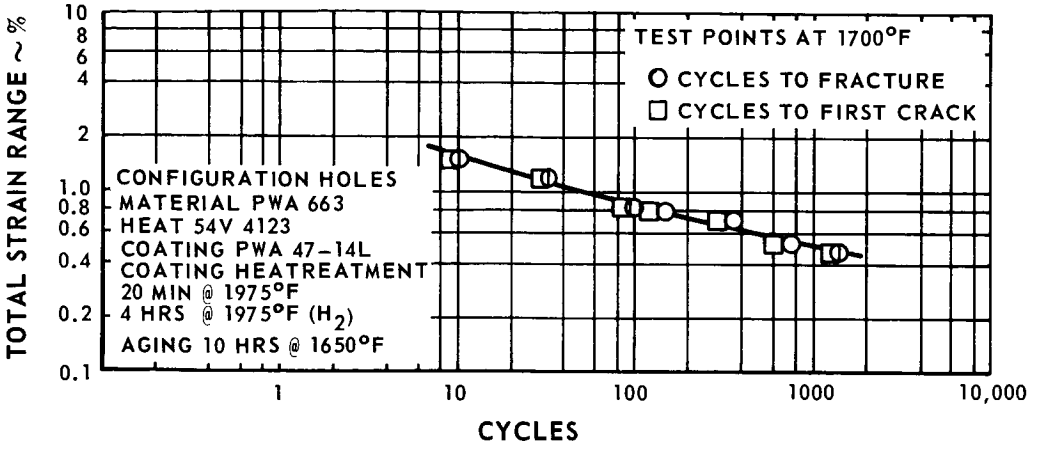


Figure C-20 Total Strain Range vs. Cycles. Constant Temperature Strain Cycling Fatigue Test of PWA 663 Holes, 1700°F

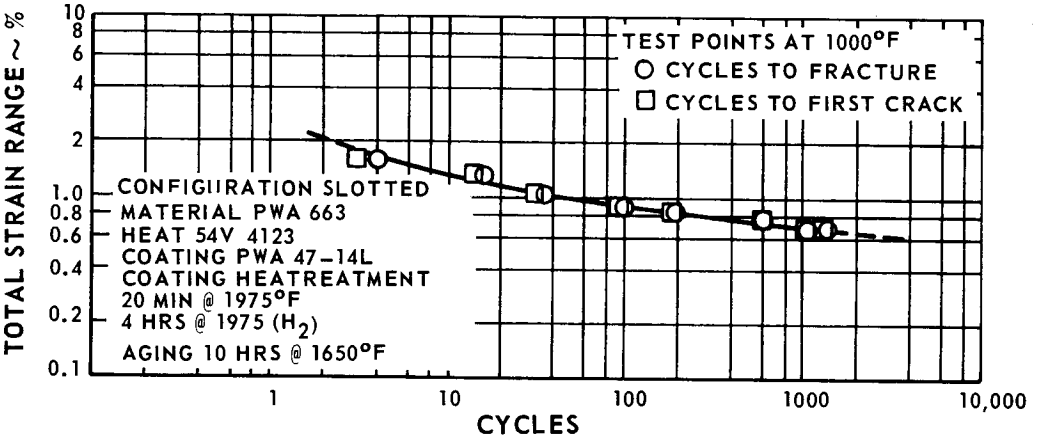


Figure C-21 Total Strain Range vs. Cycles. Constant Temperature Strain Cycling Fatigue Test of PWA 663 Slotted, 1000°F

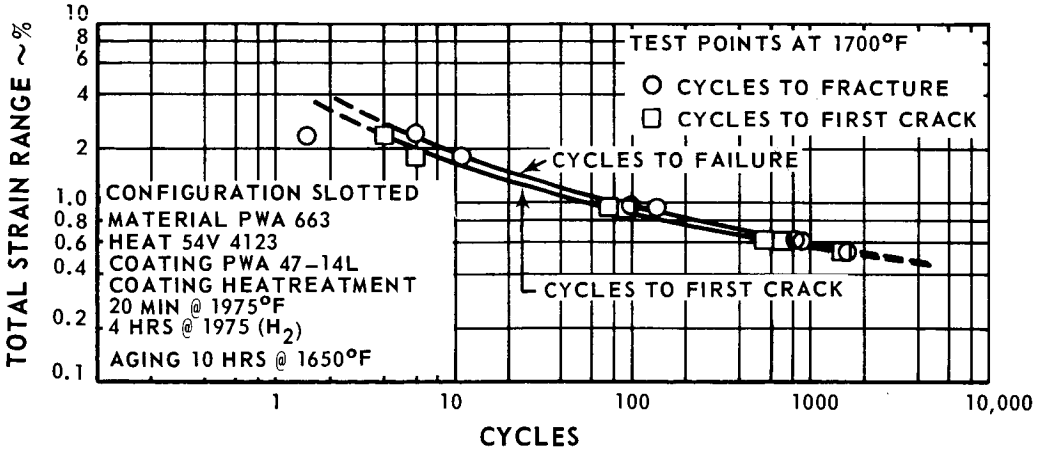


Figure C-22 Total Strain Range vs. Cycles. Constant Temperature Strain Cycling Fatigue Test of PWA 663 Slotted, 1700°F

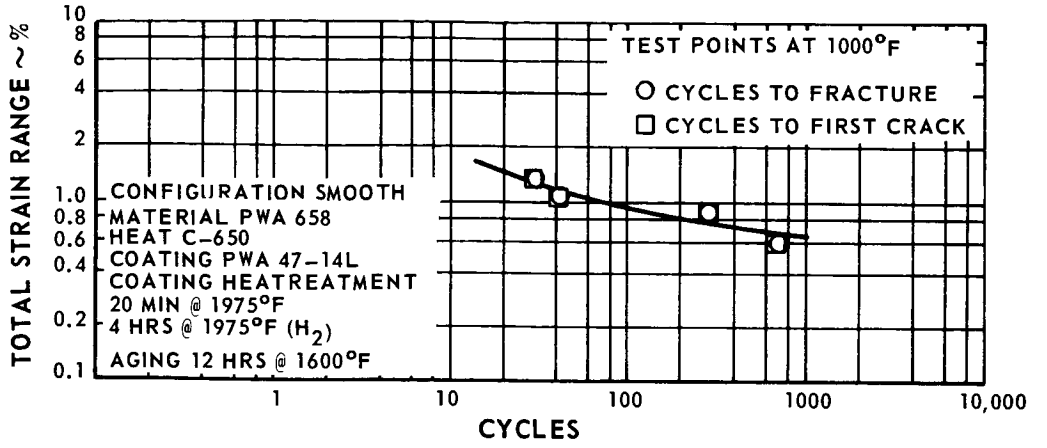


Figure C-23 Total Strain Range vs. Cycles. Constant Temperature Strain Cycling Fatigue Test of PWA 658 Smooth, 1000°F

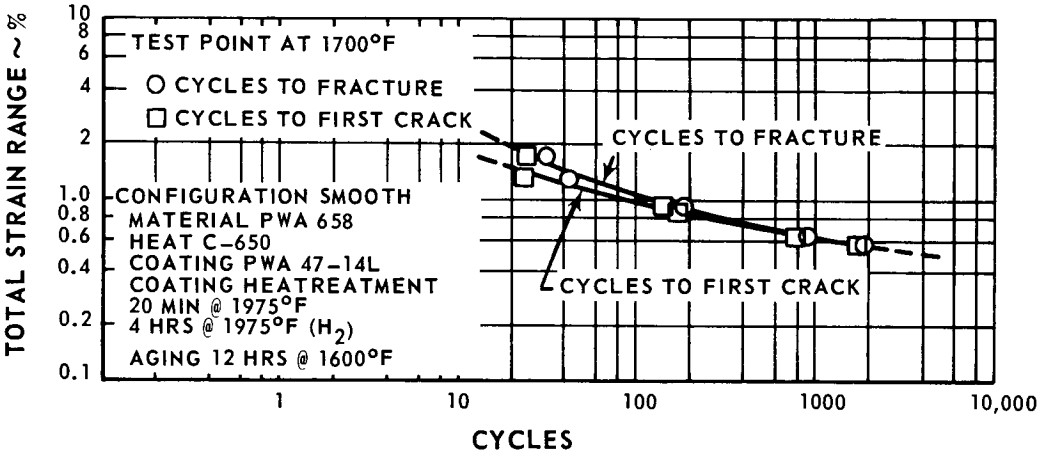


Figure C-24 Total Strain Range vs. Cycles. Constant Temperature Strain Cycling Fatigue Test of PWA 658 Smooth, 1700°F

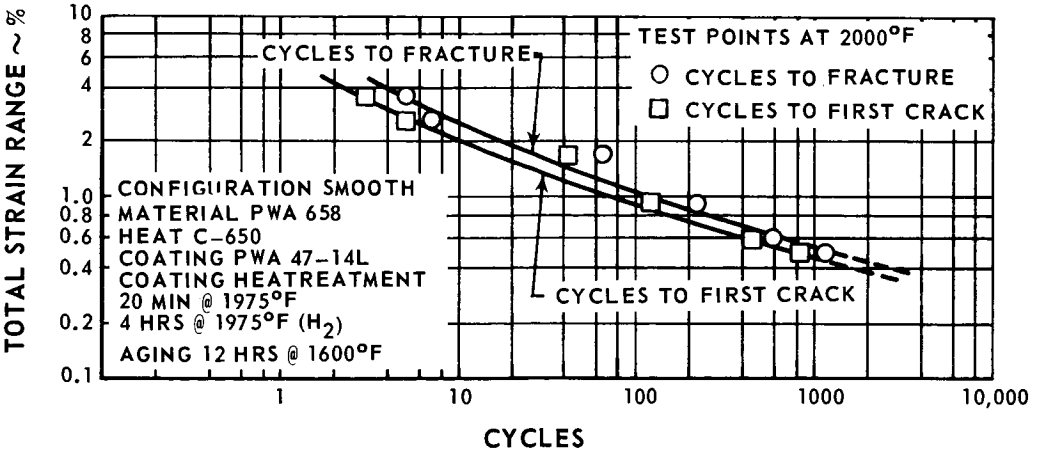


Figure C-25 Total Strain Range vs. Cycles. Constant Temperature Strain Cycling Fatigue Test of PWA 658 Smooth, 2000°F

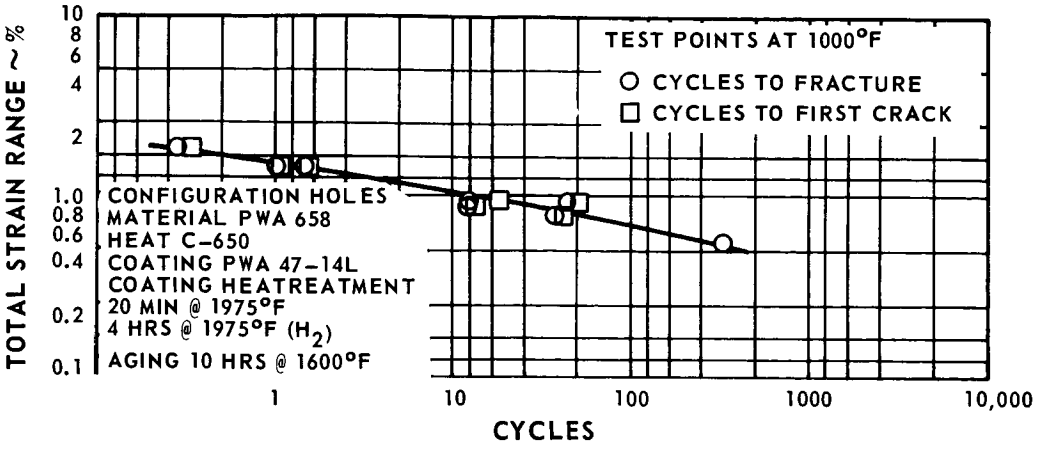


Figure C-26 Total Strain Range vs. Cycles. Constant Temperature Strain Cycling Fatigue Test on PWA 658 Holes, 1000°F

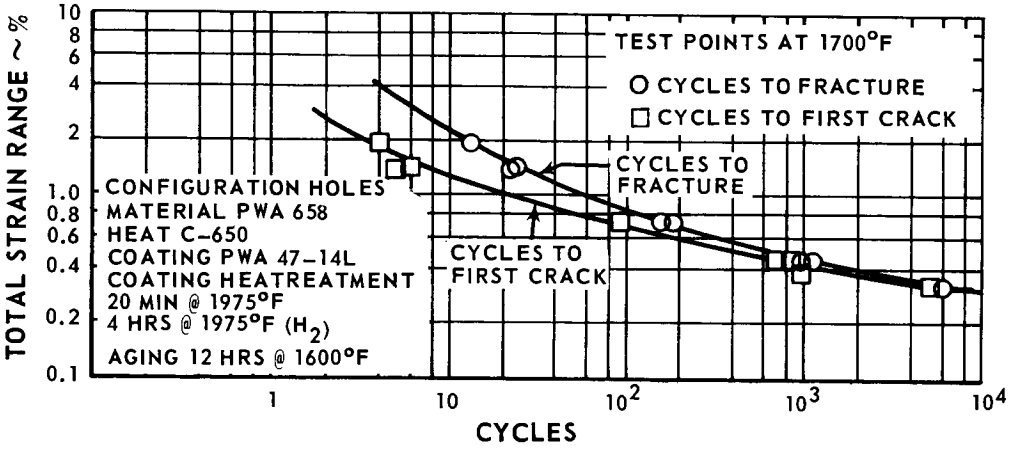


Figure C-27 Total Strain Range vs. Cycles. Constant Temperature Strain Cycling Fatigue Test of PWA 658 Holes, 1700°F

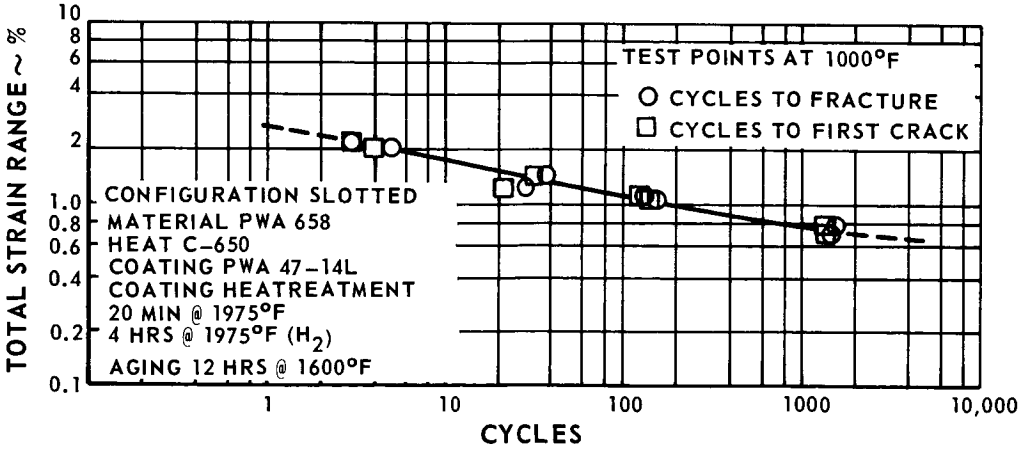


Figure C-28 Total Strain Range vs. Cycles. Constant Temperature Strain Cycling Fatigue Test of PWA 658 Slotted, 1000°F

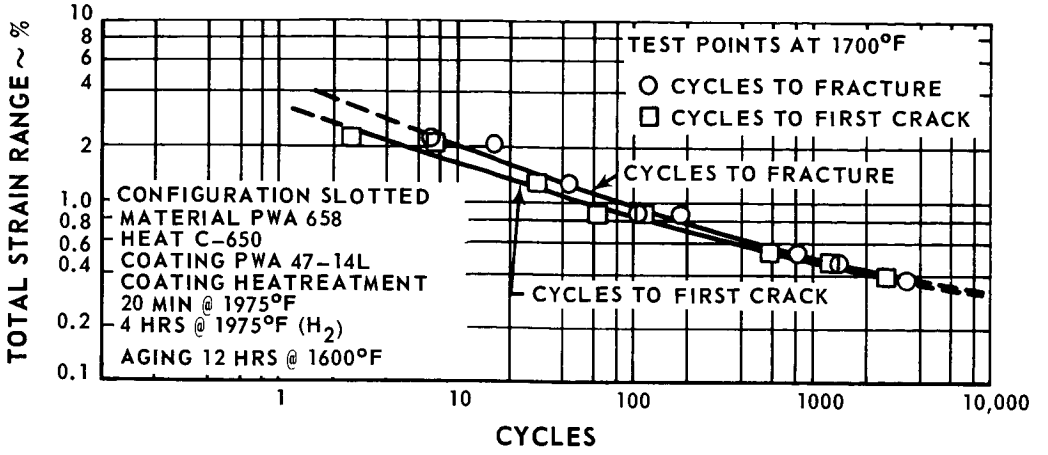


Figure C-29 Total Strain Range vs. Cycles. Constant Temperature Strain Cycling Fatigue Test of PWA 658 Slotted, 1700°F

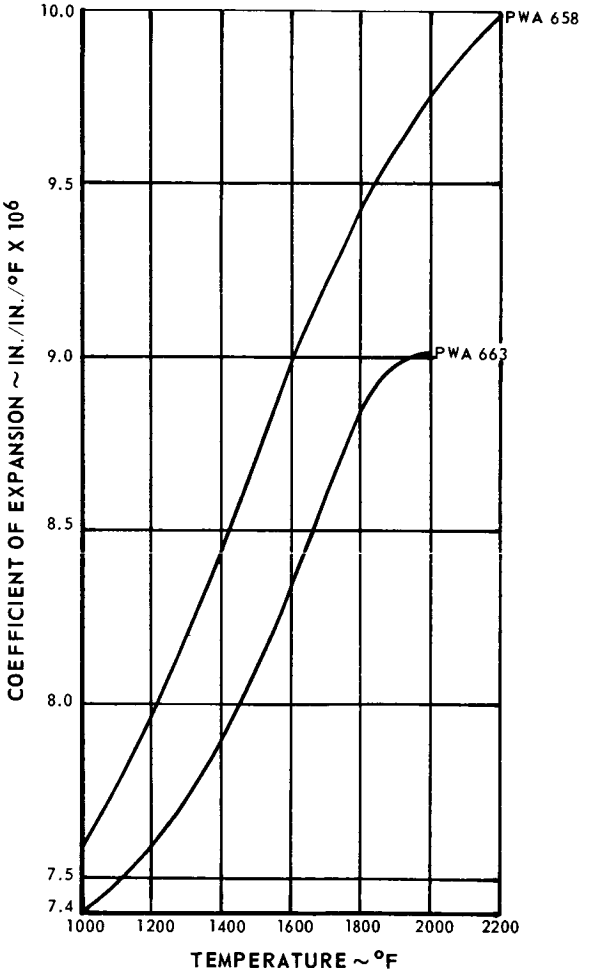


Figure C-30 Coefficient of Expansion vs. Temperature for PWA 663 and PWA 658

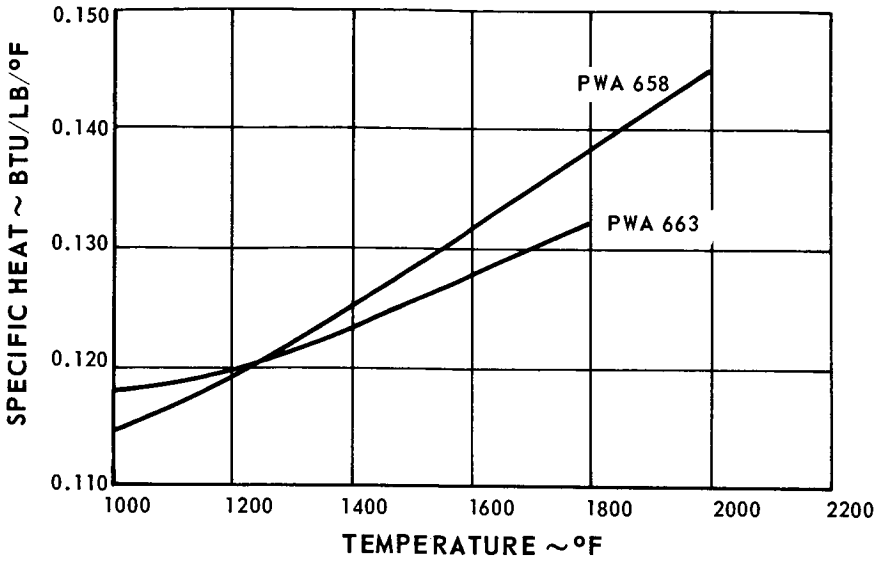


Figure C-31 Specific Heat vs. Temperature for PWA 663 and PWA 658

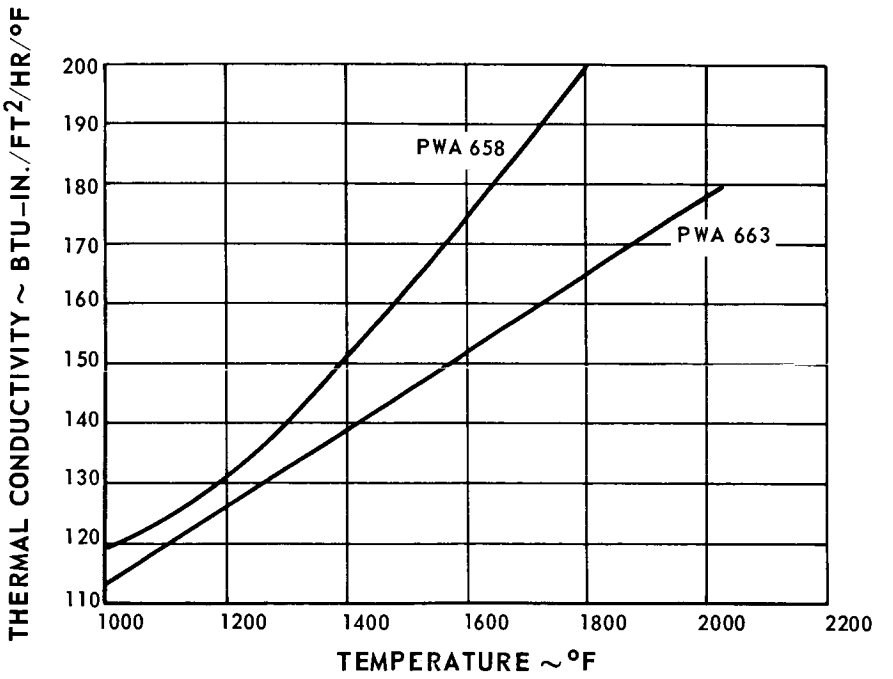


Figure C-32 Thermal Conductivity vs. Temperature for PWA 663 and PWA 658

# APPENDIX D

## METHOD OF CALCULATING BENDING STRESSES IN SPECIMENS

Prepared by: W. H. Vogel

## GENERAL APPROACH

To obtain the stress-strain history of the specimen at the mid-span section, it was necessary to ascertain the bending moments at that section. These moments, induced by such factors as curvature of the specimen due to thermal gradients when simultaneously subjected to axial loading, eccentricities between the bearing axis and the specimen axis, and flexibility in the test rig and loading mechanism, were determined as described in the following section. The moments due to the gas loading were less than 5 inch-pounds at the mid-span and were, therefore, neglected. The analytical method discussed below is applicable to moments about both axes, it being necessary to vary only the geometry.

Bending strains were measured with strain gages in the upper and lower pull rods. These strains, in turn, were related to the mid-span bending moments. The net mid-span moment was obtained by combining the forementioned with those moments resulting from eccentricities induced by the thermal gradients in the specimen which assumes a curvature in an effort to relieve the resultant thermal strains. The latter component was determined through a relationship incorporating the axial load, specimen length and grip geometry, and the angular rotations of the pull rods. These rotations ( $\theta_T$ and $\theta_B$) were determined by using the values calculated in the stress analysis program, as a fixed approximation. These rotations could be more accurately determined by direct measurement.

## ASSUMPTIONS

The assumptions on which this method of calculation is based are that:

- Frictional forces and moments may be neglected.
- The reactions, $R_T$, and $R_B$, act through the centroid of the axial cross section of the specimen.
- The angles $\theta_T$, $\theta_S$, $\phi_T$, and $\phi_B$ are sufficiently small so that the following approximations may be made.

$$\sin \theta_T \approx \theta_T \qquad \sin \theta_B \approx \theta_B$$

$$\sin \phi_T \approx \phi_T \qquad \sin \phi_B \approx \phi_B$$

$$\cos \theta_T \approx \cos \theta_B \approx \cos \phi_T \approx \cos \phi_B \approx 1.0$$

## CALCULATIONS

From these assumptions and upon summing forces in the X-direction (shown in Figure D-1), it is seen that

$$P_{MEAS_{TOP}} \cos \theta_T = P_{MEAS_{BOT}} \cos \theta_B$$

or

$$P_{MEAS_{TOP}} \approx P_{MEAS_{BOT}}$$

By breaking the forces on the rod into components, it is seen that

$$P_{ACT_{TOP}} = P_{MEAS_{TOP}} / \cos \phi_T \approx P_{MEAS_{TOP}}$$

Similarly

$$P_{ACT_{BOT}} = P_{MEAS_{BOT}} / \cos \phi_B \approx P_{MEAS_{BOT}}$$

Thus

$$P_{ACT_{TOP}} \approx P_{MEAS_{TOP}} \approx P_{MEAS_{BOT}} \approx P_{ACT_{BOT}}$$

For simplicity in notation these forces will be represented by the symbol P.

To get an expression for $M_c$, the moment in the center of the specimen, in terms of P , $\theta_t$, $\theta_b$, $\phi_t$, and $\phi_b$, two equations must be found to solve for the reactions $R_T$, and $R_B$. This may be done by summing forces in the y-direction and by summing moments about the Point 0' :

$$\sum Fy = 0$$

$$\rightarrow R_b + R_t = P\left[(\theta_b + \phi_b) + (\theta_t + \phi_t)\right]$$

$$\sum M_{o'} = 0$$

$$[P(\theta_b + \phi_b)][L + \ell + 2e] = P[(L + e)(\theta_b - \theta_t)]$$

$$+ R_b[\ell + 2e] + P(\phi_t + \theta_t)[L]$$

$$R_b = \frac{P\left\{(\theta_b + \phi_b)[L + \ell + 2e] - (L + e)(\theta_b - \phi_t) - L(\phi_t + \theta_t)\right\}}{\ell + 2e}$$

$$= P\left\{(\theta_b + \phi_b) + \frac{1}{\ell + 2e}[L(\phi_b - \phi_t) - e(\theta_b - \theta_t)]\right\}$$

$$R_t = P\left\{(\theta_t + \phi_t) - \frac{1}{\ell + 2e}[L(\phi_b - \phi_t) - e(\theta_b - \theta_t)]\right\}$$

The moment in the center of the specimen may now be formulated.

$$\sum M_c = R_b\left(\frac{\ell}{2} + e\right) - P(\theta_b + \phi_b)\left(L + e + \frac{\ell}{2}\right) + P[(L + e)\theta_b + y_m]$$

$$= P\left\{-L\left(\frac{\phi_b + \phi_t}{2}\right) + e\left(\frac{\theta_b + \theta_t}{2}\right) + y_m\right\}$$

But the moment, $m_a$, a distance (a) up from the bottom joint of the loading arm is:

$$M_a = a(P \sin \phi_b) \approx a P \phi_b$$

It follow that:

$$\phi_b = M_a/aP$$

Similarly,

$$\phi_t = m_b/bP$$

The expression for the moment in the center may then be written as:

$$M_c = P\left\{-L\frac{(M_a/a + m_b/b)}{2P} + e\left(\frac{\theta_b + \theta_t}{2}\right) + Y_m\right\}$$

If a moment $M_y$ were to be found, as well as $M_x$, the derivation would be exactly the same. In the y-bending direction, the distances L, a, and b would have smaller values, since there is a different joint configuration in that direction.

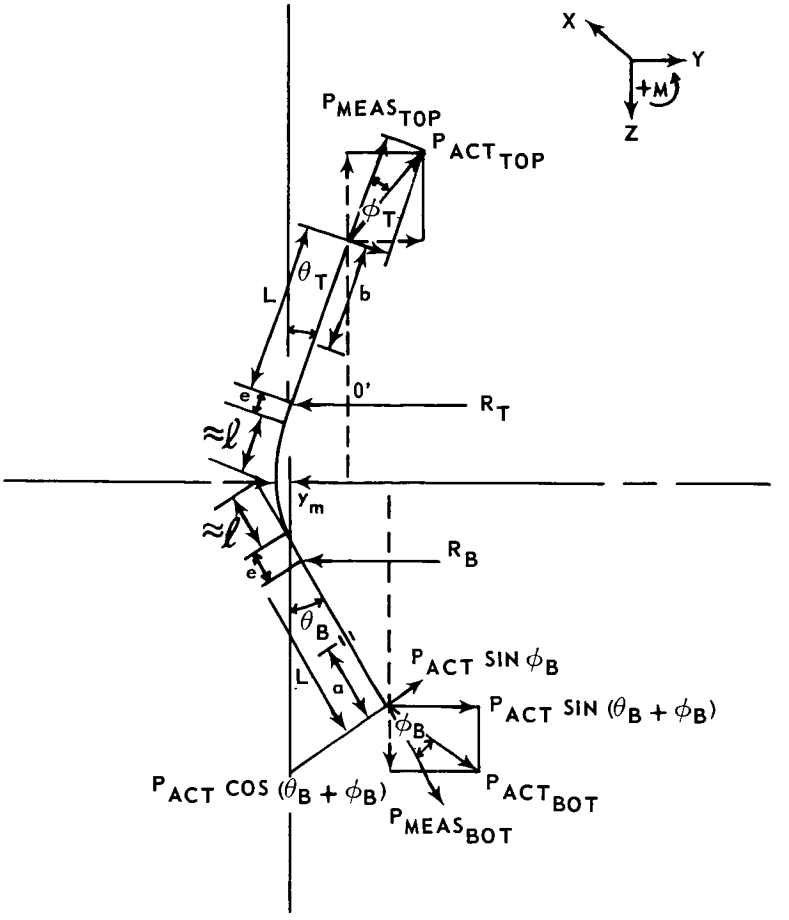


Figure D-1 Specimen Loading Diagram

# SUMMARY REPORT
# METHODS FOR PREDICTING THERMAL STRESS CRACKING IN TURBINE STATOR AND ROTOR BLADES

Written by
O. L. Stewart and W. H. Vogel

Approved by
R. A. Doak

## ABSTRACT

NASA's purpose in originating this program was to develop a method for predicting the initiationof thermal fatigue cracking in aircraft gas turbine blades and vanes and to verify the prediction method by testing simulated turbine blade specimens. A method for predicting thermal fatigue cracking in turbine blades and vanes, developed by Pratt & Whitney Aircraft prior to this contract, was delivered to NASA as part of this program. A single specimen test rig and simulated turbine blade specimens were designed and constructed. The specimen designs included uncooled solid, convectively cooled, and film cooled airfoil configurations of two materials, B-1900 (PWA 663) and IN-100 (PWA 658). Instrumented specimen tests were conducted to measure airfoil metal temperatures. Thermal fatigue life predictions were made for some of the specimens based on the measured specimen metal temperatures. Analytical and experimental investigations were performed to develop a satisfactory test procedure and some preliminary verification tests were conducted. Isothermal fatigue and other physical properties of the two specimen materials are included.